

THE UNIVERSITY OF MICHIGAN  
INDUSTRY PROGRAM OF THE COLLEGE OF ENGINEERING

DETERMINATION OF  $(d, \alpha)$  REACTION CROSS SECTIONS

Kenneth Lynn Hall

This dissertation was submitted in partial fulfillment of the requirements for the degree of Doctor of Philosophy in the University of Michigan. The research was partially supported by the Atomic Energy Commission under University Project No. 7, Contract No. AT (11-1)-70.

November, 1955

IP-134

### ACKNOWLEDGEMENT

We wish to express our appreciation to the author for permission to distribute this dissertation under the Industry Program of the College of Engineering.

## TABLE OF CONTENTS

	Page
List of Tables	ix
List of Figures	x
Abstract	xiii
 Part I: Absolute (d,α) Reaction Cross Sections	
Introduction	1
Statement of Problem	5
Description of Apparatus	6
A. Bombardment Chamber	6
Design	8
B. Window Box Probe	17
C. Beam Integrator	18
Description	20
Operation	24
D. Metal Evaporator	24
Electrical Controls	26
Vacuum Gauge	26
Vacuum System	28
Heaters and Target Assembly	33
Operation	34
E. 4π Proportional Counter	35
Description	36
Performance	42
Experimental Procedures	44
A. Beam Determination	44

	Page
Suppression of Secondary Electrons	44
1. Preliminary Experiments	45
2. Secondary Electrons Emitted from the Cup	48
3. Secondary Electrons Emitted from the Target	49
Primary Calibration of the Beam	52
Integrator	
1. Direct Measurement of Current	54
2. Potentiometer Method	58
Secondary Calibrations	62
B. Target Preparation	63
Magnesium	66
Sulfur	67
Titanium	69
Cadmium	70
C. Chemical Separations	72
Sodium from Magnesium Targets	75
Phosphorus from Sulfur Targets	78
Scandium from Titanium Targets	80
Silver from Cadmium Targets	84
D. Absolute Beta Counting	87
Summary of Existing Methods	87
1. Rate of Energy Release	87
2. Coincidence Counting	88
3. Particle Counting with Known Counting Efficiency	89



	Page
4π Proportional Counting	93
1. Plastic Film Preparation	95
2. Film Thickness Measurement	98
3. Film Absorption Correction	102
4. Self Absorption	109
5. Effect of a Conducting Coating	110
6. Effect of Gain, Trigger and Voltage Settings	114
7. Dead Time Correction	117
8. Counting of National Bureau of Standards Samples	124
Experimental Results	128
A. Derivation of Equations	128
Cross Section	128
Chemical Yield	133
B. Bombardment Procedure	140
C. Magnesium Bombardments	141
Target Preparation	143
Chemical Procedure	145
Absolute Beta Counting	146
Analysis of Decay Curves	151
Half-Life of Na <sup>24</sup>	152
Cross Section for Na <sup>22</sup> and Na <sup>24</sup>	155
D. Sulfur Bombardments	158
Target Preparation	160
Chemical Procedure	160
Absolute Beta Counting	163

	Page
Analysis of Decay Curves	166
Cross Section for $P^{32}$	167
E. Titanium Bombardments	169
Beam Determination	172
Target Preparation	172
Chemical Procedure	173
Absolute Beta Counting	173
Analysis of Decay Curves	177
Cross Section for $Sc^{46}$	180
F. Cadmium Bombardments	181
Target Preparation	183
Chemical Procedure	183
Absolute Beta Counting	185
Analysis of Decay Curve	185
Cross Section for "1.2" hr $Ag^{104}$ , $Ag^{111}$ , and $Ag^{112}$	185
G. Loss of Recoil Nuclei	188
H. Energy of the Deuteron Beam	189
Discussion	191
Part II: Mass Assignment of $Ag^{104}$	
Introduction	195
Experimental Procedures	196
A. Target	196
B. Chemical Separations	197
C. Counting	200

	Page
Experimental Results	201
Discussion	203
Appendix I	205
Appendix II	208
Bibliography	212

## LIST OF TABLES

<u>Table No.</u>	<u>Title</u>	<u>Page</u>
I	Target Materials	65
II	Spectrographic Analysis of Foote Titanium	70
III	Spectrographic Analysis of Johnson, Matthey Cadmium Rods	72
IV	Surface Density Data for Films made from 33 per cent Zapon Solution	101
V	Aliquot Reproducibility	108
VI	Summary of Bombardment Data for Mg(d, $\alpha$ )Na	144
VII	Analysis of Decay Curves of Sodium	153
VIII	Summary of Half-Lives of Na <sup>24</sup>	154
IX	Propagation of Errors in Cross Section for Mg(d, $\alpha$ )Na	157
X	Summary of Bombardment Data for S(d, $\alpha$ )P	161
XI	Summary of Bombardment Data for Ti(d, $\alpha$ )Sc	171
XII	Summary of Bombardment Data for Cd(d, $\alpha$ )Ag	184
XIII	Mass Analysis of Cadmium Oxide Target Materials	197
XIV	Relative Yields of Silver Isotope	201
XV	Ratio of the Relative Yields from Enriched(Bombardment 5) and Normal Cadmium Targets(Bombardments 1 and 4)	202

## LIST OF FIGURES

<u>Figure No.</u>	<u>Title</u>	<u>Page</u>
1.	Cyclotron Layout - Schematic	7
2.	Cyclotron Bombardment Chamber - Front View	13
3.	Cyclotron Bombardment Chamber - Top View	14
4.	Cyclotron Bombardment Chamber - Side View	15
5.	Faraday Cup and Target Probe Assembly	16
6.	External Focused Beam Bombardment Chamber for Cyclotron	16
7.	Cyclotron Probe Head	19
8.	Current Integrator - Schematic	21
9.	Power Supply for Current Integrator - Schematic	22
10.	Metal Evaporator	25
11.	Types of Heaters for Metal Evaporator	25
12.	Electrode, Heater and Target Assembly for Metal Evaporator	25
13.	Evaporator Control Panel - Schematic	27
14.	Evaporator Vacuum System - Schematic	30
15.	4 $\pi$ Proportional Counters	37
16.	Cylindrical 4 $\pi$ Proportional Counter - inside housing	37
17.	Modification of Model 162 for Proportional Counting	40
18.	Integrator-Monitor Comparison	47

<u>Figure No.</u>	<u>Title</u>	<u>Page</u>
19.	Suppressor Ring Curves	50
20.	Calibration Schematics	56
21.	Calibration of Beam Integrator	60
22.	Chemical Separation of Sodium from Magnesium	77
23.	Chemical Separation of Phosphorus from Sulfur	81
24.	Chemical Separation of Scandium from Titanium	83
25.	Apparatus for Making Thin Plastic Films	97
26.	Mounting the Film on a 4π Counting Plate	97
27.	Trimming the Mounted Film	97
28.	Transmission of Ni <sup>63</sup> Radiation	103
29.	Film Absorption Curve of NBS P <sup>32</sup>	107
30.	Self Absorption Curve of Co <sup>60</sup>	110
31.	Plateau Curves	113
32.	Sample for 4π Counter	115
33.	Discrimination Curves of NBS P <sup>32</sup>	116
34.	Decay of In <sup>116</sup>	121
35.	Coincidence Correction	123
36.	Decay of NBS P <sup>32</sup>	127
37.	Nuclide Chart of the Magnesium Region	142
38.	Discrimination Curves of Sodium-- 3% Na <sup>22</sup>	147
39.	Discrimination Curves of Sodium-- 100% Na <sup>22</sup>	148
40.	Film Absorption Curve of Sodium	149

<u>Figure no.</u>	<u>Title</u>	<u>Page</u>
41.	Decay of Sodium	150
42.	Nuclide Chart of the Sulfur Region	159
43.	Decay of Phosphorus-pure P <sup>32</sup>	162
44.	Discrimination Curves of Phosphorus	164
45.	Decay of Phosphorus-P <sup>32</sup> plus P <sup>33</sup>	165
46.	Decay of P <sup>33</sup> Tracer	168
47.	Nuclide Chart of the Titanium Region	170
48.	Discrimination Curves of Scandium-- 70% Sc <sup>46</sup>	174
49.	Discrimination Curves of Scandium-- 100% Sc <sup>46</sup>	175
50.	Film Absorption Curve of Scandium	176
51.	Decay of Scandium	178
52.	Calculated Decay of Sc <sup>44,47,48</sup>	179
53.	Nuclide Chart of the Cadmium Region	182
54.	Discrimination Curves of Silver	186
55.	Decay of Silver	187
56.	Chemical Separation of Silver from Cadmium	199

# DETERMINATION OF (d, alpha) REACTION CROSS SECTIONS

by  
Kenneth Lynn Hall

## ABSTRACT

The objectives of this research were to assemble the necessary apparatus and establish procedures for the accurate measurement of (d,  $\alpha$ ) reaction cross sections, and to apply these techniques to determine several cross sections using the 7.8 Mev deuterons from the University of Michigan cyclotron.

The measurement involved the bombardment of thin targets, subsequent chemical separation of the product nuclei, and determination of the absolute disintegration rate of the  $\beta$ -ray emitting products. To obtain the irradiations a bombardment chamber was designed and installed as an integral part of the cyclotron vacuum system. The deuteron beam was stopped in a Faraday cup, after traversing the target. The beam current was measured by means of a current integrator which was built for this work. A metal evaporator was assembled for use in fabricating thin targets. After bombardment, the targets were dissolved, and the low yield (d,  $\alpha$ ) reaction products were chemically separated from relatively large amounts of (d, n) and (d, p) radioactive products. This was achieved without the addition of



inactive carriers in the case of three of the four elements studied. Absolute counting of the separated products was accomplished by application of the techniques of  $4\pi$  proportional counting.

The experimental (d,  $\alpha$ ) reaction cross sections for the formation of the isotopes indicated are:

Na <sup>22</sup> :	$\sigma = 0.094 \pm 0.004$	barn at $7.8 \pm 0.1$ Mev
Na <sup>24</sup> :	$\sigma = 0.151 \pm 0.006$	barn at $7.8 \pm 0.1$ Mev
P <sup>32</sup> :	$\sigma = 0.3 \pm 0.2$	barn at $7.7 \pm 0.1$ Mev
Sc <sup>46</sup> :	$\sigma = 0.00044 \pm 0.00033$	barn at $7.0 \pm 0.8$ Mev
1.2-hr Ag <sup>104</sup> :	$\sigma = 0.0017 \pm 0.0002$	barn at $7.8 \pm 0.1$ Mev
Ag <sup>112</sup> :	$\sigma = 0.00049 \pm 0.00002$	barn at $7.8 \pm 0.1$ Mev
Ag <sup>111</sup> :	$\sigma = 0.0004 \pm 0.00004$	barn at $7.8 \pm 0.1$ Mev

The errors quoted are estimated standard deviations. The result for Sc<sup>46</sup> quoted above is an average of two determinations which differed from one another by a factor of four. The half life of Na<sup>24</sup> was evaluated by the method of least squares and found to be  $14.93 \pm 0.04$  hours. Separated isotopes were bombarded to assign the 27-minute and the "1.2-hour" periods in silver to Ag<sup>104</sup>.

## PART I: ABSOLUTE (d,alpha) REACTION CROSS SECTIONS

### INTRODUCTION

The study of the properties of the nucleus and of the reactions which it may undergo has received an enormous amount of attention during the past two decades, and it appears that the field will continue to increase in popularity at an even greater rate than it has in the past. Thus the expenditures of the United States Atomic Energy Commission have quadrupled since 1948, (1) and in seven years the dollar volume to be spent on nuclear reactors is predicted to undergo a tenfold increase. (2) Particle accelerators are fairly common on college campuses nowadays (3) so that high energy sub-atomic projectiles are available to many workers for the purpose of producing radioactive species for study or application, or for the purpose of investigating the details of the reaction between the projectile and the nucleus.

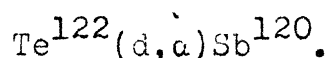
In speaking of nuclear reactions one of the important questions to ask is "What will the yield of a certain nuclear species be if bombarded under a given set of conditions?" In the field of reactions between molecules the organic chemist is similarly concerned with the chemical yield, i.e., the percentage of the starting materials which react to give a specific product among the various by-products which are produced in the same reaction mixture. Pursuing this analogy a little further, the rate of production of a given chemical species is many times expressed

in terms of the concentration of the reactants, and a rate constant characteristic of the reaction. A similar situation exists in the reactions between nuclei and high energy bombarding particles, with the important difference that in this case equilibrium conditions do not exist and the reaction must be discussed in terms of individual collisions. The rate of production of a given nuclear species is expressed in terms of the "concentration" of nuclei and incident particles, and a constant of proportionality characteristic of the reaction (cf. the rate constant for chemical reactions). This constant is known as the cross section and it may be defined as the probability that a given nuclear reaction will occur. There may be several possible courses for the reaction to follow (as in the chemical case), but the cross section usually refers to only one.

Just as in writing chemical equations a nuclear reaction may be written with the reactants on the left and the products on the right:



In words, this means that one nucleus of tellurium-122 reacts with a deuteron and a nucleus of a new element, antimony-120, is produced with the release of an alpha particle. A shorter notation is usually preferred, so that the above reaction is written as



These symbolizations refer to a single event (cf. chemical equations where each symbol refers to one mol). The heats of nuclear reactions are tremendous when compared with ordinary chemical reactions. Thus the "Q" for the above reaction is exothermic by 9.0 Mev per nucleus, or  $2.1 \times 10^{11}$  cal/mol.

Rate constants for chemical reactions are dependent upon the temperature of the reactants. Remembering that temperature may be related to the mean kinetic energy of the molecules, a change in the temperature produces a change in the average energy with which the reacting molecules collide. Thus the rate constants may be said to depend upon the mean collision energy. The nuclear case is analogous in that the cross section is a function of the energy of the incident particle. A graph exhibiting this dependence is called an excitation function.

There have been many studies of these functions carried out during the past two decades. In 1944 Clarke and Irvine (4) presented a bibliography of experimental excitation functions produced by cyclotron accelerated deuterons. The Neutron Cross Section Advisory Group of the Atomic Energy Commission (5) has more recently compiled neutron excitation functions and thermal neutron cross section data. A program is currently underway at Los Alamos under the direction of R. F. Taschek (6) to assemble the existing experimental charged particle cross sections. Many of the excitation functions appearing in the literature have been

in terms of relative values of the cross section, as the shape of the curve was the main object of interest. Sometimes an absolute scale has been established by normalizing the relative curve to one point which is an absolute cross section at a particular energy. Other times each point was determined absolutely.

Less attention has been devoted to the careful measurement of absolute cross sections at an accurately known energy, especially for low-yield reactions such as the  $(d,\alpha)$ ,  $(p,\alpha)$ ,  $(d,\gamma)$ , etc. This may be due in part to the experimental difficulties attendant in these measurements. The present work is concerned with such absolute determinations for the  $(d,\alpha)$  reaction using 7.8 Mev deuterons of the University of Michigan cyclotron.

## STATEMENT OF THE PROBLEM

The objectives of this research were (a) to set up the apparatus and establish procedures by which absolute cross sections may be routinely determined with an overall accuracy of  $\sim 4$  per cent, and (b) to apply these techniques to the measurement of the (d, $\alpha$ ) cross sections of several nuclei.

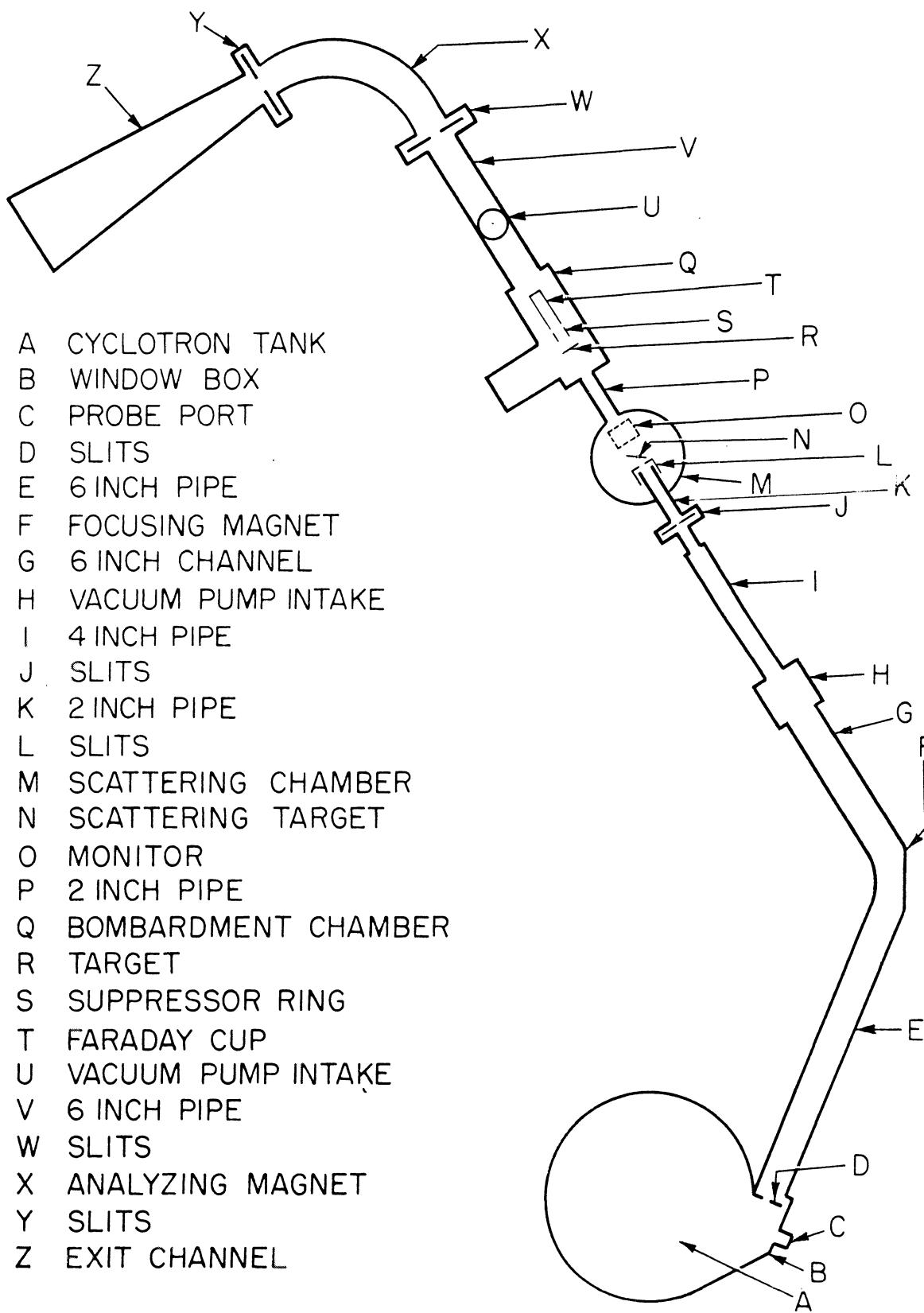
## DESCRIPTION OF APPARATUS

### A. Bombardment Chamber

The 42 inch University of Michigan cyclotron produces 7.8 Mev deuterons in high intensity beams. The external beam is as great as 100 microamperes just beyond the deflector. An additional system was installed within the last two years to bring the deflected beam out to a "scattering chamber" via a focusing magnet, and finally through an analyzing magnet to a detector. The layout of the cyclotron vacuum system as it now stands is shown schematically in figure 1. It was known that the nuclear chemistry group was to have a bombardment chamber incorporated into the system and it fell to the writer to design, test, and install the chamber. It was to be placed somewhere between the two magnets F and X. Simple geometrical considerations demonstrated that to take advantage of the focusing magnet the chamber must be behind the focal plane and as close to it as possible. Slits may then be placed at L (the calculated focal plane passes through the center at N) to select various combinations of energy definition and beam intensity.

Referring to figure 1 the deflected beam emerges from the cyclotron vacuum tank A through the window box B, passes the vertical and horizontal slits D into a 6 inch diameter iron pipe E. A focusing magnet F directs the beam past the vertical and horizontal slits J and L toward the scattering chamber M on the other side of the shielding wall.

### CYCLOTRON LAYOUT — SCHEMATIC



- A CYCLOTRON TANK
- B WINDOW BOX
- C PROBE PORT
- D SLITS
- E 6 INCH PIPE
- F FOCUSING MAGNET
- G 6 INCH CHANNEL
- H VACUUM PUMP INTAKE
- I 4 INCH PIPE
- J SLITS
- K 2 INCH PIPE
- L SLITS
- M SCATTERING CHAMBER
- N SCATTERING TARGET
- O MONITOR
- P 2 INCH PIPE
- Q BOMBARDMENT CHAMBER
- R TARGET
- S SUPPRESSOR RING
- T FARADAY CUP
- U VACUUM PUMP INTAKE
- V 6 INCH PIPE
- W SLITS
- X ANALYZING MAGNET
- Y SLITS
- Z EXIT CHANNEL

Fig. 1. Schematic representation of the layout of the cyclotron vacuum system.



The slits L consist of a set of collimators containing rectangular holes all  $1/4$  inch high, but of several horizontal dimensions from  $1/8$  to  $3/4$  inch. They were machined from  $1/8$  inch lead sheet and mounted on a brass collar which slides over the 2 inch pipe K. Normally the  $1/2$  inch horizontal aperture was used in this work. (This choice was more or less arbitrary, but it was based upon the observation that whenever the  $1/8$  and  $1/4$  inch slits were used, the maximum beam was roughly  $0.05 \mu a$ , whereas as much as  $0.5 \mu a$  has been observed with the  $1/2$  inch slits.) The remaining apparatus pivots about the scattering chamber, riding on a circular railroad track. This system may be oriented to zero degrees when the chemistry bombardment chamber Q is used. The Faraday cup T and target R retract when not in use so that the beam can pass into the analyzing magnet X for the physics experiments. Vacuum pumps located at H and U are equipped with valves so that various parts of the pipe system may be let down to air independently. One other control over the beam (in addition to the deflector and magnets) is a variable 10,000 volt D. C. power supply which is applied to vertical deflector plates so the beam may be aimed up or down as it enters the focusing magnet.

### Design

The design of the bombardment chamber with the associated Faraday cup and target arrangement was the subject of much consideration. Its primary purpose was

to fulfill the requirements dictated by this research, but in addition it was to be made versatile enough to permit other problems to be investigated with a minimum of modification. Thus the angular distribution of recoil nuclei, excitation function studies, and the bombardment of radioactive targets were among the problems for which the chamber was designed. Furthermore, it had to be integrated with the cyclotron system such that only a few minutes would be required to change from a chemistry bombardment to a physics experiment. With this in mind a design was worked out which meets these demands and works quite satisfactorily in practice.

A search of the literature revealed that many diverse arrangements of the target system have been used in previous work.

Two ways are apparent of arranging the target with respect to the Faraday cup to measure the number of incident particles. The target may be placed inside of the cup or in direct contact with it. (7 - 13) In the other arrangement the target foil is placed in front of the Faraday cup so that the beam passes through the target and is caught in the cup. (4, 10, 13 - 20) Panofsky (10) found no difference in results when the two arrangements were tried. In either case some provision must be made to stop secondary electrons from either escaping (if produced inside) or entering the cup (if produced outside). While some workers have ignored this detail (12, 15, 20) most of them have made

use of an electric field to suppress the secondaries. Others have used magnetic fields, e.g. the fringe field of the cyclotron, to insure that the electron orbits are spirals which are small compared with the dimensions of the collector. Since the target must be removed from the chamber rapidly after bombardment and because of other requirements, it was decided to use the scheme in which the target is placed before the Faraday cup with a suppressor ring between.

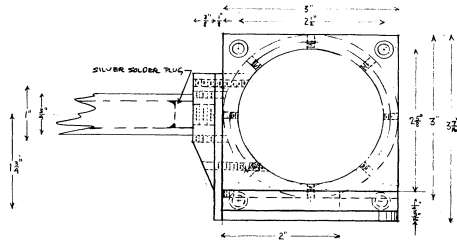
The machine drawings of the bombardment chamber are shown in figures 2, 3 and 4, and the photographs of the completed chamber are shown in figures 5 and 6. The construction was made of brass, with all joints silver-soldered except as noted below or where O-rings were used. Before installation the entire assembly was vacuum tested, first by filling with water under pressure and secondly with a helium leak detector. Ten inch diameter brass pipe used in the construction made the chamber large enough to accomodate apparatus to be used in future work as well as to permit the retraction of the Faraday cup assembly to the side of the chamber when not in use. Both the cup and target are on the end of probes manipulated from the outside. Geometrical considerations show that a cone of scattered particles defined by the center of the scattering chamber as its apex, and the end of the 6 inch brass pipe V, figure 1, as its base, is undisturbed by the protrusion of the Faraday cup when in its retracted position.

The Faraday cup assembly is mounted on teflon slides which engage in grooves in the brass floor of the chamber for easy positioning of the cup. The probe consists of a 3/4 inch brass pipe screwed into a part of the teflon structure. This pipe slides in and out of the chamber through an O-ring port. The suppressor ring was cut from 1/4 inch brass plate, and a hole was machined in the center to match the inside diameter of the Faraday cup. It is mounted permanently on the front of the cup and insulated with teflon. Electrical leads are brought into the chamber via kovar seals (Stupakoff Ceramic and Manufacturing Company, Latrobe, Pennsylvania, No. 95.1029) which were soft-soldered over the 1/2 inch holes atop the chamber. The cup and ring are provided with binding posts, and ~10 inch lengths of RG-62/U cable are attached at one end to the posts, the other end being soldered to the kovar seals. To protect the outside of the seals from breakage and dirt, removable brass housings are provided. The outer terminals of the kovar seal were soldered to the pin of cable connectors mounted on the brass housings. Type UG-560/U (teflon insulated) was used with the Faraday cup while UG-496/U was used with the suppressor ring. The entire cup assembly and connecting wires were scrupulously cleaned of dirt, grease, and lint before final assembly, with special attention paid to the teflon parts and the electrical contacts.

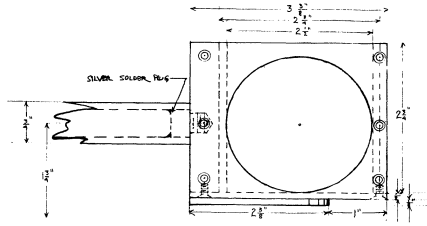
The target probe may be introduced through a side chamber so as not to disturb the main vacuum. The vacuum lock is constructed of 6 inch brass pipe, and a vacuum valve with a 4 inch opening isolates it from the main vacuum system. A 3/4 inch modified steam valve was soft-soldered into a pipe fitting in the side of the 6 inch pipe to serve as the connection for the vacuum pump. (For details see the section describing the metal evaporator.) A Cenco-Hypervac 4 mechanical pump (Central Scientific Company, Chicago, Illinois) was used to evacuate the side chamber in about 10 minutes. A 3/8 inch Hoke valve (oriented with the arrow pointing out) was soft-soldered into a pipe fitting protruding from the 6 inch pipe. This provides a means of letting air into the chamber slowly without rupturing the delicate targets. An O-ring port in the end plate of the side chamber maintains the vacuum seal and supports the target probe. The end plate must be removed before the probe can be inserted or withdrawn, but this can be done in a matter of seconds. This design is seen to fulfill the original objectives, since it has given very satisfactory service over the past year.

The brass probe head with provision for eight separate target mounts engages in the Faraday cup assembly. The eight target positions vary from 1 1/2 to ~ 2 2/3 inches in front of the cup to accommodate collimators, absorbers, targets, etc. The positions were assigned numbers 1, 2, ..., 8

FARADAY CUP - FRONT VIEW



TARGET PROBE - FRONT  
FINISH ALL OVER



UNIVERSITY OF MICHIGAN  
DEPT. OF CHEMISTRY

CYCLOTRON BOMBARDMENT CHAMBER  
DRAW NO. UM 2022  
DRAWN BY *J. S. H.*  
DATE 11-27-53  
SCALE 1/8" = 1"

VACUUM CHAMBER - FRONT VIEW  
SECTION A-A

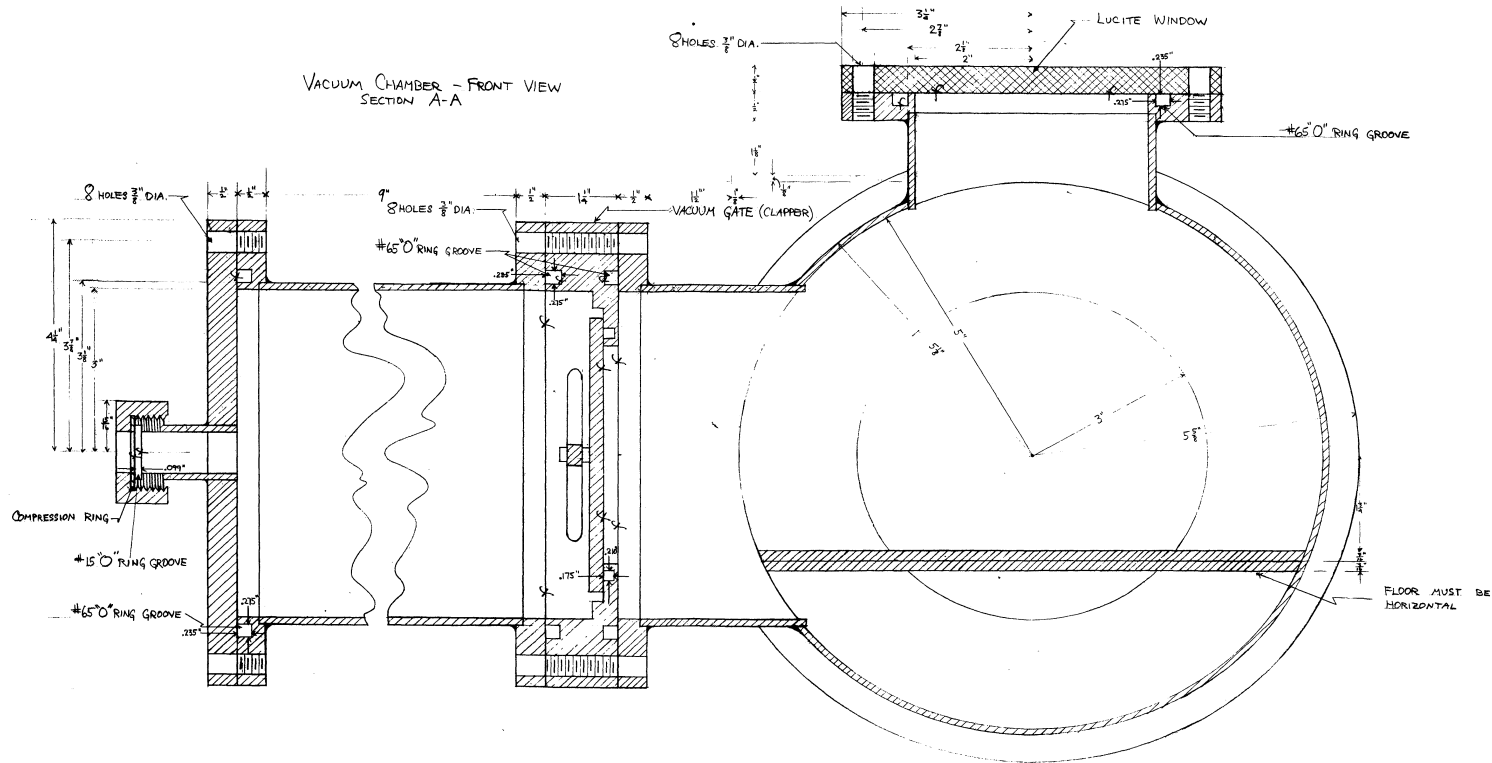


Fig. 2. Machine drawing of the cyclotron bombardment chamber - front view.

UNIVERSITY OF MICHIGAN  
DEPT. OF CHEMISTRY

CYCLOTRON BOMBARDMENT CHAMBER  
DRAW. NO. UM 2223  
DRAWN BY X244  
DATE 11-27-53  
SCALE ONE INCH

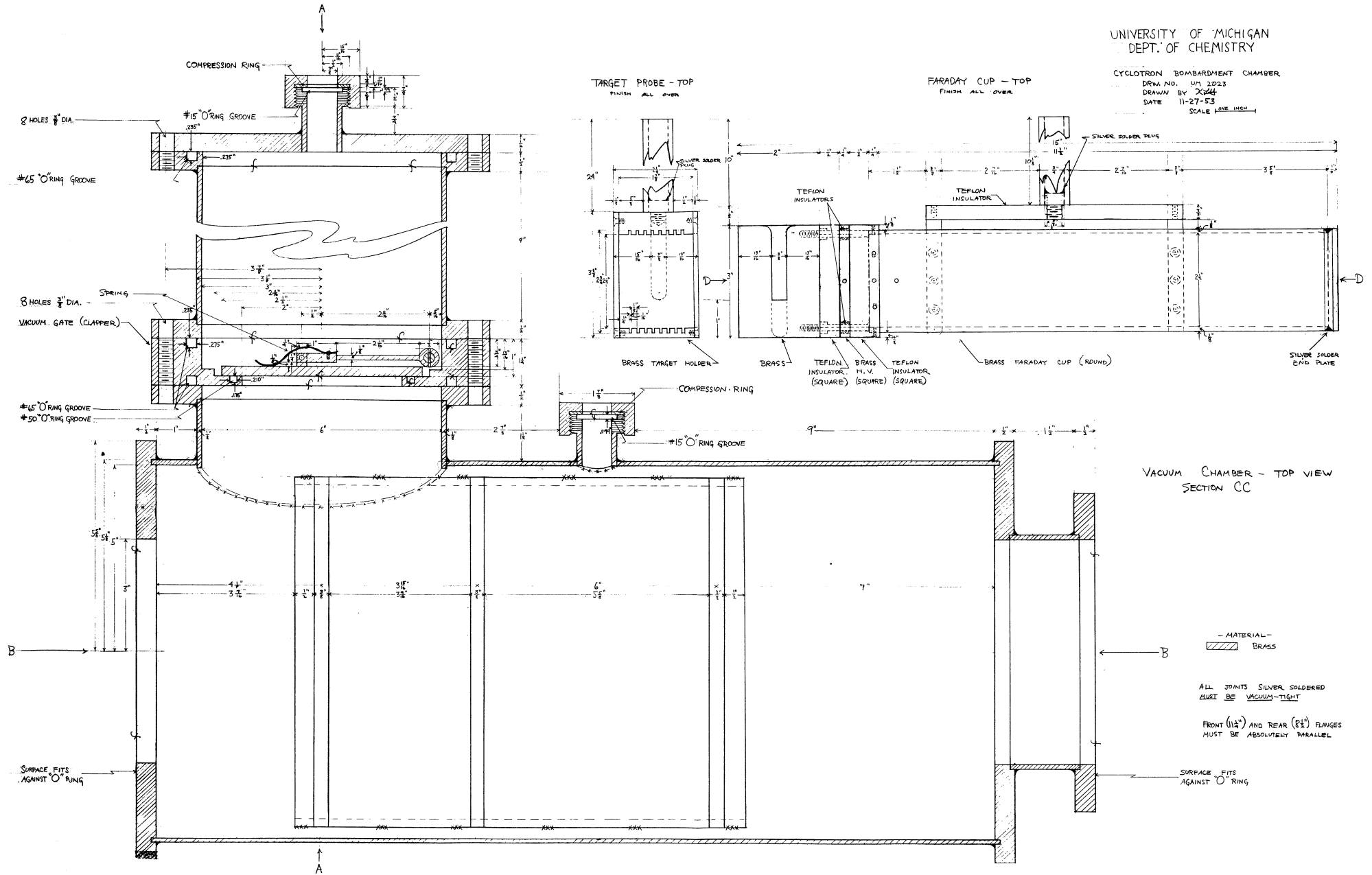


Fig. 3. Machine drawing of the cyclotron bombardment chamber - top view.

TARGET PROBE - SIDE  
FINISH ALL OVER

FARADAY CUP - SIDE  
SECTION DD  
FINISH ALL OVER

UNIVERSITY OF MICHIGAN  
DEPT OF CHEMISTRY

CYCLOTRON, BOMBARDMENT CHAMBER  
DRAW. NO. UM2021  
DRAWN BY *Xell*  
DATE 11-27-58  
SCALE 1/8" = 1"

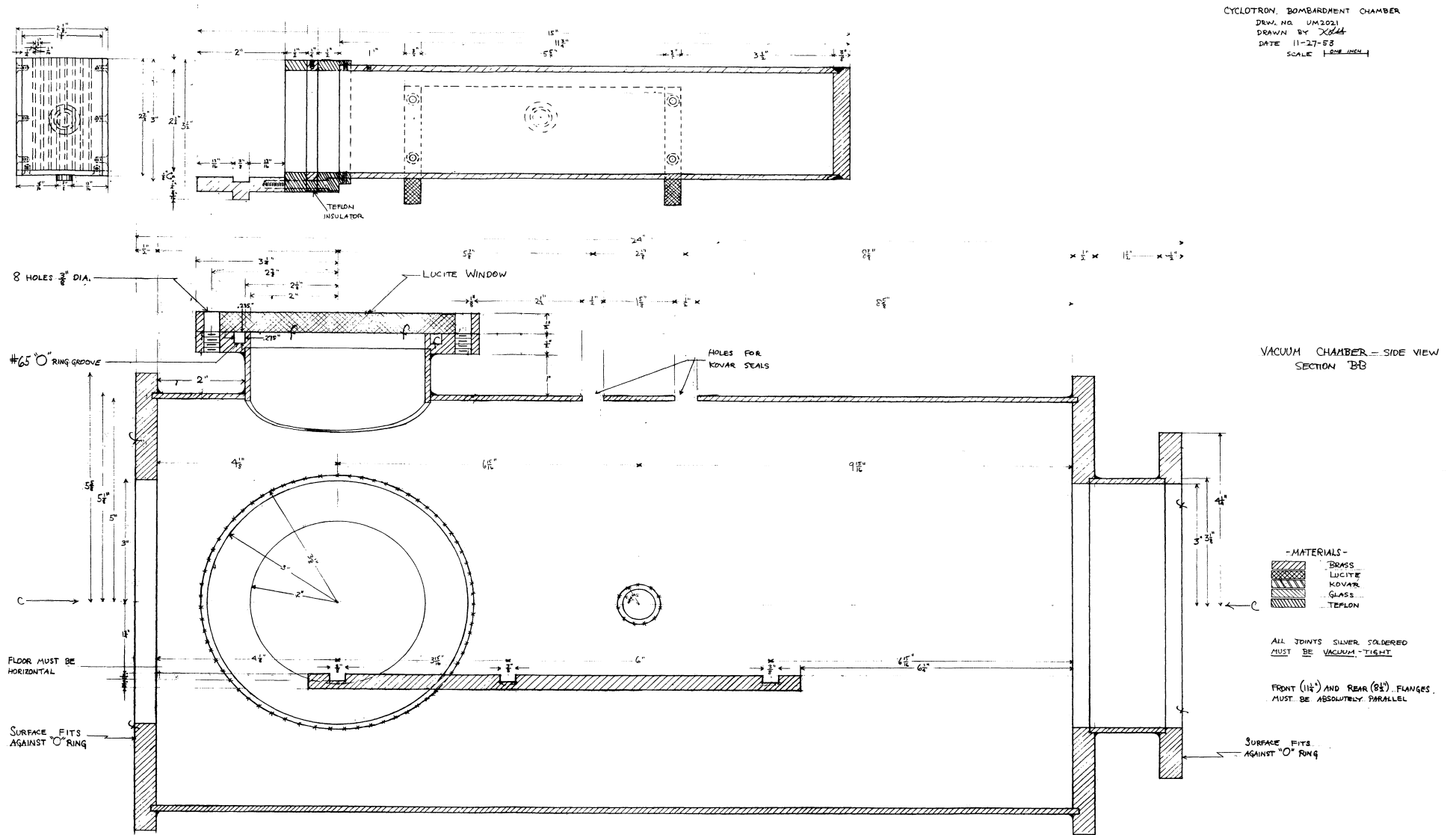


Fig. 4. Machine drawing of the cyclotron bombardment chamber - side view.



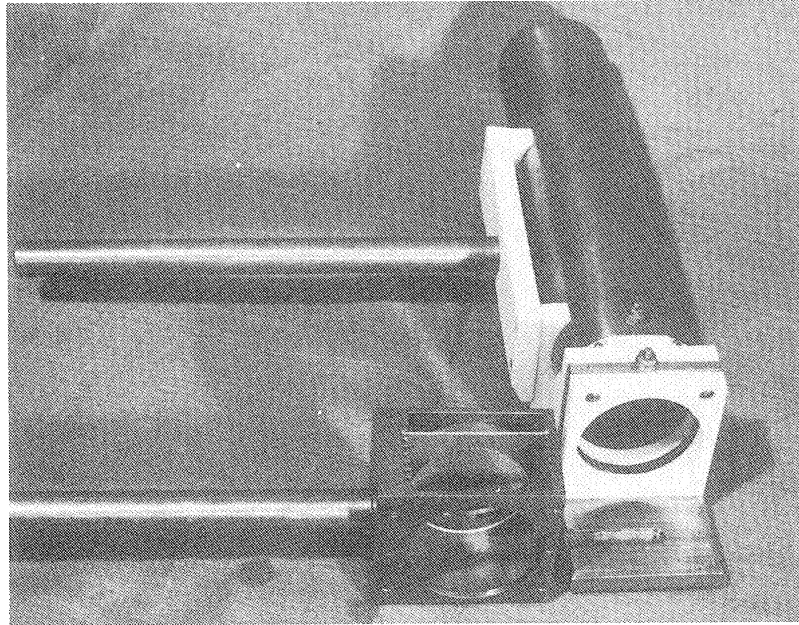


Fig. 5 Faraday Cup and Target Probe Assembly.

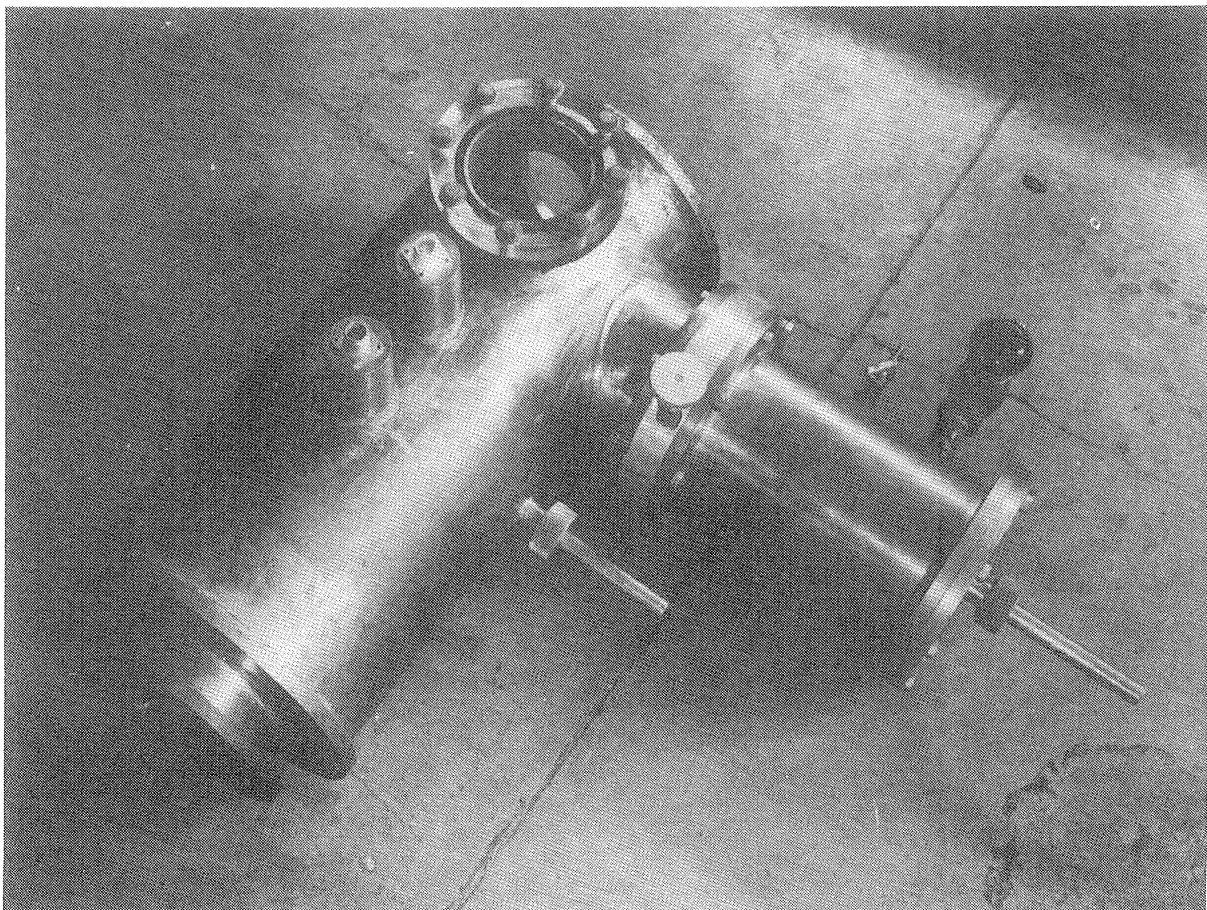


Fig. 6 External Focused Beam Bombardment Chamber for Cyclotron.

for easy reference, position 1 being closest to the Faraday cup.

#### B. Window Box Probe

In the early phase of this work, a number of bombardments had to be obtained in order to test chemical procedures, to explore the order of magnitude of (d,a) yields that could be expected, etc. Beam currents of 50 - 100  $\mu$ a are available at the window box probe, (C of figure 1), making it easy to obtain large amounts of activity. The probe for use in this position was made from 3/4 inch brass pipe in which the target was clamped to a copper head. When the probe was withdrawn from the cyclotron after being bombarded, it was extremely radioactive - many targets were obtained which measured 2 roentgens per hour at a distance of one foot! The need thus arose for a new probe design from which the target could be quickly removed. Fast removal would result in lower radiation exposures for personnel since most of the induced activities are in the copper probe head. Moreover, the investigation of short-lived activities would be aided by the use of a quick opening device.

The result of these considerations was a new probe design, the details of which are shown in figure 7. The essential feature is that a single Phillips head screw secures the hinged clamp against the probe head thus holding the target foil tightly. A spring normally forces the clamp away from the head so that after bombardment the screw is loosened and the clamp springs away releasing the

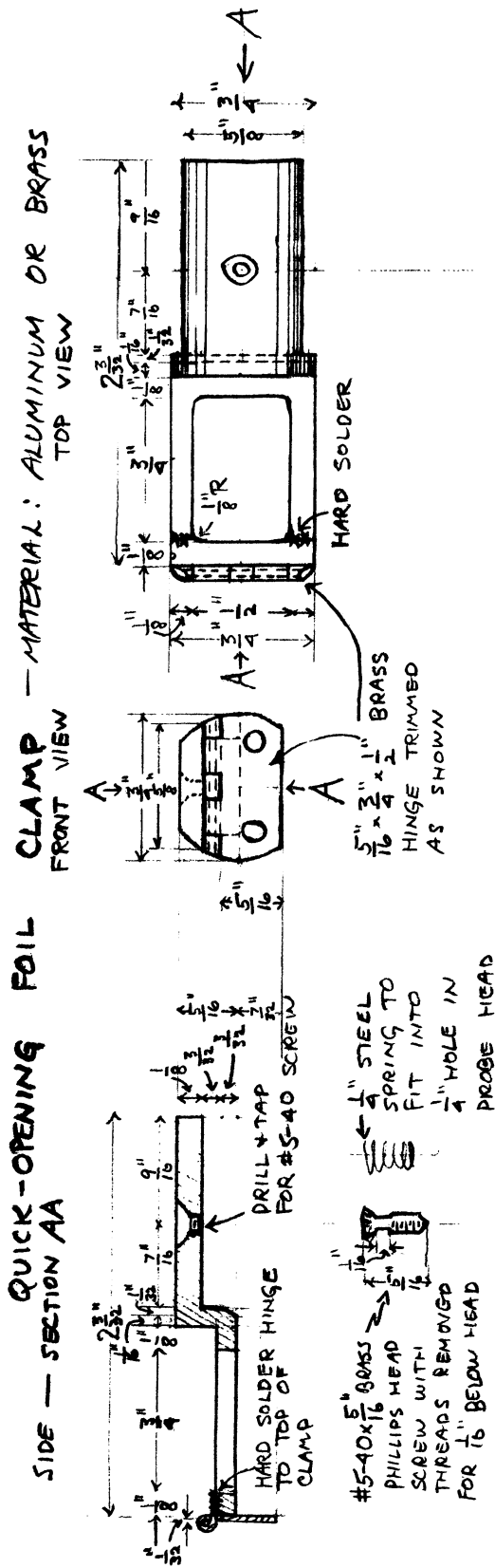
target. To prevent the screw from flying out of the clamp, the threads were machined off for 1/16 inch close to the head of the screw. The entire operation of releasing the target from the probe and dropping it into a beaker can be done at a distance of several feet by employing a Phillips head screw driver mounted on the end of a long aluminum rod.

This new design has been in use for about three years, and has given very satisfactory service. Spare clamps, springs, and screws allow one probe to be used many times before it must itself be repaired.

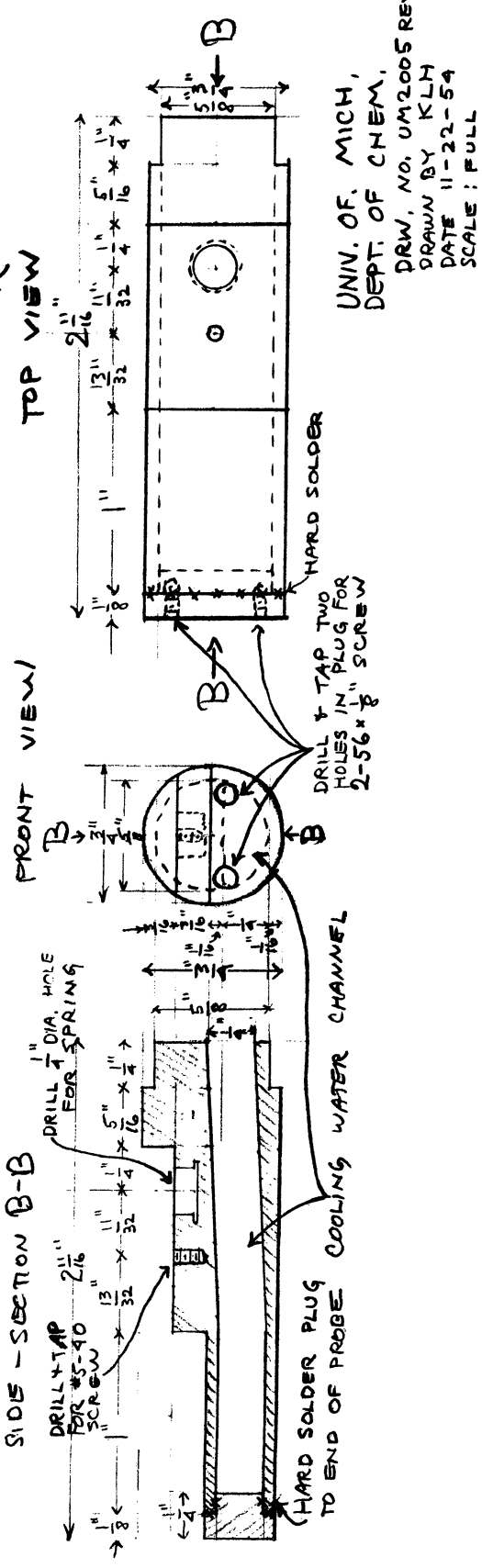
### C. Beam integrator

There are two principle methods for recording the current produced by the incident deuterons. They may be caught in a Faraday cup and the current amplified and fed into a pen recorder. Otherwise some form of current integrator may be used to record the total charge collected. From the point of view of accuracy, Kelley and Segre (18) claim only  $\pm 0.5$  per cent by integrating under the curve of current vs time, whereas  $\pm 0.1$  per cent has been reported for many of the integrators reported in the literature. (8, 10, 13, 21 - 34) Since an integrator patterned after the one described by Watts (30) had previously been used with the University of Michigan cyclotron by King (35) and was available to us, it was decided that this would be the logical starting point. The only modifications foreseen were the improvement of its stability and the extension of its range up to  $\sim 5 \mu\text{a}$ .

# CYCLOTRON PROBE HEAD



## PROBE HEAD - MATERIAL: COPPER



UNIV. OF. MICH,  
DEPT. OF CHEM,  
DRW. NO. UM2005 REV.  
DRAWN BY KLM  
DATE 11-22-54  
SCALE: FULL

Fig. 7. Machine drawing of the cyclotron window box probe head.

Accordingly, Trott Electronics Company of Rochester, New York, was contracted to make these changes. However, the unit as received was far from satisfactory. With no input current it counted at a rate corresponding to several microamperes. It was found that the integrating condensers did not fully discharge after each count. Several errors in wiring were discovered. These and other difficulties necessitated extensive modifications before the integrator could be used.

#### Description

The circuit as finally adopted is shown schematically in figures 8 and 9. Briefly the operating cycle is as follows. The deuterons strike the Faraday cup, extract electrons and cause one of the integrating condensers A...D to charge. The grid of V3 then becomes positive, and V3 starts to conduct when the grid potential reaches about 5 volts. This cuts off one half of V4 and results in a rise in the grid potential of one half of V5, a univibrator circuit. This half of V5 starts to conduct, cutting off the other half. This means that the grids of V1 and V2 rise and these tubes conduct, discharging the integrating condenser. A positive pulse is also received on the grid of V6 which drives the register and records a count. V6 also actuates a relay (Potter and Brumfield, Princeton, Indiana, Type SM5LS, 10,000 ohm.) whose closing time is ~3 milliseconds and opening time is less than

# CURRENT INTEGRATOR — SCHEMATIC

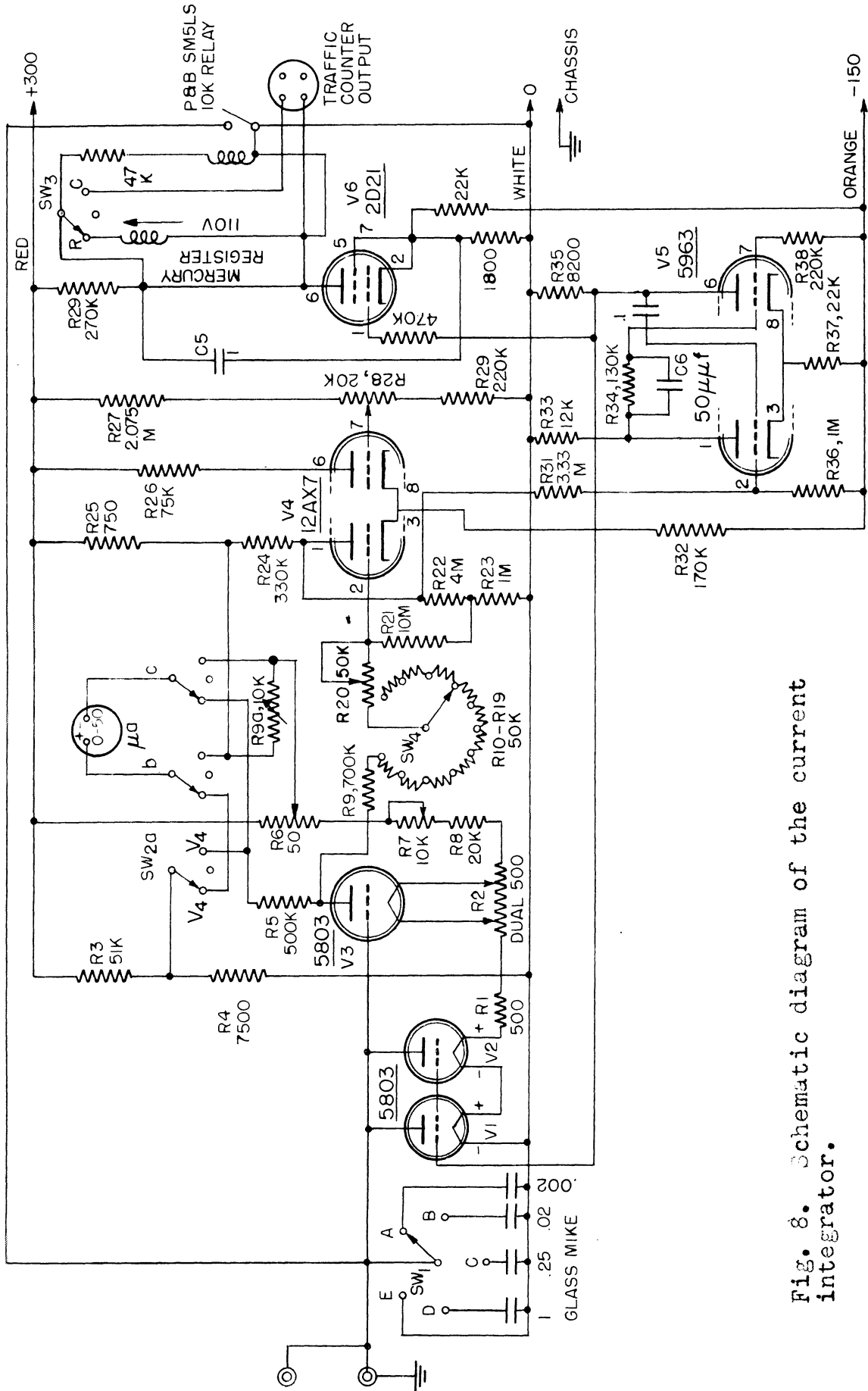


Fig. 8. Schematic diagram of the current integrator.

# POWER SUPPLY FOR CURRENT INTEGRATOR - SCHEMATIC

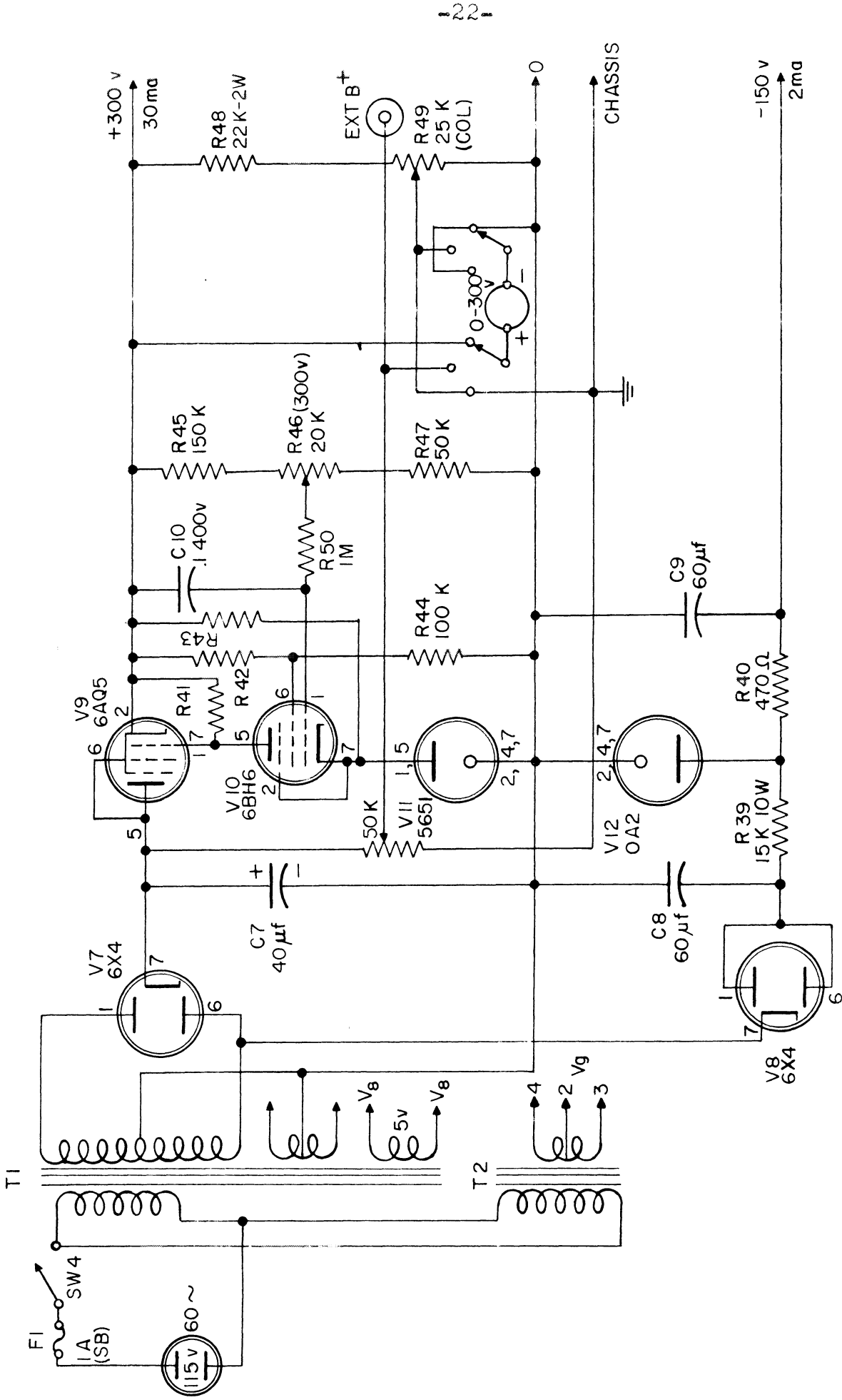


Fig. 9. Schematic diagram of the power supply for the current integrator.

1 millisecond. The condenser is thus completely discharged. The counts may be recorded either on the Mercury register, or on a traffic counter (Streeter-amet Company, Chicago, Illinois, Model SCl-5) which stamps out the number of counts at equal time intervals.

The 5803 electrometer tubes were sealed in a light tight box along with a small bag of silica gel. The integrating condensers are similarly sealed and desiccated. All the exposed input wires were cleaned and sprayed with Krylon and the cable connectors kept scrupulously clean and dry. These precautions were found to be absolutely essential in order to reduce the drift rate (counting rate with zero input current) to a tolerable level. Now the drift rate corresponds to  $\sim +0.001 \mu\text{a}$  on range B and  $\sim -0.001 \mu\text{a}$  on range D. The Faraday cup is connected to the integrator by about 67 feet of RG-8/U cable using teflon insulated connectors, UG-59B/U. The second input connector is for the calibration equipment.

In order to maintain the B+ constant and at 300 volts it was necessary to use a Sola constant voltage transformer and a Variac between it and the integrator. Even with these precautions B+ drops several volts whenever the register is activated. It was noted later in the work that if the traffic counter and the integrator are both plugged into the same line circuit, every time the traffic counter prints a number, a certain amount of extraneous charge appears on the integrating condenser.



### Operation

It was found that it is necessary for the integrator to be warmed up at least two hours before reproducible results can be obtained. The B+ is then adjusted to 300 volts by means of R46 of figure 9. Referring to figure 8 the range switch SW<sub>1</sub> is set to E (shorting out the grid of V3), and the meter switch SW<sub>2</sub> set to V3. The bias on V3 is adjusted by means of R2 so that the meter reads 8  $\mu$ a. Next SW<sub>1</sub> is switched to D, and a small current is fed into the instrument. If the meter does not indicate 22  $\mu$ a when the register trips, R28, R20, and/or R10-19 are adjusted until it does. Finally SW<sub>2</sub> is changed to V4, and the meter is made to read from zero to full scale to indicate fractions of a count. This is done by varying R6 and R9a.

The performance of this instrument is best discussed in terms of its accuracy and stability, and this will be reserved for the Experimental Procedures section on the calibration of the beam integrator. The calibration curves presented there are not linear except at very low counting rates, and this together with the difficulties discussed above led to the conclusion that an entirely new integrator should be constructed. The design of Higinbotham and Rankowitz (28) was chosen, and the parts ordered, but there wasn't time to complete the new unit for use in this work.

#### D. Metal Evaporator

A high vacuum metal evaporator was constructed for use in this work. It operates at pressures from  $10^{-3}$  to  $10^{-6}$  mm

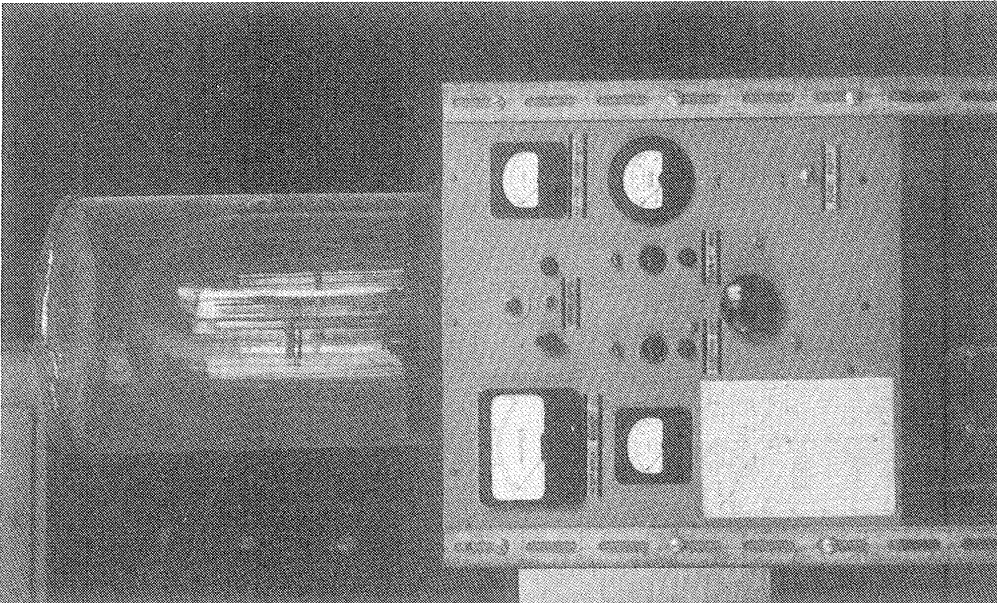


Fig.10 Metal Evaporator.

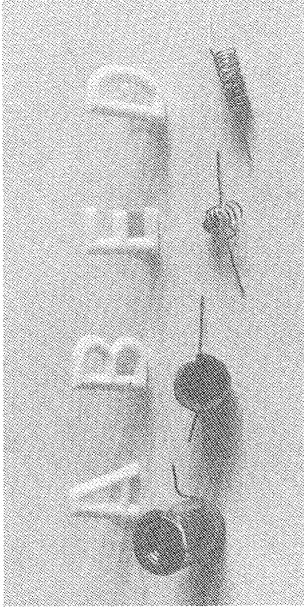


Fig.11 Types of Heaters for Metal Evaporator.

- A: Vycor crucible
- B: Alundum crucible
- C: Tungsten wire basket
- D: Tungsten wire helix.

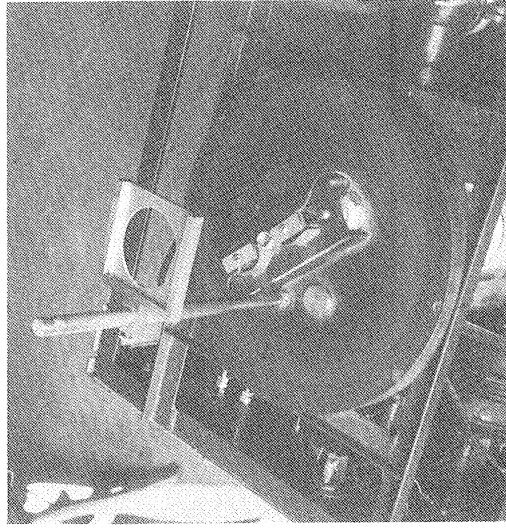


Fig.12 Electrode, Heater, and Target Assembly for Metal Evaporator.

of mercury and is powered by a transformer system capable of delivering about 250 watts to the heating element. The completed unit is pictured in figures 10, 11 and 12.

Thin even films of various target materials may be prepared with this apparatus starting with metal chips, shavings, powder, or metallic compounds such as oxides, etc. The films so produced are very uniform in their thickness, as indicated by the data presented in the Experimental Procedures section on target preparation. Another use made of the evaporator is to evaporate gold onto thin Zapon films for absolute beta counting with the  $4\pi$  counter.

#### Electrical Controls

The vacuum evaporator used in this work was patterned after one in use at the University of California Radiation Laboratory. Dr. E. H. Fleming of that laboratory kindly furnished us with the drawings and specifications. The control panel was built in 1951 by W. A. Cassatt and was only slightly modified for its present use. The schematic diagram of the panel as it now stands is shown in figure 13. The heater output is capable of delivering up to ~13 volts when the Powerstat is wired for 135 volts output.

#### Vacuum Gauge

A thermocouple vacuum gauge, RCA type 1946, was sealed directly to the base plate of the evaporator by means of Apiezon W wax. (All attempts to make a vacuum seal through an O-ring connection failed. Presumably this was because

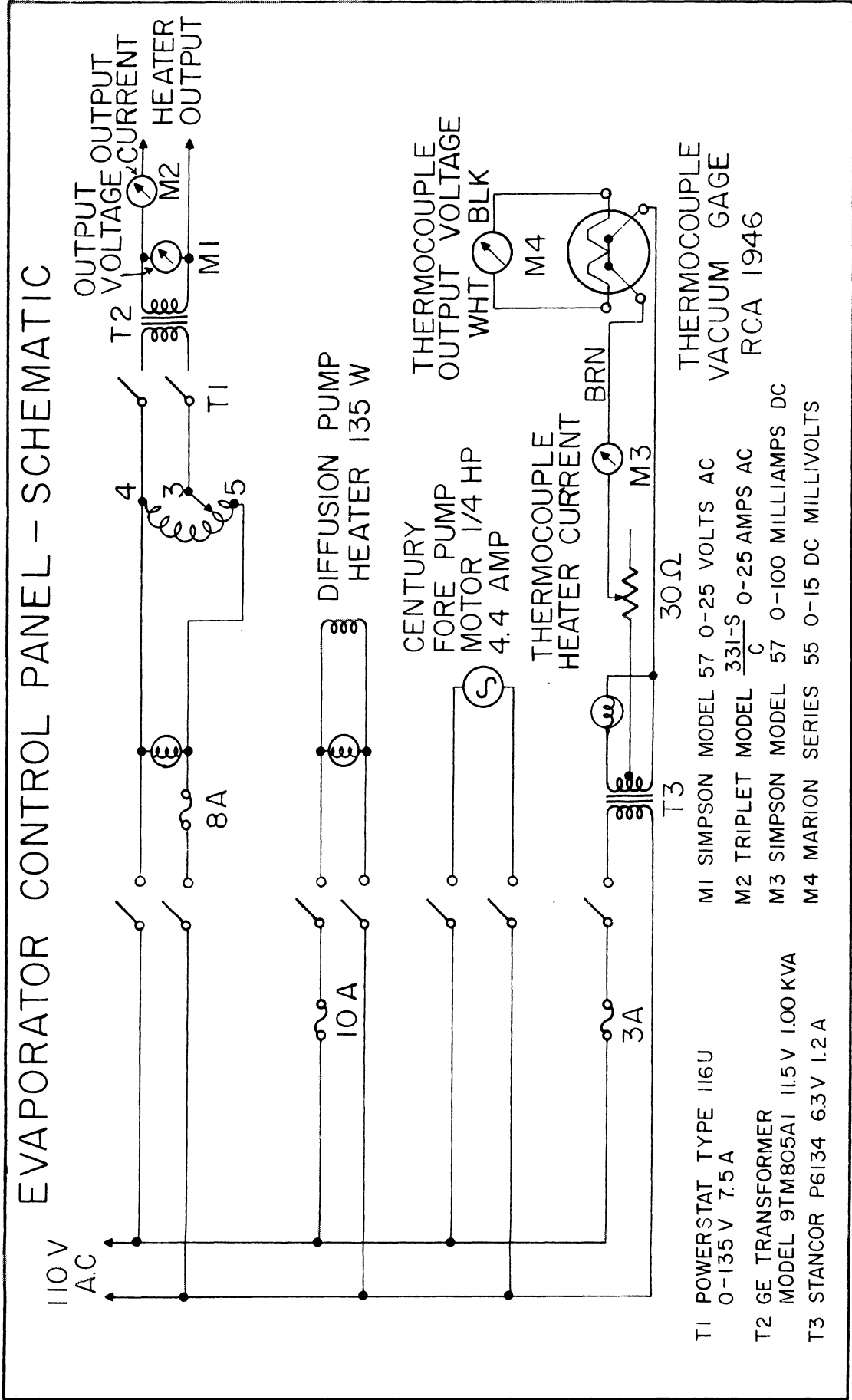


Fig. 13. Schematic wiring diagram of the metal evaporator control panel.

the base plate was machined from a casting so that the recessed surface originally provided in the base plate for the gauge could not be polished sufficiently.)

A McLeod gauge was used for the calibration. Both gauges were connected to the vacuum system through holes provided in the base plate. The pressure was varied by isolating the vacuum system at various stages of evacuation. The pressure was the same in the two gauges and remained constant over a period of time much longer than necessary to take readings, as proved by repeated readings. Calibration curves were taken for various values of the heater current in the 1946 tube. Subsequent calibrations showed that the curve shifts as the tube ages, but not enough to affect the day-to-day operation of the evaporator. The thermocouple gauge becomes quite insensitive at pressures below  $10^{-4}$ , but since most evaporations do not require a vacuum better than this value, the gauge serves the purpose.

#### Vacuum system

A schematic representation of the system is shown in figure 14. The vacuum system of the original unit was rebuilt to include a liquid nitrogen trap and a system of valves to bypass the diffusion pump. The original Cenco-Hyvac forepump was replaced with the faster Cenco-Hypervac 4, which reduced the pump-down time for rough vacuum from 30 to 5 minutes. The inclusion of the cold trap was found to be essential for the rapid attainment of pressures in the range of  $10^{-6}$  mm, especially on humid summer days. The

valves make it unnecessary to cool the diffusion pump between evaporations, as the pumping system can be closed off while air is being admitted to the main vacuum chamber and the diffusion pump alone can be isolated while "roughing out" the main chamber. These modifications permit greater efficiency and more rapid operation - it takes only 10 to 15 minutes to obtain the vacuum needed to proceed with an evaporation!

The pipe system consisted of ordinary 1 inch brass plumbing fittings joined together with silver solder. A short 1 inch brass nipple was soft-soldered to the intake of the diffusion pump. The threads of this nipple were tinned with soft solder, then coated with red Glyptal enamel No. 1201, (General Electric Company) and finally screwed into valve 3. A second coat of Glyptal assures a vacuum tight connection. The entire pipe system (including the diffusion pump and cold trap) is attached to the base plate of the main vacuum chamber by means of a brass flange and an O-ring seal.

The diffusion pump used, a VFM-10 (Consolidated Vacuum Corporation, Rochester, New York), was thoroughly cleaned out with C. P. ether and filled with Octoil. (Each time the bottom plug is removed the copper gasket must be replaced to assure a vacuum tight seal.) The fore pump was filled with light grade Cenco-Hyvac oil. As the pump is broken in through usage, their heavy grade

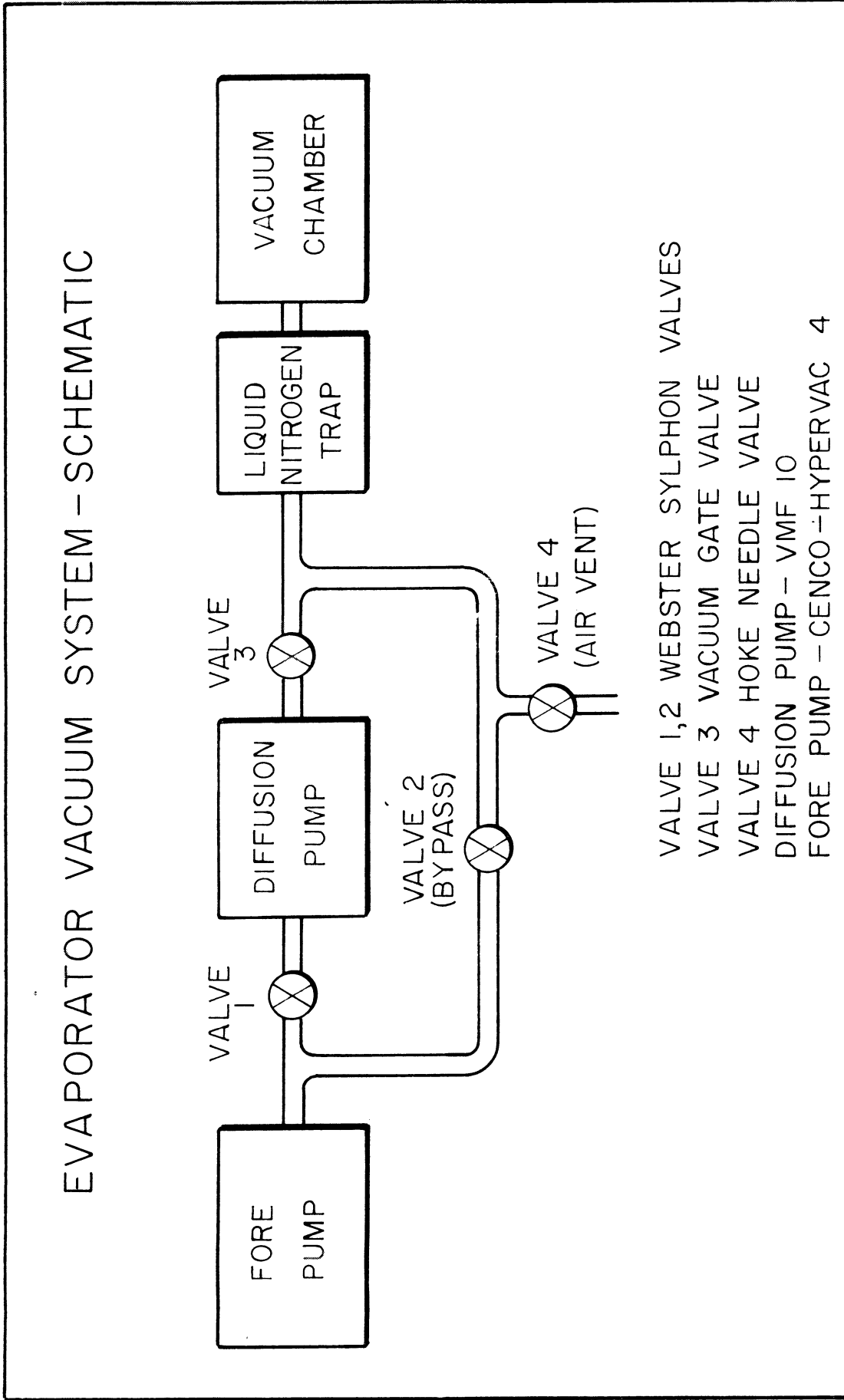


Fig. 14. Schematic representation of the metal evaporator vacuum system.

oil is necessary to prevent the vacuum from becoming soft as the oil heats up.

The valves used in constructing the bypass system are of three kinds. Valve 3, directly above the diffusion pump, is a commercial high vacuum valve. The air vent, valve 4, is simply a 1/4 inch Hoke needle valve properly oriented.

The other two valves and the one used on the bombardment chamber (see page 12) deserve special attention. Several ways of modifying ordinary commercial valves for use in vacuum systems have been suggested. (36 - 38) However, ordinary steam radiator valves containing sylphon bellows can be modified much easier for conversion to serviceable high vacuum valves. (39) First, the fiber gasket was replaced with one of soft rubber (e.g. neoprene). Next, the leakage path around the screw in the gasket holder was closed off by soft-soldering the two parts together. The valve seat and the top of the body (where the bonnet screws down) were polished with emery cloth. An O-ring was inserted between the top of the body and the sylphon flange. A piece of soft solder in the form of a ring was useful to act as a spacer in keeping the O-ring centered. For assembly the O-ring (coated with Apiezon T if desired) was placed in position on the body and the sylphon inserted with the gasket in place. Next the valve was pumped down so that atmospheric pressure held the pieces in place. The shaft was removed from the bonnet and screwed into the



syphon. Finally the bonnet was lowered into position with the solder spacer and screwed down tightly to effect a vacuum seal around the O-ring. Using this procedure there was no twisting of the O-ring which can cause leaks.

The cold trap consisted of a 2 inch brass tube with a 3/4 inch brass pipe extending concentrically almost to the bottom. A flange with an O-ring groove was provided so that the trap can be cleaned. The cold trap was thermally insulated from the rest of the metal system with the rubber O-ring and teflon washers on the flange bolts.

An inordinately large amount of time was spent in leak-hunting and in making vacuum-tight connections. Large leaks were found by filling the system with water under a pressure of several pounds, or by applying air pressure inside and soap solution outside. A spare vacuum gauge was found to be very handy when it came to hunting smaller leaks. The pressure was then checked in one section at a time, making use of the valves either assembled or with the bonnet and stem replaced by rubber stoppers. A hydrogen leak detector was also used with some success, but the helium leak detector is far superior in detecting minute leaks.

Both wax seals and screw threads coated with glyptal have been used to effect vacuum-tight connections, but the only fool-proof method is to employ O-rings in properly constructed grooves. Bolts were designed with O-ring grooves in the under side of their heads to seal off the

spare holes in the base plate. Great care was exercised in making the grooves. Their dimensions were made to conform closely to those recommended by the manufacturer (Crane Packing Company, Bulletin No. P-308) except that the groove width "D", was made equal to the O-ring cross-sectional diameter. All surfaces contacting the O-rings were honed or polished free from radial scratches and tool marks. It was found that the metal used must not be porous, i.e., castings can not generally be used.

The original bell jar provided was made of steel with a window in the top. The welded joints made it impossible to work with, as leaks developed when a modification was attempted. A Pyrex bell jar 10 1/4 inches in diameter and 14 inches high, (Consolidated Vacuum Corporation, Rochester, New York, No. 5728) was found to be very satisfactory. An L-shaped rubber gasket fits around the rim of the bell jar to make a vacuum tight seal with the base plate. No grease was necessary. An effective method of preventing the bell jar from becoming coated with an opaque deposit of evaporated material is to apply a thin layer of Dow Corning High Vacuum Grease on the inner surface.

#### Heaters and target assembly

Several types of heaters described in the literature (40 - 41) were tried. Figure 11 illustrates four different designs: a Vycor crucible with a tungsten heater coiled around it, a crucible made from alundum (impure alundum was

used because the pure variety crumbled and would not stick to the conical wire frame), a tungsten wire basket, and a tungsten wire helix. These designs met with varying degrees of success, but the most generally satisfactory heater for this work consists of a strip of 0.005 inch tungsten foil with the sides bent up to form a boat. A large amount of material may be placed in the boat with little danger of it falling out, and a white heat is easy to obtain. However, each material to be evaporated presents its own problems and the solution is an individual matter. The heaters were clamped between steel plates mounted on steatite stand-off insulators, as illustrated in figure 12. The current was conducted into the vacuum chamber by commercial electrode assemblies (Consolidated Vacuum Corporation, No. 7299). Figure 12 also shows the substrate upon which the metal vapor condenses supported above the heater from a specially designed ring stand. In the case of plastic substrates a 1/2 inch thick aluminum block is placed behind and in contact with it to help dissipate the heat. The choice of substrate is also an individual consideration, and will be treated along with the choice of heater in the Experimental Procedures section on target preparation.

#### Operation

The detailed instructions for use with this evaporator are given in Appendix I.

### E. $4\pi$ Proportional Counter

When this research was undertaken there were no  $4\pi$  counters available commercially. The choice of this type of counter for absolute disintegration rate determination will be explained later in the Experimental Procedures section on absolute beta counting. There are four different designs of  $4\pi$  chambers described in the literature. European workers employed a cylinder with the sample placed on a support dividing the cylinder into two halves along its axis. (42 - 46) Two wires stretched parallel to the cylinder axis above and below the sample support served as anodes. A "pillbox" arrangement has been used at the National Bureau of Standards and at Harwell. (46 - 47) A rectangular chamber was divided into two halves by a sample plate, with the anode wires stretched above and below the plate and parallel to it. Borkowski (48) is responsible for the third design which consists of two cylindrical halves clamping the sample plate between them. (47 - 48) The anode wires are stretched along a diameter of each half. Finally two hemispheres placed together with the sample plate in between constitute the fourth type. (47, 49-52) The center wires are two small loops suspended above and below the sample.

The two anodes were usually connected together in parallel and fed into a proportional or geiger counting unit. Some workers have made studies of the coincidences between the two halves. (42 - 44)

The counting gas flows continuously or a pump may be used to evacuate the chamber after which the gas is intro-

duced at the desired pressure. In the proportional counters both pure methane and a mixture of 90% argon and 10% methane have been used. (The latter, sometimes called P10 gas, is reported to give a plateau at a lower voltage than pure methane.) (48, 53) The pressure is usually atmospheric, although Borkowski (48) has conducted experiments in which the pressure was varied from 10 to 76 cm of mercury without noticeable ( $\pm 0.2\%$ ) change in counting rate on the plateau.

#### Description

A cylindrical (Borkowski type) and a spherical  $4\pi$  chamber were constructed for use in this work. They are pictured in figures 15 and 16. The cylindrical type was patterned after that used by Borkowski (48) who very kindly sent us the machine drawings. The two hemi-cylinders were  $2 \frac{3}{4}$  inches in diameter and  $1 \frac{5}{16}$  inches deep, machined from aluminum. These two halves are placed on top of one another, clamping a thin aluminum sample plate between them. A gas tight seal is provided by an O-ring between the hemi-cylinders. The sample to be counted is mounted on a plastic film covering the hole in the center of the plate. The plate then rests just inside the O-ring. The electrodes are stainless steel wires 0.002 inches in diameter (obtainable from Sigmund Cohn, New York). They are stretched horizontally across each half of the cylinder at a distance of  $\frac{11}{16}$  inches from the central plate. Since it is frequently necessary to change these wires the details



Fig. 15 4 pi Proportional Counters: left, spherical; right, cylindrical.

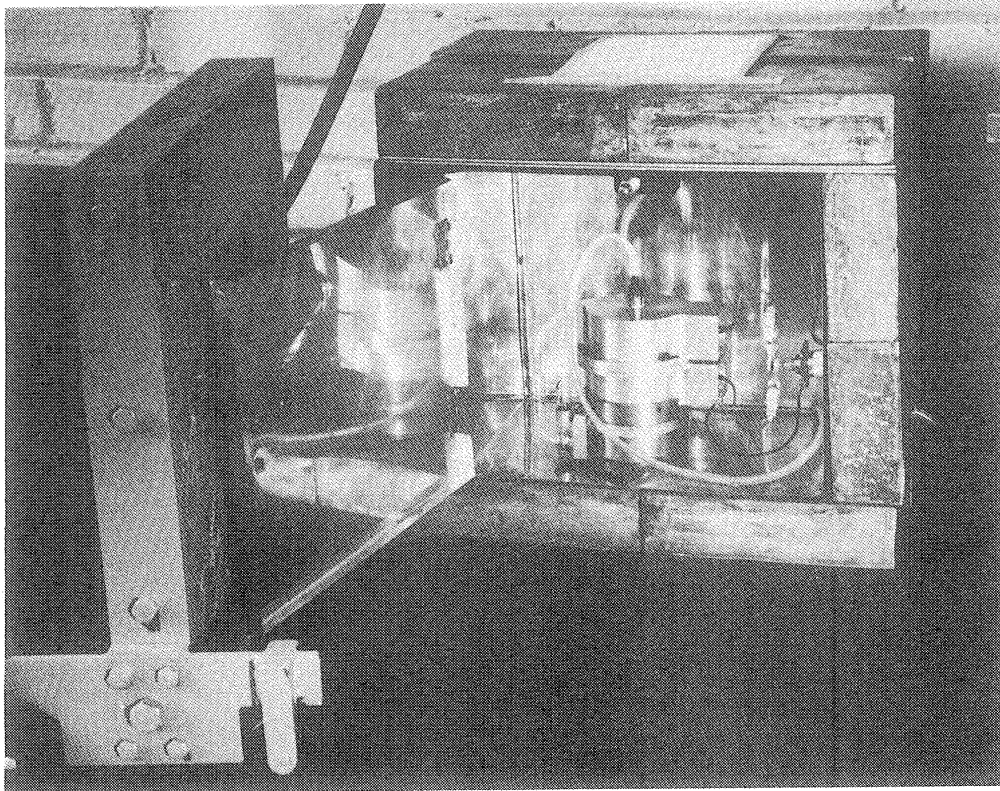


Fig. 16 Cylindrical 4 pi Proportional Counter inside housing.

of this operation are described in Appendix II.

The other chamber, patterned after the ones in use at the National Bureau of Standards (47, 49 - 50) consists of two stainless steel hemispheres  $2 \frac{7}{16}$  inches in diameter. The sample plate is clamped between them. A gas-tight seal is effected by two O-rings compressed against opposite sides of the sample plate. (Here the O-rings actually form a part of the inside spherical surface.) The anodes are made from 0.001 diameter wire, either stainless steel or platinum. They are formed into loops  $\frac{3}{16}$  inch in diameter and are suspended above and below the sample from teflon insulators  $\frac{3}{4}$  inch from the sample plate. Both loops and hemispheres are commercially available (Nuclear Measurements Corporation, Indianapolis, Indiana). The loops can also be made in the laboratory, and the following directions for making them are given in Appendix II.

The sample plates for these chambers are made from 0.010 inch aluminum sheet. Three  $\frac{1}{8}$  inch holes spaced 120 degrees apart and  $\frac{1}{4}$  inch from the edge permit the flow of methane from one half of the chamber to the other. Plastic films can be mounted directly over a  $\frac{1}{2}$  inch central hole upon which is deposited the active source. Another arrangement is to lay across this hole a smaller disk (1 inch diameter) which itself has a central hole punched in it and across which the sample-bearing film can be secured. The latter is illustrated with the cylindrical counter in figure 15. Usually the active

deposit is covered with another layer of film to prevent contamination of the chambers.

The counting gas used is 99 mol per cent methane (Phillips Petroleum Company, Bartlesville, Oklahoma) and the flow rate is adjusted by means of a bubbler filled with Dow Corning 702 fluid. The chamber is flushed for about 10 minutes at a rate of ~10 bubbles per second after introduction of each sample. This length of time was determined by observing the counting rate of Sr-Y<sup>90</sup> as a function of the length of flushing time. After 3 minutes the sample counted within the statistical error of the normal rate. Care must be exercised with the Zapon films as they will be ruptured by too great a flushing rate. The flow rate is reduced to ~3 bubbles per second for the duration of the count.

The counters were operated in the proportional region so that very high counting rates may be measured without the application of a large dead time correction. This is due to the fact that the dead times of proportional counters are intrinsically low in comparison with those of Geiger counters: of the order of 5  $\mu$ sec as compared with ~200  $\mu$ sec for Geiger counters.

A Nuclear-Chicago Model 162 scaling unit modified for proportional counting (54) was used in conjunction with the cylindrical chamber. The amplifier stage was modified by the addition of two 1N38 diodes and a 1 megohm, 1/2 watt resistor in the grid circuit of the



# MODIFICATION OF MODEL 162 FOR PROPORTIONAL COUNTING

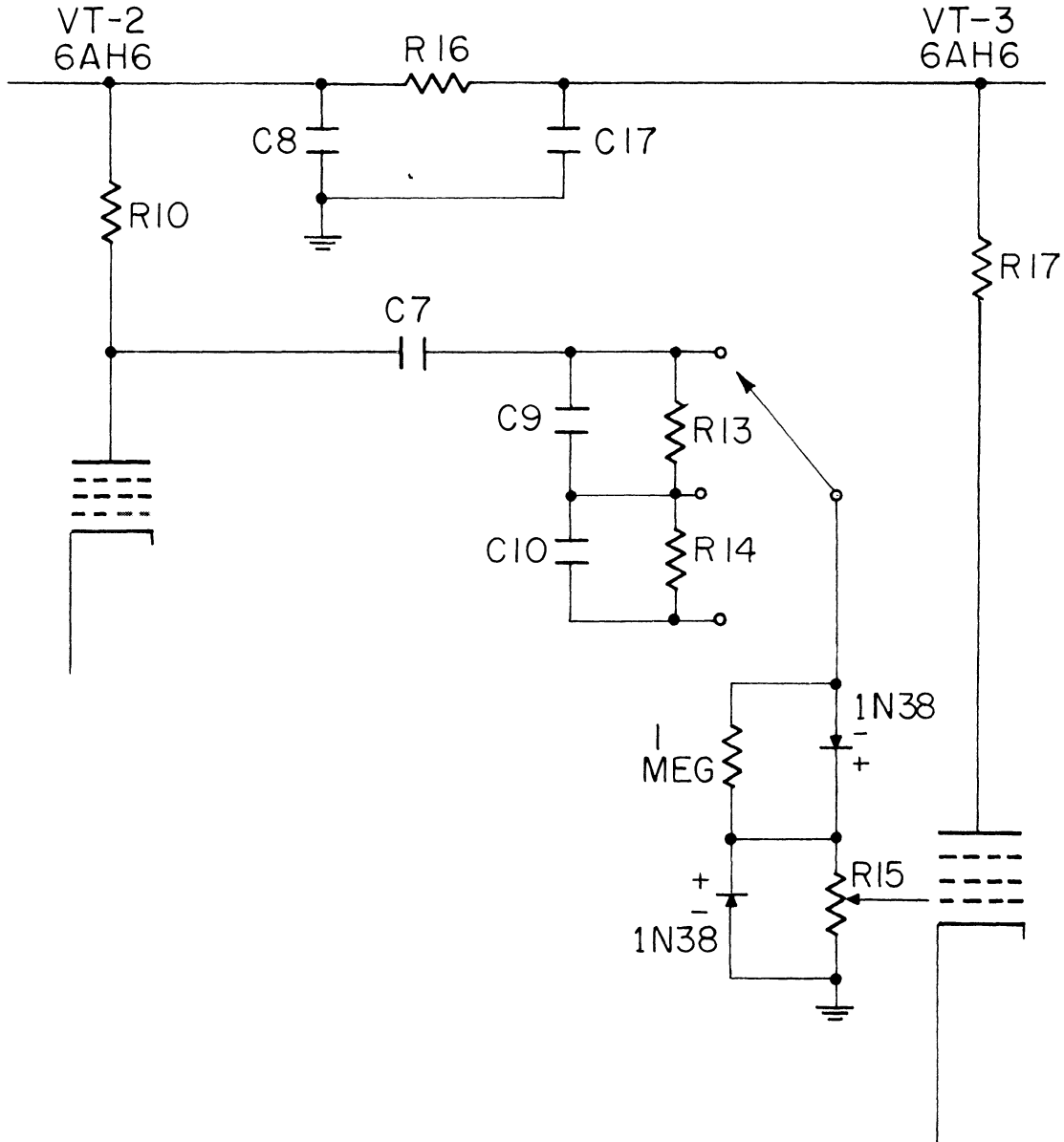


Fig. 17. Schematic diagram of a portion of the Nuclear Instrument Corporation Model 162 scaling unit circuit which has been modified for proportional counting.

third 6AH6 tube (VT-3, per the circuit diagram of the Model 162 scaler given in the accompanying instruction manual). The modified part of the circuit is shown in the figure 17 which is a portion of the Model 162 circuit diagram. This alteration is to prevent the amplifier from overloading and double pulsing with very large pulses and high counting rates. The high voltage was supplied by a Radiation Instrument Development Laboratory Model 80 dual high voltage supply. The amplifier and scaler for use with the spherical chamber was built by the Trott Electronics Company. The pulse amplifier is the same as designed by Rexroth. (55) The scaler is a modification of the one described by Kemp. (56) (The end window proportional counters used at Los Alamos utilize the same amplifier-scaler combination as reported by Rexroth and Kemp.)

The 4 $\pi$  chambers are placed in a copper box for electrical shielding, as shown in figure 16. At first heavy bare copper wires connected the chamber to the UG-496/U cable connector in the side of the copper box. Later flexible rubber covered wire (5,000 volt insulation) was found to stand up better. These wires were attached to the cable connector by clip leads so that the chamber may be easily disconnected for changing samples, cleaning, or for using the top and bottom halves independently. A short length of RG-11/U cable runs from the box to the proportional amplifier. This copper box arrangement is used at the National Bureau of Standards for the purpose

of lowering the input capacitance and thus reducing the resolving time and the attenuation of the pulses entering the amplifier. (57)

The copper box is surrounded by two inches of lead for shielding purposes. The background is then ~100 counts/min on the cylindrical counter and 40 counts/min on the spherical counter.

### Performance

A good deal of trouble was experienced in getting the counters to operate properly. This was especially true of the spherical chamber. The difficulty was that after a period of operation the voltage plateau would become almost nonexistent, except at very high methane flow rates. The cylindrical chamber seemed to consistently give better looking plateaus, and for this reason it was used almost exclusively in the cross section work. But even it gave spurious counts which would sometimes jam the scaler. The several precautions that were found necessary for proper performance are treated below.

First of all the methane must be flowing through the chambers at all times when the high voltage is on. Otherwise a continuous discharge may occur and a brown deposit may accumulate inside the chamber. (58 - 59) If this happens, the anode wires and/or chambers must be cleaned as described in Nuclear Measurements Corporation Instruction Manual for their Model PC-1 counter. Further details are given in Appendix II.

Special attention must be paid to any dust, lint, etc. which may lodge on the high voltage connections, for this will surely cause a discharge to occur.

The gas connections are another possible source of grievance. It was found that the chamber must really be gas-tight in order for proper counting to result. Thus the Tygon (type R3603) connecting tubing was wired tightly to the chamber connections. Apiezon W wax was used to insure that the chamber connections were sealed. The chamber was frequently tested for bad leaks by watching the 1/2 inch head of oil in the bubbler when the system is closed.

Lastly a phenomena occasionally takes place that so far defies an explanation. When certain samples are counted for more than several minutes the counter goes into continuous discharge, while other samples, the background, etc., all count normally. Furthermore the questionable sample appears to count all right when the bottom half of the chamber is used alone, but it jams the counter if the top half is used alone! Perhaps it has something to do with the way in which the sample is prepared, because little trouble has been experienced ever since the procedure has been adopted of cleaning the sample plates with acetone and drying the final sample under a heat lamp and hot air current.

## EXPERIMENTAL PROCEDURES

### A. Beam Determination

#### Suppression of Secondary Electrons

As pointed out in the section describing the bombardment chamber, page 9 , secondary electrons, or delta rays, produced when deuterons strike the target, collimator, etc., must not be allowed to enter the Faraday cup if produced outside of it. Otherwise the positive current collected would be smaller than that produced by the deuteron beam. Conversely, electrons produced within the cup must not be allowed to escape or too high a positive current would be indicated. Most workers have taken secondary electron emission into consideration using 200 - 300 volts to suppress them in lieu of a magnetic field, although Panofsky (10) used 8,000 volts. Since the geometric arrangement was different in each case reported in the literature it was deemed necessary to experimentally determine the proper potential to use.

To take into account the fluctuation in the deuteron beam, a scattering target of Mylar, a DuPont polyester film, usually 0.00025 inch (1/4 mil) thick, was in the scattering chamber at N of figure 1. The scattered particles which passed through both monitor counters O, were recorded as events by a coincidence analyzer whose output was fed into a scaler. Bach (60) has given a complete description of the monitors. The main beam passed through the Mylar target N,

traversed the target R, and was stopped in the Faraday cup T. The potential of the suppressor ring S was varied and the amount of charge collected in the cup was measured in terms of the ratio  $B_M$  of the number of counts recorded by the integrator per 64 monitor counts. The integrator was set on range B (see figure 8) for those experiments. The procedure was to measure  $B_M(0)$  when no potential is applied to the suppressor ring, i.e., with the ring shorted to ground. Secondly  $B_M(v)$  was measured when  $v$  volts were applied. Thirdly  $B_M(0)$  was again determined, etc., alternating between readings with no potential and with  $v$  volts.

#### 1. Preliminary Experiments

A great deal of difficulty was experienced in that  $B_M(0)$  tended to drift during the course of an experiment. This could have been the result of part of the beam striking the monitor target N then failing to hit the Faraday cup target R, or vice versa. Multiple scattering from the monitor was ruled out on the basis of a calculation following Rossi and Greisen.(61) A quick check with an oscilloscope showed that the discrimination settings on the proportional amplifiers of the monitors were not set on a steep part of the discrimination curve. (In the final run, experimental discrimination curves were taken to determine how to adjust the amplifier.)

The principle source of difficulty lay in the geometrical arrangement. The lead slits L of figure 1

in front of the monitor foil must be small compared to the area of the foil. Decreasing the vertical and horizontal slits J in front of the scattering chamber reduced the amount of extraneous scattered beam. That the main beam was actually going through target R was demonstrated by the observation of the beam pattern. It appeared as a yellow discoloration ~1 inch wide and ~1/2 inch high in the center of the many Mylar targets that were bombarded during the course of this work. (Since the slits L were most often 1/2 inch wide and 1/4 inch high, some idea may be gained of the divergence of the beam from these figures.) With the "background" (counting rate of the monitor with the Mylar target N removed from the beam path) thus reduced to less than 50 monitor counts per integrator count (range B) some improvement was observed in the constancy of  $B_M(0)$ . Finally the correct alignment of the monitor counters, i.e. "aiming" them exactly at the center of the monitor foil, provided the means of reducing the drift over a period of roughly 4 hours to ~8 per cent. This is illustrated by data from the final run in figure 18 which shows the fluctuations in  $B_M(0)$  as a function of the total number of counts recorded by the integrator. The latter increases with time, but is not proportional to it because of the variations of the cyclotron beam. The drift that is still present may be due to the deterioration of the Mylar target (it becomes brittle and turns yellow under bombardment),

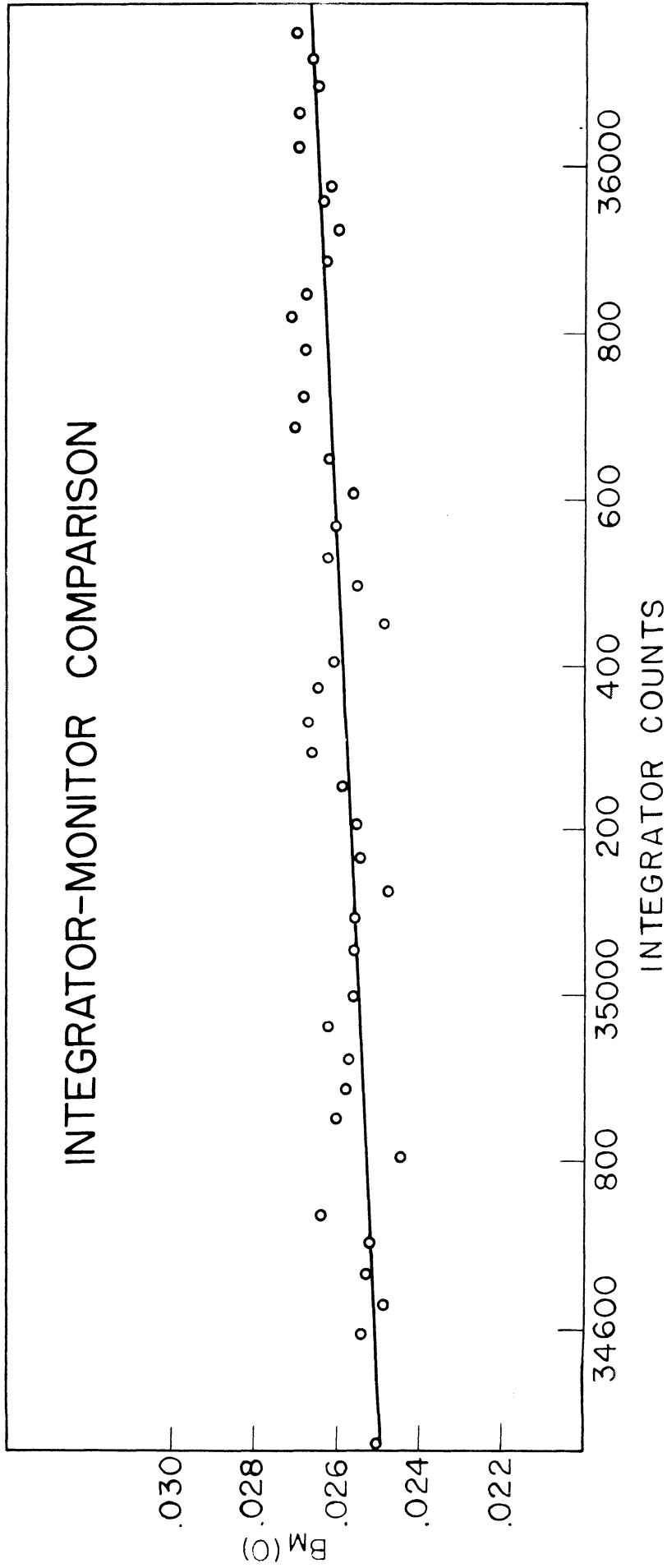


Fig. 18. Comparison of the current integrator and the monitor. The line indicates the amount of drift (~8 per cent) over a 4-hour period. The ordinate is defined on page 45.



or some electronic instability of either the monitor or integrator. Although range B of the integrator was not calibrated with the same care that was taken with ranges C and D (see next section), early experiments indicated that its linearity was as good as the other two higher ranges if the counting rate remains below ~10 counts/min.

The fluctuations of the individual values of  $\underline{B_M(0)}$  are higher than expected from an accumulation of the errors of counting statistics, timing, etc. However, by averaging  $\underline{B_M(0)}$  taken before and after  $\underline{B_M(V)}$  was taken, the ratio  $\underline{B_M(V)/B_M(0)}$  is fairly reproducible. This is the function which is of interest in determining the effect of suppressing potential.

## 2. Secondary Electrons Emitted from the Cup

In an early experiment with no target foil R in front of the Faraday cup, the potential of the ring was set at -295 volts, and the readings taken. Next, the ring was grounded and the cup itself was biased at -200 volts by means of the R49 control on the integrator (see figure 9). In these experiments there was no detectable change in the amount of charge collected by the cup. That is,  $\underline{B_M(0)}$  equaled  $\underline{B_M(V)}$  to within the  $\pm 2$  per cent deviations observed for these number.  $\underline{B_M(0)}$  itself drifted by about 4 per cent during the two hour course of this experiment. The result is evidence that the cup was well designed insofar as its geometry is concerned--less than 2 per cent

of the secondary electrons can escape that are produced when the beam is stopped in the cup.

### 3. Secondary Electron Emitted from the Target

The target R was a 0.9 mil aluminum foil placed in one of the eight positions of the probe head in front of the Faraday cup (see page 12 ). A marked effect was observed as shown in figure 19. This curve and the one of figure 18 were the results of the final run lasting ~14 hours. (The many earlier runs were much less conclusive because the techniques were still in the process of being worked out.) The ordinate is the ratio  $B_M(V)/B_M(0)$  referred to above, and the abscissa is the suppressor potential. The errors are the mean deviation of at least four determinations. The figure gives the results for two different target positions. When the aluminum foil was close to the Faraday cup in position 3, the positive charge collected for a given number of monitor counts was ~27 per cent higher when a suppressing potential of more than -200 volts than when no potential was applied. When the target was moved further away making the solid angle subtended by the cup smaller, the observed effect was also smaller. Thus in position 7 the discrepancy was ~16 per cent.

Several corrections might have been applied to obtain a more nearly correct value of  $B_M$ , but they were considered negligible. Thus the integrator drift rate (see section describing the beam integrator page 23 ) amounts to about

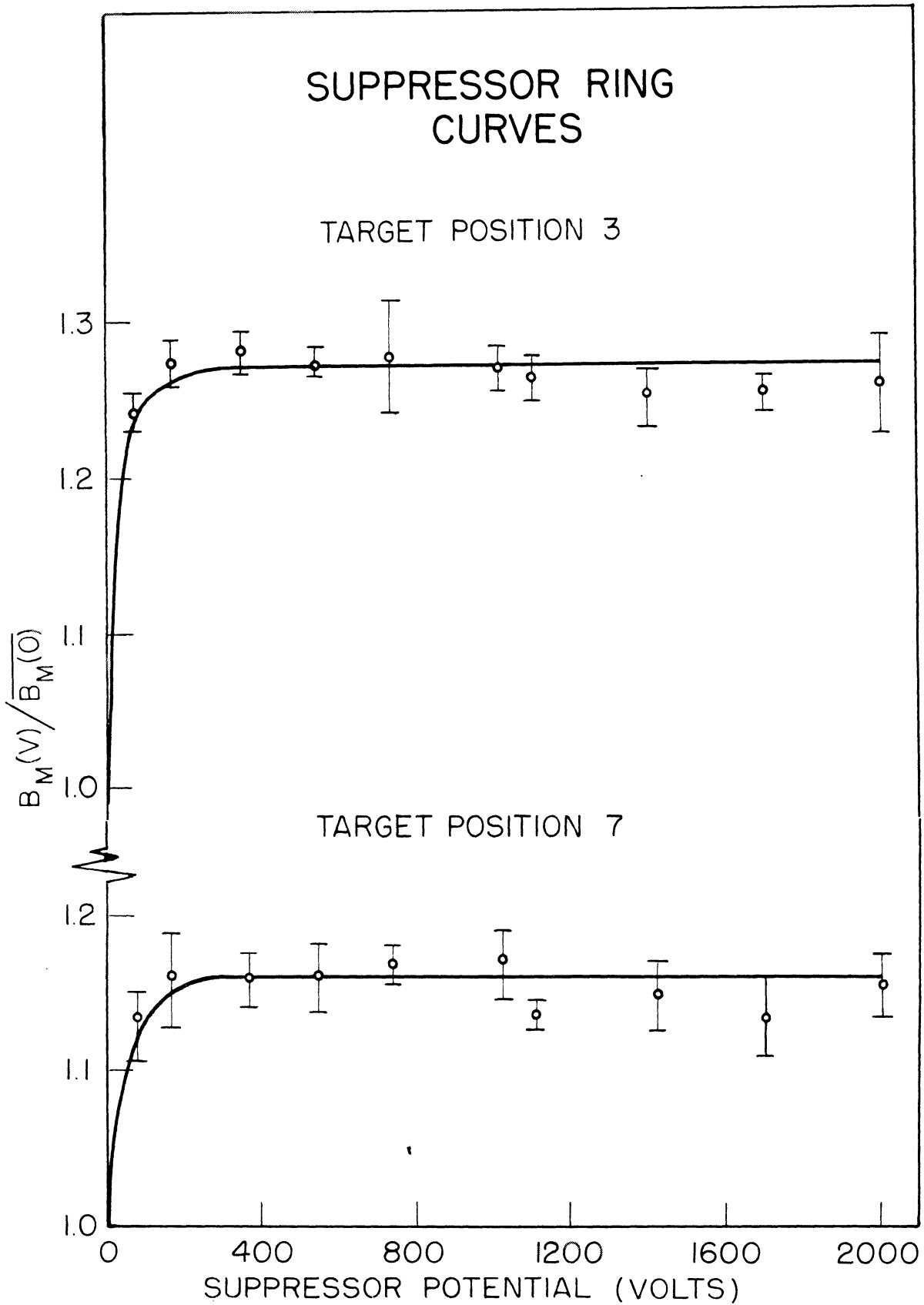


Fig. 19. The effect of applying a potential to suppress secondary electrons produced by the deuteron beam. The ordinate is defined on page 48.

+0.03 counts/min on range B. This nearly constant correction, when compared to typical counting rates of 5 counts/min with the cyclotron beam on, is of little importance. Then there is the monitor background, mentioned above, due to extraneous scattered radiation, but this is only about 0.3 per cent of the counting rate registered with the monitor target in place. Finally there is a very small background in the monitor due to electronic noise, cosmic rays, etc. This was found negligible at about 0.01 per cent of the counting rates observed during a run.

The curves in figure 19 indicate that in practice, as long as the potential on the suppressor ring is maintained below -200 volts, the effect of secondary electrons is negligible. Theoretically a slight positive slope might be expected out to 8500 volts, which is the maximum possible energy of a secondary electron ejected by a 7.8 Mev deuteron. Bethe and Ashkin (62) give the formula for calculating  $\underline{N}$ , the number of delta rays emitted per centimeter of path of the incident heavy particle. Applied to 7.8 Mev deuterons in 0.9 mil aluminum, the number of delta rays with energies between  $\underline{W}$  and  $d\underline{W}$  (kev) is

$$dN = 0.020 \frac{d\underline{W}}{(\underline{v}/c)^2 \underline{W}^2} \quad (1)$$

where  $\underline{v}$  is the velocity of the incident particle and  $\underline{c}$  is the velocity of light. Note that the  $\underline{N}$  will be inversely proportional to the energy of the delta rays. The energy  $\underline{W}$

is a function of the angle of ejection of the electron,  $\theta$ :

$$W = 2mv^2 \cos^2 \theta \quad (2)$$

where  $m$  is the mass of the incident particle. Taking the target in position 7 as an example, and considering the cone defined by the center of the target and the mouth of the Faraday cup, the maximum value of  $\theta$  is  $\sim 25^\circ$ . From equation (2) this corresponds to electrons of 7 kev energy. The total number emitted from 7 to 8.5 kev in 0.9 mil aluminum is found to be 1.38 electrons per deuteron, by integrating and solving equation (1). Considering the range of these electrons (33) only those produced in the last  $6 \times 10^{-5}$  cm will escape from the aluminum. This amounts to 0.038 electrons per deuteron, which represents delta rays from zero on up to 8.5 kev energy emerging from the target. Scattering in the aluminum will further reduce the number emitted at angles from 0 -  $25^\circ$ . It was therefore assumed that the plateau reached at  $\sim 200$  volts in figure 19 was real, and that energetic electrons passing the suppressor ring were too small in number to be observed.

#### Primary Calibration of the Beam Integrator

The integrator was calibrated by feeding in a known current and observing the counting rate. The current was supplied by a power supply in series with a high resistance. The connecting cable and Faraday cup were included in the calibration, as they are in parallel with the integrating

condensers. (The RG-8/U cable, rated at 29.5  $\mu\mu\text{f}$  per foot, contributes a capacitance of  $\sim 2 \times 10^{-9} \mu\text{f}$ .) These are small compared with 0.25 and 1.0  $\mu\text{f}$  of ranges C and D.

The description of the integrator has been given in the apparatus section, page 18, Referring to figure 8, the condensers A.....D discharge when their potential  $\underline{V}$  rises to  $\sim 5$  volts. The fluctuation in the condenser potential produces variations in the calibration current. If  $\underline{R}$  is the total series resistance across the condenser of capacitance  $\underline{C}$ ,

$$V = E(1 - e^{-\frac{t}{RC}}), \quad (3)$$

where  $\underline{E}$  is the value of the power supply voltage, and  $\underline{t}$  the time measured from end of the discharge. The value of the current  $\underline{i}$  is

$$i = \frac{E - V}{R}. \quad (4)$$

It may be seen from equation (4) that the larger  $\underline{E}$  is, the less effect the variations in  $\underline{V}$  will have on the average current. For this reason the power supply was operated at 500 volts or more. Even so, noticeable fluctuations were observed, and the integrator was switched to range E (input shorted to ground) for the current measurement.

The magnitude of the discrepancy between the range E (maximum) value and the average value of the current on, say, range D can be estimated as follows. Consider the instantaneous current in the R-C circuit: substituting

equation (3) into (4) yields

$$i = \frac{E}{R} e^{-\frac{t}{RC}}. \quad (5)$$

The initial current  $\underline{i_0}$  is simply  $i_0 = E/R$ , and the average value of the current is

$$\bar{I} = \frac{EC}{T} (1 - e^{-\frac{T}{RC}}) = \frac{i_0 RC}{T} (1 - e^{-\frac{T}{RC}}) \quad (6)$$

where  $T$  is the time between counts. Substituting typical experimental numbers in the equation (6) shows that the  $\bar{I}$  differs from  $\underline{i_0}$  by 0 - 0.5 per cent. This constitutes the justification for using the maximum value of the current in plotting the calibration curves.

The exact value of the current may be ascertained by two general methods: (a) the current may be observed directly with a sensitive current meter, or (b) the potential drop across a known standard resistor in series with the high resistor may be measured. Both of these methods were tried in the primary calibration of the integrator, but only the second one (employing a potentiometer) gave satisfactory results. However, the details of both will be given.

#### 1. Direct measurement of current

Watts (30) suggested the use of a micromicroammeter for calibration purposes. No such instrument was available in this laboratory but it was possible to borrow a sensitive portable galvanometer, (Leeds and Northrup type R No. 2500

rated sensitivity  $0.0005 \mu\text{a/mm}$ ). It was used in conjunction with a lamp and scale employing a 2 meter optical path. If the current sensitivity is known accurately, the galvanometer may be used as a microammeter. This expedient was used by Poole. (24)

The sensitivity was determined according to the potential divider method given by Smith (63) and indicated schematically in figure 20A. P was a decade box (Leeds and Northrup No. 4750), Q another decade box (General Radio type 602-J), R a wire-wound 1 per cent IRC resistor, and S a decade box (Leeds and Northrup No. 4775). A potentiometer (Rubicon type B No. 2780) was used rather than a voltmeter. Current flowed through the potentiometer coils for at least 24 hours before use. The 10,000 ohm coil of P was used as a standard of comparison for the 10,000 ohm coil of Q and R. Shielded cables (RG-62/U) were used everywhere except with the potentiometer. The contacts were carefully cleaned, and solder connections made with 50-50 (50 per cent lead, 50 per cent tin) solder. The galvanometer coil was warmed up with several wide deflections before a series of readings was taken.

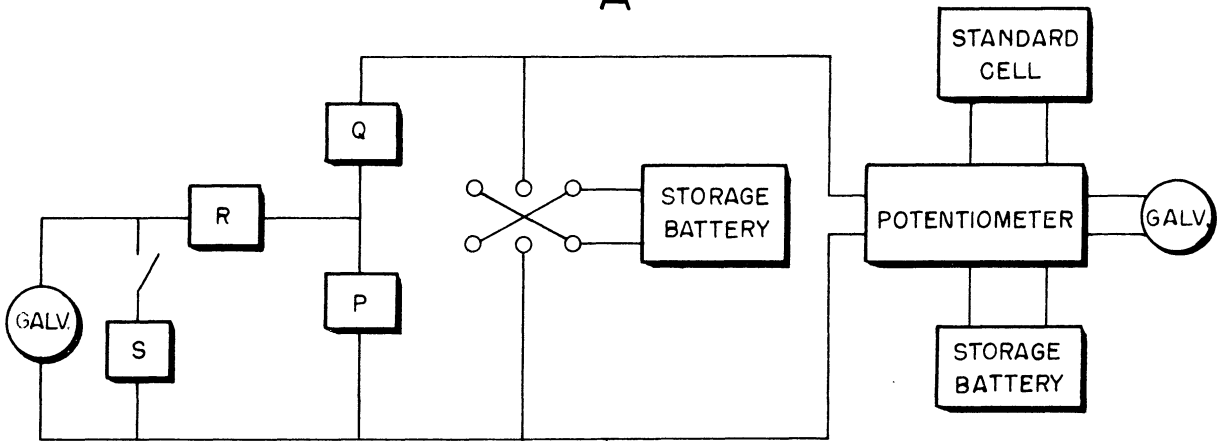
During use, the zero point shifted by about 1 per cent or less of the deflection after the passage of current. Therefore the average of the zero point readings immediately before and after a deflection was assumed to be the true point.

The results of four calibrations gave smooth curves from +250 to -250 mm deflection except in the neighborhood

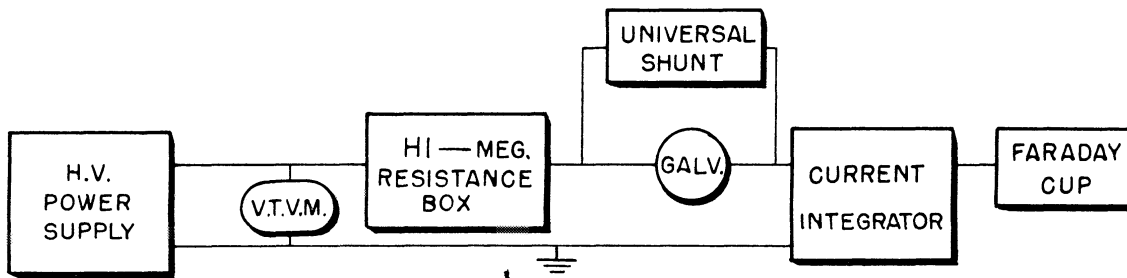


# CALIBRATION SCHEMATICS

A



B



C

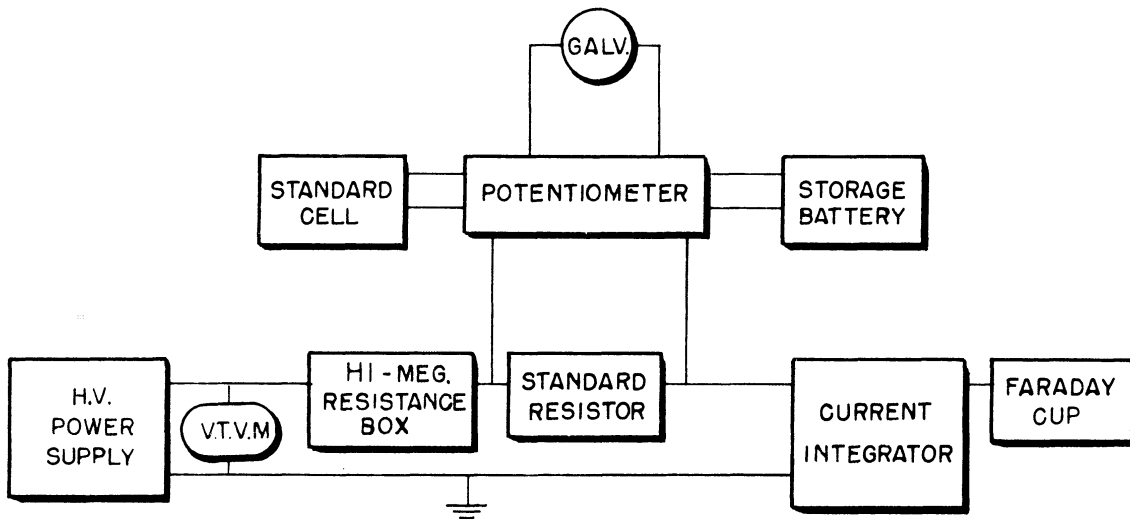


Fig. 20. Schematic representation of the apparatus to A, measure the current sensitivity of the galvanometer; B, calibrate the current integrator by direct measurement of the current with a galvanometer; and C, calibrate the current integrator by the potentiometer method.

of zero, where it becomes much more sensitive. This discontinuity in the smooth curve was considered abnormal, but a more serious drawback was the fact that successive calibrations over a period of several days gave curves showing decreasing sensitivity (all in the vicinity of  $0.00035 \mu\text{a}/\text{mm}$ ) which was still lower than the rated sensitivity. The differences amounted to several per cent. Even when the galvanometer was not moved between two runs, the second curve lay about  $1/3$  per cent above the first. After using the galvanometer to calibrate the integrator, the current sensitivity was redetermined by O. U. Anders, using slightly different techniques. His results, although somewhat more reproducible than the first calibration, were higher by  $\sim 5$  per cent.

The non-reproducibility of this method is not attributable to temperature or humidity differences. The explanation may lie in the fact that no particular care was taken to assure the galvanometer was perfectly level. Other workers have observed difficulties similar to those experienced here until the instrument was leveled. (64)

Two attempts were made to calibrate the integrator using the set up shown in figure 20B. The universal shunt was used to extend the range of the galvanometer. The vacuum tube voltmeter V.T.V.M. was used merely to read the H.V. power supply output. The calibration curves obtained by this method were not to be trusted because of the uncertainty in the galvanometer calibration.

## 2. Potentiometer method

In this method the accuracy is limited due to the decrease in sensitivity brought about by the high values of the standard resistance necessary to give measurable potential drops for very low currents. Potentiometers are not designed to measure potentials in circuits containing very high resistances. A practical limit was found to be ~10,000 ohms for the standard resistance. If much larger values are tried the galvanometer does not respond to slidewire changes of less than 1 per cent of the indicated potential. The particular potentiometer used also makes a difference, e.g. it was found that the Rubicon type B, and Leeds and Northrup type K are satisfactory, but that the Leeds and Northrup No. 8662 microvolt potentiometer is not, as it provided much less sensitivity.

There are several ways to surmount this difficulty: by the use of a more sensitive galvanometer, by increasing its optical path, or by connecting a condenser in parallel with the standard resistance, etc. However, it was felt that the integrator would serve adequately for the final cross section determinations if calibrated only for its two highest ranges C and D, corresponding to currents from 0.05 to 5  $\mu$ a. These values provide 0.05 to 5 volt potential drops across a 10,000 ohm standard resistor which can be measured with the Rubicon potentiometer and the Leeds and Northrup type R galvanometer to good precision.

The schematic block diagram of the calibration set up is shown in figure 20C. In the early runs, the Hi-Meg resistors (The Victoreen Instrument Company, Cleveland, Ohio) were out in the open, but for the final calibration they were enclosed in an air tight box with steatite selector switches and two UG-496/U cable connectors. Care was taken to clean the resistors, and a bag of silica gel was placed inside the box. Ceresin wax was used to seal the box. The standard resistor at first was an IRC 1 per cent wire-wound product, but later a 10,000 ohm Leeds and Northrup No. 4040 resistor, standardized by the National Bureau of Standards in 1954, was used. For the power supply, an Atomic Instrument Company model 312 High Voltage Power Supply was used. (Earlier, the integrator control R49, figure 9, was used for this purpose, but the highest potential available was generally too low.) The vacuum tube volt meter, a Voltohmist Senior (Radio Corporation of America), measured the power supply output. A Rubicon type B potentiometer was used in conjunction with an Eplab standard cell and a Leeds and Northrup type R No. 2500 galvanometer.

The results of the calibration are depicted in figure 21 for ranges C and D. Although data were obtained extending to ~40 counts/min, only the lower portion of the curves are shown since deviation from linearity is noticeable beyond 12 counts/min on range C and 6 counts/min on range D. Treating the points below these limits by the method of

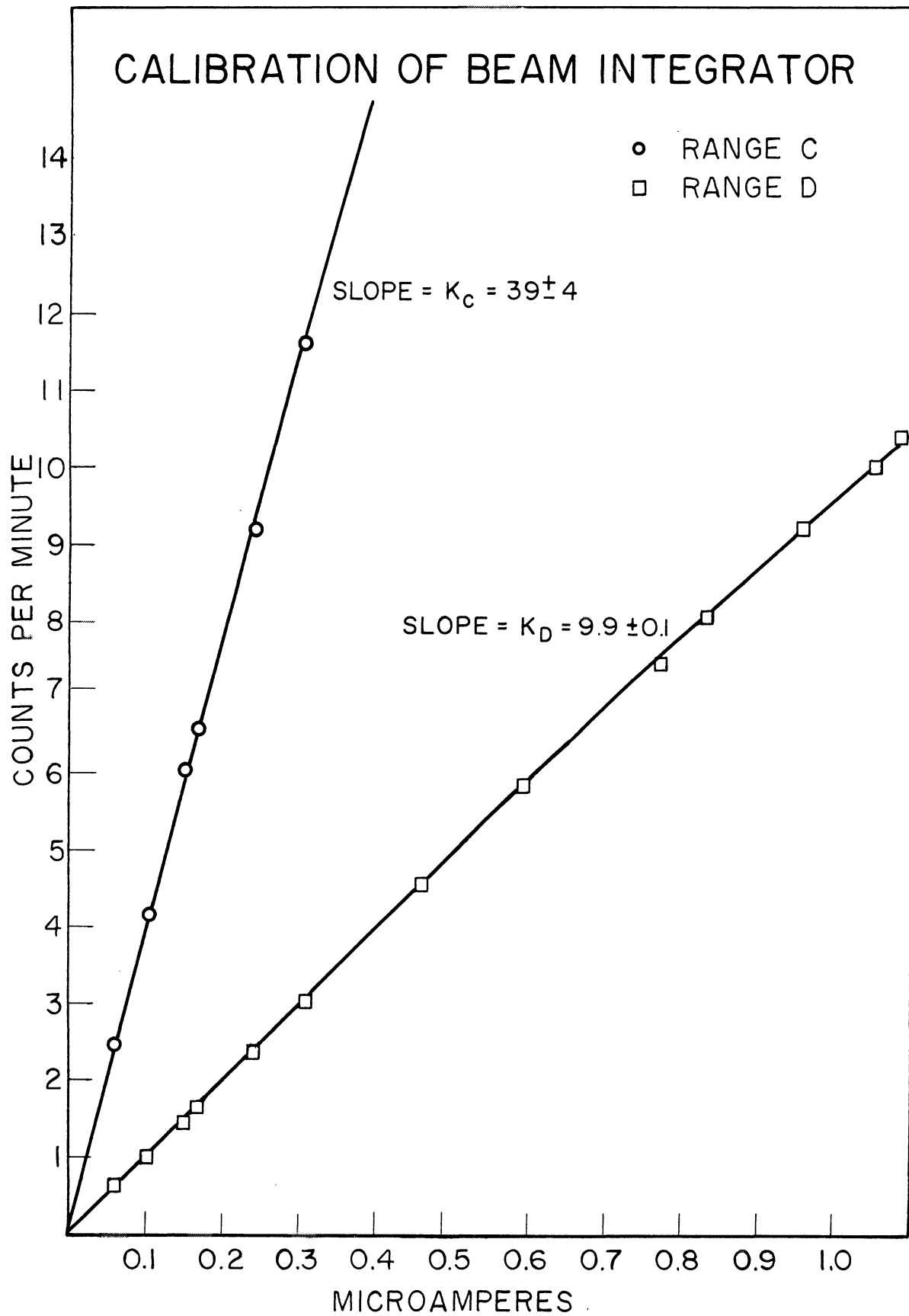


Fig. 21. Calibration curves of the beam current integrator.

least squares gives the following values for the slopes,  $K_C$  and  $K_D$  for ranges C and D respectively:  $37.6 \pm 3.6$  counts/min/ $\mu$ a and  $9.80 \pm 0.03$  counts/min/ $\mu$ a. The intercepts were not zero, as would be expected for an ideal integrator, but were  $0.30 \pm 0.15$  and  $0.045 \pm 0.010$  counts/min for ranges C and D. This could be the drift rate encountered when no input current is fed into the integrator, except that in this case the intercept should be negative for range D to agree with observation! If the intercept is assumed to be zero,  $K_C$  and  $K_D$  become 39.4 and 9.97 counts/min/ $\mu$ a respectively, but the deviations show a trend when plotted.

The curves obtained about six months previously using less care in the measurements exhibited approximately the same slope: 43.4 and 10 counts/min/ $\mu$ a for ranges C and D respectively.

The following values were taken as the calibration factors for use in obtaining absolute measurements of the beam:

$$K_C = 39 \pm 4 \text{ counts/min}/\mu\text{a}$$

$$K_D = 9.9 \pm 0.1 \text{ counts/min}/\mu\text{a}.$$

These numbers represent the average of the two least squares slopes, one with the both constants determined and the other assuming the intercept equal to zero. The errors assigned are the mean deviation except when the statistical standard deviation was larger, it was chosen. Note that

the errors thus assigned bracket the early values, so that during the succeeding two month period in which the cross section bombardments were obtained, the change in calibration factor should be less than these errors.

### Secondary Calibrations

Secondary calibrations were made every time bombardments were obtained to detect any day-to-day variation in the instrument. For this purpose a more rugged apparatus was used than in the primary calibrations. The vacuum tube voltmeter and Hi-meg resistance box were used as a microammeter, and the set-up is the same as in figure 20C, except that the standard resistor and potentiometer were removed. (The readings thus obtained indicated drifts not only in the integrator but also in the V.T.V.M.-Hi-meg resistance combination.)

During the two month course of the bombardment work the secondary calibrations were found to show no long term drift (except perhaps at the very end) and the readings for a given V.T.V.M.-Hi-meg resistance combination on range D always duplicated themselves with an average deviation of  $\pm 0.7 - 1.6$  per cent. These variations might be attributed to changes in the V.T.V.M., the Hi-meg resistors, temperature or humidity. It was noted, however, that the integrator must be warmed up at least two hours before use, in order to reproduce the readings within the above limits.

## B. Target Preparation

In order to measure cross sections at well-defined deuteron energies it is essential that the target material not degrade the incident energy significantly. The target itself must therefore be made quite thin in order to take advantage of the 6.5 keV/mm resolution of the focusing magnet. For example, aluminum only 0.00026 inches thick will degrade the energy of 7.8 MeV deuterons by 127 keV, which represents the resolution obtained from a 3/4 inch slit at L, figure 1.

A second consideration is that the targets must be made free from thickness gradients. A uniform thin film may then be bombarded with a deuteron beam inhomogeneous with respect to intensity variations over the beam area, and the cross section calculated without a knowledge of the beam intensity distribution.

Thirdly, the target must be free from impurities which might give rise to interfering activities which would follow the product element sought in the chemical separation. This is particularly important in the present study because the (d, $\alpha$ ) yields are typically a factor of  $10^3$  lower than those of the (d,n) and (d,p) reaction which are the major reactions induced by 7.8 MeV deuterons. For example, the (d,n) reaction on a 0.1 per cent impurity might produce comparable numbers of radioactive atoms compared to the (d, $\alpha$ ) product.



For this reason considerable time was spent in locating the highest purity target materials commercially available. In those cases in which the material was evaporated onto a substrate some additional purification may result from the process, but there is also the possibility that it may actually introduce impurities. The possibility of magnesium oxide formation in this manner is discussed below.

Several general methods of producing thin films have been reviewed by Hudswell. (65) The metal evaporator described earlier on page 24 was used for this purpose, but it was soon found that this approach has its drawbacks. Data on the techniques for evaporating various metals from different types of heaters are presented in the literature. (40-41)

The problem of finding a suitable substrate to which the evaporated material will adhere was the subject of many trials. Several different substrates were tried for each of the target elements. These were polystyrene, rubber hydrochloride, Mylar, Saran, cellophane and aluminum. Table I lists the four target elements encountered, some of their properties and the target preparation method.

Table I. Target materials

	Mg	S	Ti	Cd
mp(°C)	651	113	1800	321
bp(°C)	1110	445	>3000	767
mg/cm <sup>2</sup> /mil	4.4	5.3	11.4	22.0
purity	---	99.98%	99.99%	"spec-pure"
availability	Dow	Stauffer	Foote	Johnson, Matthey
preparation	evap.	poured	foil	evap.
substrate	Mylar	polystyrene	---	Al
evaporator heater	W boat	---	---	W boat

Target mounts were made to fit the slots of the probe head of the bombardment chamber and were machined from 1/16 inch aluminum stock. A hole 2 1/4 inches in diameter was cut in the mounts to match the 2 1/4 inch opening of the Faraday cup. The substrate was glued over the hole with rubber cement. In practically all cases the target material was restricted to this 2 1/4 inch area by means of a spare target mount placed over the substrate to serve as a collimator during the deposition of the target. To prevent shadows of the edge of the spare mount from being cast in the evaporation the circular edges of the collimator were beveled.

The details of the target preparation for each of the four elements studied will be given below.

### Magnesium

Magnesium metal purified by sublimation was kindly furnished by Mr. A. D. Brooks of the Dow Chemical Company. This material sublimes in vacuo, and the unscreened granules of the Dow magnesium have a tendency to pop out of the heater unless the heating is done extremely slowly. At first Vycor crucibles were used to contain the magnesium, but their deep shape made them very efficient little cannons which shot large particles of magnesium right through the thin substrate! Alundum crucibles were also tried before settling upon the shallow tungsten boat. With care, a full boat load could be sublimed with little loss from popping out.

When polystyrene was tried as a substrate, the magnesium would not stick and in addition the heat in the evaporation process is enough to melt the plastic. Magnesium adheres well to Teflon, but it can't be easily decomposed in the chemical procedure (see Chemical Separations section). Mylar (1 mil thick) appeared to be the best backing material. In order for even deposits to result, the surface of the Mylar had to be carefully cleaned with ether and acetone and then wiped dry to eliminate drying marks. Two or three evaporations were required to produce a film thick enough to bombard.

A curious effect that was sometimes noted was that the surface of the evaporated magnesium was grayish and metallic looking, while at other times it had a whitish cast. There

is some indication that this was due to inadvertently allowing the pressure to rise while the evaporation was in progress. Thus air or water vapor may have reacted with the magnesium resulting in the formation of the oxide.

A check was made on the uniformity of evaporation by cutting one of the 2 1/4 inch diameter films into eight rectangular pieces and determining their thicknesses in milligrams per square centimeter (metal plus substrate). The pieces were weighed on an Ainsworth type FDJ micro-balance and their areas measured with the aid of a pocket magnifier with a scale attached (Edmund Scientific Corporation, Barrington, New Jersey). The standard deviation of the surface densities was 0.4 per cent which is of the same magnitude as the experimental errors of the individual measurements. Thus it is seen that individual films can be made extremely uniform in thickness, although these results are not directly applicable to specific targets bombarded since the films had to be cut up in order to make the measurement.

#### Sulfur

The sulfur used was 99.98 per cent flowers purified by redistillation (66) furnished as a sample lot by H. O. Thomas of the Stauffer Chemical Company.

Sulfur could be evaporated from Vycor or alundum crucibles onto Mylar substrates, but a much simpler

process was finally adopted. This amounted to pouring sulfur vapor onto the substrate.(67) Sulfur was melted in one arm of a Y-shaped tube, which was then tilted so that the liquid would run into the other arm while the vapor pours out the open mouth of the tube.

Difficulty was experienced with this element in that under bombardment the sulfur would tend to vaporize from the plastic backing. This could be partially overcome by sandwiching the target between two layers of polystyrene, according to the following procedure. Sulfur vapor was poured onto a cleaned 0.9 mil polystyrene film and the weight of the sulfur was determined. Next acetone was sprayed over the sulfur side and another piece of polystyrene placed on top of the target. The sandwich was pressed together to "glue" the sulfur firmly in place. When this assembly was subjected to the beam of the cyclotron, the vaporization noted earlier was lessened.

It was noted that the target films made in this way were not as uniform as those made by evaporation. The sulfur condensed in small individual grains. On standing, crystallization occurred, no matter which way they were prepared. An attempt was made to assess the evenness by scanning the target with a photomicro-densitometer, but the grain size proved to be too large for good results. There was, however, evidence for slight thickness gradients

over larger parts of the film. A second attempt to measure the uniformity was made by cutting up a film and weighing the pieces. Some of the sulfur stuck to the razor as the pieces were being cut, however, and the reproducibility of the surface density of individual pieces was not nearly so good as with magnesium films. In this case the standard deviation of 11 pieces was  $\pm 2.2$  per cent. A gradient amounting to differences of 15 per cent may have been in evidence in going across the film.

Some success was experienced with evaporating sodium sulfate onto Mylar. This approach should yield much better targets both from the point of view of uniformity, ease of dissolution of the target, and stability under bombardment. However, the techniques of evaporating salts were not fully worked out, and the targets used in the bombardments were made of elemental sulfur.

### Titanium

A sample lot of 99.99 per cent titanium sheet 0.0026 inches thick was supplied by W. M. Raynor of the Foote Mineral Company. A typical analysis is given in Table II.

This metal is so refractory (see Table I) that vacuum evaporation is difficult. Not only are evaporated films difficult to prepare, but too thin a target won't result in much yield of the (d, $\alpha$ ) product. This is due to the long half-lives of the scandium isotopes involved and the cyclotron beam available. Therefore it was decided to

use the titanium foils as received from Foote Mineral Company.

Table II. Spectrographic Analysis of Foote Titanium

Si	0.005%	Cr	0.0005	Ca	0.0005	C	<0.001
Al	0.0001	Sn	0.0001	Cu	0.001	O <sub>2</sub>	0.002
Mo	0.0002	Fe	0.003	Ti	---	N <sub>2</sub>	0.002
Pb	ND	Ni	0.001	W	ND	H <sub>2</sub>	---
Mn	0.001	Mo	ND	HF	---		

Note: ND Not detected

--- Not determined

The thickness and uniformity was established by measurement of a portion of the titanium foil (not the same portion that was bombarded) with a micrometer. It was found to be  $0.00256 \pm 0.00013$  inches thick, where the error is the average deviation of 32 readings.

#### Cadmium

The metal used was Johnson, Matthey and Company, Limited H. S. Cadmium Rod, greater than 99.99 per cent pure. The spectrographic analysis is given in Table III. Pieces were cut from the rod with wire cutters, then cleaned with dilute hydrochloric acid and distilled water. The evaporation was best carried out from a tungsten boat, although alundum crucibles also work well.

It proved to be no small task to find a substrate to which cadmium would adhere in the evaporation. The plastic films tried include Mylar, Saran, polystyrene, cellophane, rubber hydrochloride, Formvar and Zapan. Cadmium oxide was also tried instead of cadmium, but with no more success. Finally it was found that aluminum foil such as Reynold's Wrap works, provided that its surface is first roughened with Dutch Cleanser. Targets so produced were very even and mechanically strong.

An interesting observation was made during this evaporation. The cadmium metal had a beautiful, shiny, crystalline appearance up to the point of fusion. But just as it melted into a liquid globule, a brown scum appeared in the surface. This apparently did not evaporate with the metal but was left as a residue in the boat. Perhaps this is cadmium oxide formed from the residual gas present at pressures of  $10^{-3}$  -  $10^{-5}$  mm of mercury used in the evaporation.

No attempt was made to evaluate the uniformity of these films. The data on the magnesium foils and similar data obtained in the same way on manganese and indium foils made in this laboratory (68) were taken as sufficient evidence for the absence of significant thickness gradients.



Table III. Spectrographic Analysis of Johnson, Matthey  
Cadmium Rods

---

---

Ag <0.001%

Cu faintly visible

Ca very faintly visible

Fe barely visible

No lines of the following elements were observed: Al, As, Au, Ba, Be, Bi, Co, Cr, Ga, Ge, Hg, In, K, Li, Mg, Mn, Mo, Na, Ni, Pb, Rb, Sb, Sn, Si, Sr, Ti, Tl, V, W, Zn, Zr.

---

### C. Chemical Separations

The object of the chemical separations performed on an irradiated target is to isolate the atoms of one particular element produced by transmutation. It is not necessary to recover all of the atoms, so long as it is possible to determine the fraction recovered (chemical yield). It is important that the elemental fraction be radiochemically pure, that is, that radioactive impurities of other elements be reduced below the level of detection for the particular counting arrangement used. The disintegration rate of the product element may then be determined by the techniques of  $4\pi$  beta counting as described in the next section.

One much used method of determining the chemical yield is by gravimetric procedure. A known amount (often 10 - 20mg) of the (inactive) element in question is added to a solution of the irradiated target. This is assumed to behave chemically the same as the radioactive atoms produced, and hence is known as a carrier. Carriers are also added for the various elements suspected as radiochemical impurities. Ordinary distillations, filtrations, extractions, etc. are carried out to insure interchange of the carrier with the active species and to isolate the element of interest. The final precipitate is weighed and the chemical yield is calculated.

Disintegration rate measurements made with samples containing several milligrams of carrier are made more difficult by the necessity of making self absorption corrections to take into account the absorption of weak  $\beta$  rays in the sample itself (see next section on absolute beta counting). If the elemental fraction can be obtained in a solid-free or "weightless" state, however, self-absorption can be ignored. The chemical yield can be ascertained without the addition of a carrier by adding a known amount of a radioactive tracer of the element sought to the target solution. This tracer may be either carrier free or of very high specific activity. This method is commonly employed using  $\alpha$ -emitting tracers of the heavy elements. In this work the  $\beta$ -emitting tracer was long-lived, and after the short-lived species produced in the

bombardment had decayed out, the tracer was counted and related to the amount originally added.

There is one note of caution that should be sounded with respect to either of these methods of estimation of chemical yield. In both cases, complete interchange between the isotopes of the added tracer or carrier and those produced in the target must be established so that measurements on the added species are truly representative of the transmuted atoms. This is not necessarily so obvious a matter as obtaining a homogenous solution. For instance, the fission yield of iodine was in error by several per cent until a satisfactory oxidation-reduction cycle had been perfected which ensured complete interchange. (69) It is felt that this point has been overlooked by many workers in the field.

It was found that the purity of the water used to make up reagent solutions is a critical consideration in obtaining a final solution free from all solids. This consideration applies to all the carrier free separations performed in this research. Extra precaution must be exercised in column separations as the activity is collected over a large number of 8 ml fractions totaling in ion-exchange ~500 ml eluate. From 10 - 100 ml of solution must frequently be evaporated prior to the sample preparation with the result that very low concentrations of impurities may result in sizable residues. The best answer found to this problem is to use "conductivity water" ( $\sim 1 \times 10^{-6} \text{ ohm}^{-1} \text{ cm}^{-1}$ )

for making solutions, washing the columns, etc. Furthermore if there is a large amount of activity produced, only a fraction of the total volume need be evaporated to prepare a sample for counting. Thus in column separations only one 8 ml fraction under the peak of the elution curve may have enough activity to prepare a counting sample yet contain only a microgram of solid material.

In these procedures the substrate upon which the target element had been placed had to be dissolved and the (d, $\alpha$ ) product extracted. This is because nuclei recoiling from the collision with the deuteron may be ejected from the target. (Experiments demonstrating this effect will be described later.)

#### Sodium from Magnesium Targets

The separation of the alkali metals from each other and from the alkaline earths has been reported by several authors. (70 - 75) The work of Linnenbom (75) and Beukenkamp and Rieman (73) was found especially useful in developing the procedure used here. Several preliminary experiments indicated that by using Dowex 50, a cation resin, with dilute HCl as the eluant, the magnesium is held up by the resin so that the sodium is eluted first.

Attempting to purify colloidal Dowex 50 by settling, washing with hydrochloric acid and sodium hydroxide solutions, etc., proved ineffective in providing a resin from which no extraneous material would be extracted in the elution

process. However, "CP" grades of Dowex 50 which have been screened, purified by extraction with various reagents, and analyzed, are now commercially available (Bio•Rad Laboratories, Berkeley, California). Number AG 50-X8, 100 - 200 mesh, was the resin used in this work. After the column was loaded and rinsed with conductivity water, no further treatment was necessary.

The column was made from 22 mm i.d. 25 mm o.d. Pyrex tubing of cross sectional area  $3.8 \text{ cm}^2$ , and was ~13 inches high. A coarse sintered glass frit was fused in the bottom to support the resin column, and a buret tip and stopcock formed the outlet. The column was filled with resin to a height of about 10 inches. An automatic sample changer (University of California Radiation Laboratory, Health Chemistry design) was used to collect the eluate in ~8 ml fractions in 100x15 mm test tubes (Arthur H. Thomas Company, No. 9446).

The annotated procedure for magnesium targets is given in figure 22. The format is the same as used by Professor Meinke.(76) The initial sulfuric acid-hydrogen peroxide treatment results in the destruction of the Mylar backing. In this case, once a homogeneous solution is obtained, the sodium tracer may be assumed to be mixed thoroughly with that produced in the bombardment. By fuming off the large excess of sulfuric acid much less magnesium is needed for neutralization, and the capacity of the resin is not exceeded.

CHEMICAL SEPARATIONS

Element separated: <u>Sodium</u>	Procedure by: Hall
Target Material: Magnesium	Time for sep'n: ~8 hours
Type of bbd: 7.8 Mev deuterons	Equipment required:
Yield: ~50%	250 ml Phillips beaker
Degree of purification: $\sim 10^3$	ion exchange column
Advantages: carrier free	automatic sample changer
separation for $4\pi$ $\beta$ -counting	100x15 mm test tubes
	(Arthur H. Thomas Co., No. 9446)

Procedure:

- (1) Place 1 ml con  $H_2SO_4$  in 250 ml Phillips beaker and add tracer  $Na^{22}$  (see remark 2 ). Introduce the Mg target (~20 mg) and Mylar substrate. Heat strongly to decompose the Mylar.
- (2) Cool, add several drops of 30%  $H_2O_2$  and reheat. Repeat until a clear solution is obtained.
- (3) Fume off excess  $H_2SO_4$  and add 10 ml water. Neutralize (to pH~4) by adding an excess high purity Mg.
- (4) Absorb onto Dowex 50 column ( $H^+$  form) at a flow rate of 2.5 sec/drop. Rinse the column with 10 ml of water.
- (5) Elute with 0.5 N HCl at 2.5 sec/drop, collecting the eluates in clean 100x15 mm test tubes. Assay in scintillation well counter to determine the elution curve.
- (6) Test sodium fractions for  $Mg^+$  with quinalizarin spot test (see remark 3 ).
- (7) Evaporate the most active fractions to dryness. Take up with water and transfer to  $4\pi$  plates.

Remarks:

- (1) General references: J. Beukenkamp and W. Rieman III, Anal. Chem. 22, 582 (50), and V. J. Linnenbom, J. Chem. Phys. 20, 1657 (52).
- (2) The tracer is added for the purpose of determining the chemical yield.
- (3) Reference for quinalizarin test: Feigl, Qualitative Analysis by Spot Tests, 3rd ed. (New York, 1946), p. 172
- (4) Use conductivity water to make up solutions, etc.

Fig. 22. Procedure for the chemical separation of sodium from magnesium targets.

The elution curve is most easily obtained by counting the test tubes themselves in a scintillation well counter. (The one used in this laboratory was a Nuclear-Chicago model DS-3.) This eliminates the necessity for taking aliquots of the fractions and making separate counting samples. The  $\text{Na}^{22-24}$  starts to appear in the eluate after about 500 ml of eluant has passed through.

A bombardment to check the chemical procedure was obtained using the window box probe described on page 17. Higher intensity beams by a factor of ~100 are available here compared with the bombardment chamber and hence larger amounts of activity can be produced. The magnesium was irradiated in an aluminum envelope (without the plastic substrate.) The purified sodium fraction was counted on the spherical  $4\pi$  counter and the decay showed two components: the 2.6-year  $\text{Na}^{22}$  and the 15-hour  $\text{Na}^{24}$  as expected. No other half-lives were detected.

#### Phosphorus from Sulfur Targets

A unique application of ion exchange resins has been developed by McIssac and Voigt (77) for the carrier free separation of phosphorous from neutron irradiated sulfur. Dowex 50 was first converted to the  $\text{Fe}^{+++}$  form, and then ammonium hydroxide was passed through the column precipitating ferric hydroxide. Radioactive phosphorous is known to be carried by ferric hydroxide, so when an active solution

was passed through this column, the phosphorous was absorbed while the sulfur passed on through as sulfate. The column was then rinsed free from sulfate with water, and the phosphorous removed by eluting with dilute sodium hydroxide solution. The effluent was channeled directly into a Dowex 50 column in the  $H^+$  form. By this means the sodium was removed by the resin, and a carrier free solution of radiophosphorous was obtained in aqueous solution. Bio•Rad resin AG 50-X7.5, mesh sized 20-50, was used. The details of the preparation of the resin columns are given by McIsaac and Voigt. (77)

Figure 23 shows the procedure as finally adopted. The initial sulfuric acid-peroxide treatment destroyed the polystyrene target support. The bromine-carbon tetrachloride mixture dissolved the elemental sulfur and converted it to sulfate. (78) In the absolute cross section runs it is important that the mixture not be heated too strongly as phosphorus may be lost from sulfuric acid solutions at temperatures above  $150^{\circ} C$ . (79) The neutralization step yields a solution identical to the one with which McIssac and Voigt started.

The problem of complete interchange of the added  $P^{33}$  tracer and the  $P^{32}$  produced in the cyclotron deserves consideration. There are available a number of valence states and molecular species among which the  $P^{32}$  and  $P^{33}$  atoms might distribute themselves. A separate experiment to ascertain whether or not 100 per cent interchange



was accomplished did not seem to be worthwhile in the light of several other experimental difficulties with this element. (The targets were not uniform, the sulfur tended to vaporize under bombardment; the  $P^{33}$  tracer was impure, resolution of the decay curves was difficult, and the use of hot sulfuric acid may have resulted in losses of  $P^{32}$ .) The strong oxidizing conditions used in the dissolution step assures that the phosphorus is in the +5 state, and it was only assumed that interchange then occurs rapidly.

Sulfur was bombarded in an aluminum envelope on the window box probe in order to test the chemical procedure. The target was cooled two days before processing it chemically. No plastic film was present in this case. The decay curve showed the presence of only the single 14.3-day decay of  $P^{32}$ . An aluminum absorption curve did not give any evidence for the beta ray of  $P^{33}$  which could possibly come from an (n,p) reaction on  $S^{33}$ .

#### Scandium from Titanium Targets

Carrier free scandium separations from calcium and titanium targets have been reported by Cile et al. (82) and others. (80, 81) When a clear alkaline "solution" containing tracer amounts of scandium was filtered through filter paper the scandium was retained by the paper as a radio-colloid while the other activities passed on through. The scandium was removed with dilute hydrochloric acid.

CHEMICAL SEPARATIONS

Element separated: <u>Phosphorus</u>	Procedure by: Hall
Target Material: Sulfur	Time for sep'n: ~8 hours
Type of bbd: 7.8 Mev deuterons	Equipment required:
Yield: ~20%	250 ml Phillips beaker
Degree of purification: $\sim 10^3$	ion exchange columns
Advantages: carrier free	automatic sample changer
separation for $4\pi$ $\beta$ -counting	100x15 mm test tubes
	(Arthur H. Thomas Co., No. 9446)

Procedure:

- (1) Place 2-3 ml con  $H_2SO_4$  in 250 ml Phillips beaker and add tracer  $P^{33}$  (see remark 2). Introduce the S target (~70 mg) and the polystyrene substrate. Add several drops of 30%  $H_2O_2$  and heat gently to decompose the polystyrene (see remark 3).
- (2) Cool and add 25 ml of a 2:3 mixture of  $Br_2-CCl_4$ . Let stand 30 minutes to dissolve the sulfur. Add more  $H_2SO_4-H_2O_2$  and heat gently to complete the solution.
- (3) Neutralize to pH~6.4 with solid  $Na_2CO_3$  and dilute to 500 ml.
- (4) Absorb onto Dowex 50 column in  $Fe(OH)_3$  form at a flow rate of 1 sec/drop. Rinse with 50 ml water.
- (5) Elute with 125 ml 0.125 N NaOH at a flow rate of 1 sec/drop, channelling the effluent directly into a Dowex 50 column in  $H^+$  form. Collect the eluates in clean 100x15 mm test tubes. Assay in a scintillation well counter to determine the elution curve.
- (6) Test phosphorus fractions for  $SO_4^{=}$  with  $Ba^{++}$ .
- (7) Evaporate the most active fractions to dryness. Take up with water and transfer to  $4\pi$  plates.

Remarks:

- (1) General reference: L. D. McIsaac and A. Voigt, ISC-271, (June 1952).
- (2) The tracer is added for the purpose of determining the chemical yield.
- (3) If the  $H_2SO_4$  solution is heated to fumes, some  $PO_4^{=}$  may be lost.
- (4) Use conductivity water to make up solutions, etc.

Fig. 23. Procedure for the chemical separation of phosphorus from sulfur targets.

In this work three cycles were found adequate to give the desired decontamination.

It was discovered that Whatman No. 50 hardened filter paper is superior to either of the papers recommended in the references. A certain amount of organic matter was extracted along with the scandium when the other papers were treated with hydrochloric acid. This did not happen when the hardened paper was used.

The details of the adopted procedure are given in figure 24. One problem that Gile, et al. (82) did not mention was that of keeping the titanium in solution at pH 8.5. The hydrous oxide tended to precipitate as soon as the pH was raised to ~3. It was experimentally found that this can be overcome by adding sufficient hydrogen peroxide which is reported to form a peroxide with titanium. (83) Keeping the solution dilute also helps to prevent the precipitate from salting out.

In this case there is little cause for concern about complete interchange, as scandium exists in only the 0 or +3 state. Thus the initial oxidation assures that all the scandium is in the same form and thorough mixing of the tracer and (d, $\alpha$ ) product can be assumed.

The chemical procedure was evaluated by a window box probe bombardment of titanium. Three cycles of the procedure resulted in a sample which decayed with an initial ~3.5-day half-life tailing into an 85-day component. The  $\beta$ -ray spectrum, as observed on the  $\beta$ -ray survey

CHEMICAL SEPARATIONS

Element separated: Scandium Procedure by: Hall  
Target Material: Titanium Time for sep'n: ~5 hours  
Type of bddt: 7.8 Mev deuterons Equipment required:  
Yield: ~10% 250 ml Phillips beaker  
micro bell jar  
Degree of purification: ~10<sup>2</sup> No. 00 Hirsch funnels  
Whatman No. 50 filter  
Advantages: carrier free paper, pHyrion (short  
separations for 4π β-counting range) pH paper

Procedure:

- (1) Place 1 ml con. H<sub>2</sub>SO<sub>4</sub> in 250 ml Phillips beaker and add tracer Sc<sup>46</sup> (See remark 2). Introduce the Ti target (~130 mg) and the Mylar substrate. Heat strongly to decompose the Mylar.
- (2) Cool, add several drops of 30% H<sub>2</sub>O<sub>2</sub>, and reheat. Repeat until a clear solution is obtained above the unattacked Ti.
- (3) Add 10 ml 18 N H<sub>2</sub>SO<sub>4</sub> containing 5% 16 N HNO<sub>3</sub>. Heat, keeping the HNO<sub>3</sub> replenished until the Ti is all dissolved.
- (4) Dilute to 100 ml and neutralize to pH 8.5 (use pHyrion paper) with a 1:15 mixture of 30% H<sub>2</sub>O<sub>2</sub> and 8 N NH<sub>4</sub>OH. Add enough excess H<sub>2</sub>O<sub>2</sub> to keep the Ti in solution.
- (5) Filter twice through the same Whatman No. 50 filter paper, using suction. Wash three times with 3 N NH<sub>4</sub>Cl at pH 8.5.
- (6) Remove Sc with several portions of hot 3 N HCl.
- (7) Repeat steps 4, 5 and 6 twice, except in final cycle use conductivity water at pH 8.5 to wash the Sc "precipitate".
- (8) Evaporate to dryness. Destroy organic matter with aqua regia. Take up with water and transfer to 4π plates.

Remarks:

- (1) General reference: J. D. Gile, et al., J. Chem. Phys., 18, 1685 (50).
- (2) The tracer is added for the purpose of determining the chemical yield.
- (3) Use conductivity water to make up solutions, etc.

Fig. 24. Procedure for the chemical separation of scandium from titanium.

spectrometer (84) was consistent with the expected radiations. The  $\gamma$ -ray spectrum obtained with a scintillation spectrometer (85) also showed the expected peaks at 0.9 and 1.1 Mev for  $\text{Sc}^{46}$ .

#### Silver from Cadmium Targets

From a consideration of the data presented by Hicks et al. (86) it was thought that a rapid carrier-free separation would be possible for silver. They indicate that tracer quantities of silver can be separated from cadmium, indium, palladium, etc. by eluting tracer quantities of silver on Dowex 2 with 6 - 9 N hydrochloric acid, while the other ions remain on the column. However, it was not possible to separate  $\text{Pd}^{111}$  and  $\text{Ag}^{111}$  in this way when tried in the laboratory, which cast suspicion on the method. (Evidently their data was obtained using a bad batch of resin (87) which explains why their results could not be reproduced here.)

Next the procedure of Haymond et al. (88) for the carrier free isolation of silver from palladium targets was tried. They claimed to have co-precipitated tracer silver with mercurous chloride. To 500 ml of 0.5 N hydrochloric acid solution of the palladium target containing rhodium and ruthenium carriers they added 0.5 ml of saturated mercurous nitrate to precipitate the chloride. However, when this procedure was tried here using irradiated cadmium plus various holdback carriers

such as Cu, Zn, Ga, In, Pb, and Bi, very little silver activity coprecipitated with the mercurous chloride.

(The presence of active silver was demonstrated by precipitating silver chloride from the mercurous chloride supernate and following the decay of the silver chloride.)

It was hoped to separate the carrier mercury from the silver subsequently by an anion column procedure. However, repeated experiments failed to yield success in isolating the radioactive silver. At one stage it was noted that whenever palladium is present in the solution, the mercurous chloride precipitate turns black. Thus it may have been that the mercurous species reduced the palladium to the metal which in turn carried the silver in this procedure.

Rather than spending more time developing a carrier-free separation it was decided to resort to the addition of silver carrier. A good clean, fast procedure based upon the rapid exchange of radio-silver with inactive silver chloride suspended on a platinum gauze was developed in this laboratory by Sunderman and Meinke. (89) This, together with a more standard precipitation procedure developed for use with the  $\text{Ag}^{104}$  mass assignment problem (Part II of this thesis) was used in the cross section work. The discussion of the latter procedure is given in Part II.

Here again the question of exchange of carrier and trace amounts of silver is no problem. In fact the very rapid rate of heterogeneous exchange between the solid silver chloride and  $\text{Ag}^+$  in solution has been the subject of

study ! (89 - 90) It has been reported that silver ions tend to absorb on the walls of glass containers. (91 - 92) This effect is precluded by addition of silver carrier to the vessel before dissolving the target.

That the exchange separation does, in fact, give good decontamination from the other cadmium bombardment products was shown by a separate bombardment at the window box position. Cadmium foil of 99.99 per cent purity (Belmont Smelting and Refining Works, Incorporated, Brooklyn, New York) was backed with Reynolds Wrap aluminum foil and bombarded for about  $2\mu\text{a-hr}$ . The silver was separated and its decay followed. It showed the presence of just the same components that were found in all the previous work using the well tested silver chloride precipitation procedure (Part II of this thesis).

## D. Absolute Beta Counting

### Summary of Existing Methods

The problem of determining the rate at which a radioactive source decays in terms of actual disintegrations per unit time has been the subject of a great deal of study by many workers over the past decade. Manov (93) has presented a concise summary of the status of radionuclide standardization as of April 1, 1953. The various avenues of approach group themselves into three broad classifications. In the first method a measurement is made of the rate of energy released by the radioactive nuclei and the disintegration rate is calculated from this datum and a knowledge of the average energy per disintegration. Secondly, the coincidence counting rate of a sample may be related to the disintegration rate without knowing the efficiency of the detectors for the various radiations emitted. Finally, the particles ejected from the nucleus may be counted by a detector whose "counting efficiency" (defined as the number of counts recorded under particular conditions of geometry, scattering, absorption, etc. for each disintegration) is known.

1. Rate of Energy Release. Myers (94) has written a review article on the subject of calorimetric methods of measuring the heat emitted from a radioactive source. The rate of evolution of heat  $dQ/dt$ , the average energy per disintegration  $\bar{E}$ , and the disintegration rate  $dN/dt$  are related as follows:



$$\frac{dQ}{dt} = \bar{E} \frac{dN}{dt} . \quad (7)$$

The radiation must be completely absorbed in the calorimeter. Very intense sources are required to give off enough heat to be measured accurately. Since the limit of sensitivity of most calorimeters described is 0.001 cal/hr, this means about 20 mC ( $4 \times 10^9$  disintegrations/min) of a 1 Mev  $\beta$ -emitter is required for 1 per cent accuracy in determining  $dQ/dt$ . This follows from the equation given by Myers:

$$1 \text{ cal/hr} = \frac{0.19614}{\bar{E}} \text{ curie} \quad (8)$$

where  $\bar{E}$  is expressed in million electron volts. The sample must decay slow enough to permit the heat measurements to be made. Thus a practical limit for the half-life is ~1 day. As an example of the application of this method, the disintegration rates of  $P^{32}$  (95 - 97),  $H^3$  and  $Au^{198}$  (97) have been determined.

A method related to the calorimetric standardization has been described by Loevinger (98) and Gray (99) in which the ionization produced by  $\beta$  particles is measured in a cavity type chamber. The disintegration rate can then be expressed in terms of the ionization produced, the average energy of the  $\beta$  particles, and the average energy expended in the production of one ion pair.  $P^{32}$  has been standardized in this way. (99)

2. Coincidence Counting. This method has been described by Dunworth, (100) Barnothy and Forro (101) and others (102-103)

who give good treatments of the procedure and the errors involved. Two counters are arranged so that the first detects only one type radiation from the source (e.g. beta rays) and the second detects only radiation of a different kind (e.g. gamma rays) or of a different energy. If the decay scheme of the nuclide in question is known (there must be at least two different radiations involved in the decay) a relation may be derived between the disintegration rate, the coincidence counting rate, and the single counting rates. For instance if the nuclide decays by  $\beta$  emission followed by a  $\gamma$ -ray transition to the ground state, the disintegration rate is given by

$$\frac{dN}{dt} = \frac{N_{\beta}N_{\gamma}}{N_{\beta\gamma}} \quad (9)$$

where  $N_{\beta}$  and  $N_{\gamma}$  are the single counting rates and  $N_{\beta\gamma}$  is the coincidence rate. The source must be fairly intense:  $\sim 10^5$  disintegrations/min for a long-lived activity. This and certain other conditions and corrections serve to detract from the usefulness of this method. However, it is capable of high accuracy ( $\sim 1$  per cent) for those cases in which the requirements can be fulfilled, e.g.  $\text{Co}^{60}$ . (104)

### 3. Particle Counting with Known Counting Efficiency.

This method merits special attention because it has been used widely. L. R. Zumwalt (96, 105 - 106) has described the manner in which the disintegration rate is derived from the

observation of the counting rate in end-window Geiger-Mueller counters. The counting rate is expressed as

$$(c/m) = (d/m)Gf_Wf_Af_Bf_Hf_S \quad (10)$$

in which

- (c/m) = counts/min detected by the counter;
- (d/m) = the actual number of disintegrations/min in the sample;
- G = the solid angle geometry of the source and the counter;
- $f_W$  = the factor for the effect of the absorption of the beta particles by the window and the air between the source and the window;
- $f_A$  = the factor for the effect of air in scattering beta particles into the counter;
- $f_B$  = the factor for the increase in counting rate due to backscattering from the sample mounting ;
- $f_H$  = the factor for the scattering effect of the source support structure and housing;
- $f_S$  = the factor for the effect of the mass of the source in causing both scattering and absorption of beta particles (self-absorption and scattering).

Sometimes a sample is first standardized by another means, e.g. coincidence counting, and then counted in the

particular detection arrangement to be used. The counting efficiency is thus determined for a particular nuclide and detection arrangement. If this is not done each of the factors in equation (10) must be separately determined. In addition account must be taken of the decay scheme, i.e., contributions to the counting rate from X-rays, conversion electrons, etc. Thus an additional factor should be included in equation (10) expressing the probability that a count is registered once one of the radiations from the source enters the sensitive volume of the counting tube. Of course the observed counting rate must be corrected for background and dead time losses.

Many refinements have been made in this basic method. (107 - 121) This technique has been employed in the determination of cross sections (14,111,122 - 124), specific activities (125) etc. The accuracy of such determination is limited by the "absolute" counting error of 3 - 20 per cent.

Another extension of particle counting with defined efficiency is to place the sample within the detection chamber. With the active species in the gaseous form Libby (126), Eidinoff (127), Bernstein and Ballentine (128) have counted  $C^{14}$  and  $H^3$  by incorporating them into the counting gas. Professor H. R. Crane (129) has counted  $C^{14}$  as carbon black in an internal counter. The source may be deposited on an electrode, placed in a vacuum and the

charge carried away measured. ( 130-132 ) Nearly  $4\pi$  geometry is achieved in this case but intense sources are required. A screen wall counter is capable of 5 - 10 per cent accuracy when the activity is placed on the wall of the chamber. (135) With the sample on the bottom of an internal flow counter, the solid geometry factor alone is  $2\pi$ , but absorption and scattering problems are still present. (136-141 )

The method of " $4\pi$  counting" has recently received a great deal of attention. This is really a refinement of the particle counting techniques discussed in the last three paragraphs. An advantage is gained by the elimination of the problems of scattering and, to a large extent, those of absorption. The principle is that the sample is surrounded by the detector's sensitive volume such that one disintegration produces only one count regardless of the decay scheme, particle scattering or secondary radiation. The method is highly sensitive, so that low intensity samples may be counted,  $\sim 10$  disintegrations/min being the limit of detection (for counting volume of  $\sim 250 \text{ cm}^3$ ). Very recently scintillation techniques have been used to obtain  $4\pi$  geometry in which the source is either sandwiched between two crystals (134,142 ), or dissolved in a liquid scintillator. (143) Much more work has been done with solid samples placed inside a gas filled chamber. It is with such an arrangement that the present work has been done.

### 4 $\pi$ Proportional Counting

The technique of absolute  $\beta$ -ray counting using an internal  $4\pi$  proportional counter possesses several advantages over the other methods. As mentioned above the effect of  $\beta$ -ray scattering upon the counting rate is eliminated. If the source can be obtained in a solid-free state there will be no self-absorption correction. Absorption in the source mount may be determined, and usually amounts to a small (0 - 5 per cent) correction. Especially important in the study of low yield nuclear reactions, such as the (d, $\alpha$ ) reaction, is the detection sensitivity of  $\sim 10$  disintegrations/min which may be obtained. The probability that a count is registered once a  $\beta$ -ray enters the sensitive volume is essentially unity (to within  $\sim 1$  per cent) if the electric field in the chamber and the proportional amplifier are properly adjusted. Only if there is electron capture branching, (144) or if there are delayed states involved in the transition which have lifetimes comparable to the counter resolving time ( $\sim 5\mu$ sec) will there be any major discrepancy between the counting rate and disintegration rate.

In the past the usual procedure in applying  $4\pi$  counting techniques to bombardment work for the determination of absolute disintegration rates has been to employ them to calibrate an end window Geiger-Mueller tube. The counting of the bombardment samples is then done with the calibrated counter. In this way the same corrections for back-

scattering, geometry, etc. must be applied as in Zumwalt's technique. The innovation in the present work was the direct application of  $4\pi$  counting to bombardment work in which the decay of samples containing several components (of differing half-life,  $\beta$ -ray energy, etc.) was followed with the  $4\pi$  counter. Thus absolute decay curves were obtained, subject only to small corrections discussed below. It was felt that the  $4\pi$  method was exploited to better advantage in this way, by the elimination of scattering and geometry corrections. Since this research was undertaken the Berkeley group (145 - 146) has reported some absolute cross sections by following the decay of  $C^{11}$  and  $Na^{24}$  in the  $4\pi$  counter, but no chemical separations were performed on the target foils and only one component decays were encountered.

A description of the various  $4\pi$  internal counters which have appeared in the literature has already been given on pages 35 and 36, together with the references. In addition to those, the University of Michigan (147 - 148) and the Massachusetts Institute of Technology (149) groups have reported valuable information. The work of Pate and Yaffe (150 - 152) is particularly important in connection with the specific techniques of  $4\pi$   $\beta$ -ray counting.

The particular form used in this work has been discussed on pages 36 - 42 and was pictured in figure 15 and 16. The following sections deal with the details of the procedure that have been worked out. First the methods used to

fabricate thin plastic films for use as source mounts will be given. The measurement of the thickness of these films and the film absorption correction will then be treated. The self absorption problem and the effect of a conducting coating of the source mount will be considered. A discussion of the amplifier gain and discrimination levels at various anode potentials will follow. The experimental estimation of the dead time of the counter, and finally the application of these techniques to the counting of National Bureau of Standards samples will be presented.

1. Plastic Film Preparation. As described on page 36, the activity was placed on a thin plastic film covering a 1/2 inch hole in the center of the aluminum sample plate. The active solution was pipetted onto the film and dried with the aid of an infra red lamp and hot air current from a hair drier. The deposit was usually covered with another layer of film to prevent contamination of the counter.

Several commercially available plastics were tried, including 1/4 mil Teflon, 1/4 mil rubber hydrochloride, and 1/4 mil aluminum-coated Mylar. These proved unsatisfactory for absolute counting because too large a fraction of weak beta particles are absorbed in this thickness of film.

Fabrication of films as thin as  $20\mu\text{g}/\text{cm}^2$  (several hundred fold thinner than the commercial film) was carried



out in the laboratory. Several techniques have been worked out and reported in the literature. (149 - 153) Especially helpful was the report of Fry and Overman. (149) Their method of floating a solution of the plastic on water and picking up the film thus formed on a wire frame was adopted in this work. The apparatus, similar to that used by Professor M. L. Wiedenbeck and coworkers is illustrated in figure 25. Best results are obtained if cold fresh tap water is used for casting the films. The surface is first cleaned by drawing a brass bar across it. Next the wire frame is immersed beneath the surface and suspended from the shaft of a 3 rpm synchronous motor. Four drops of the plastic solution are pipetted onto the water and the solvent allowed to evaporate. The frame is then pulled up out of the water vertically by means of the motor, picking up the film as shown in figure 25. The double layer thus formed will henceforth be referred to as a single layer.

The film is transferred from the frame to a 4π counting plate by lowering the film onto the plate. The two are forced together with an air jet by blowing through a glass tube, as in figure 26. The film must be wet for good adhesion. Figure 27 shows how the film is cut around the edges of the sample plate. A wire dipped in solvent, makes an excellent "knife".

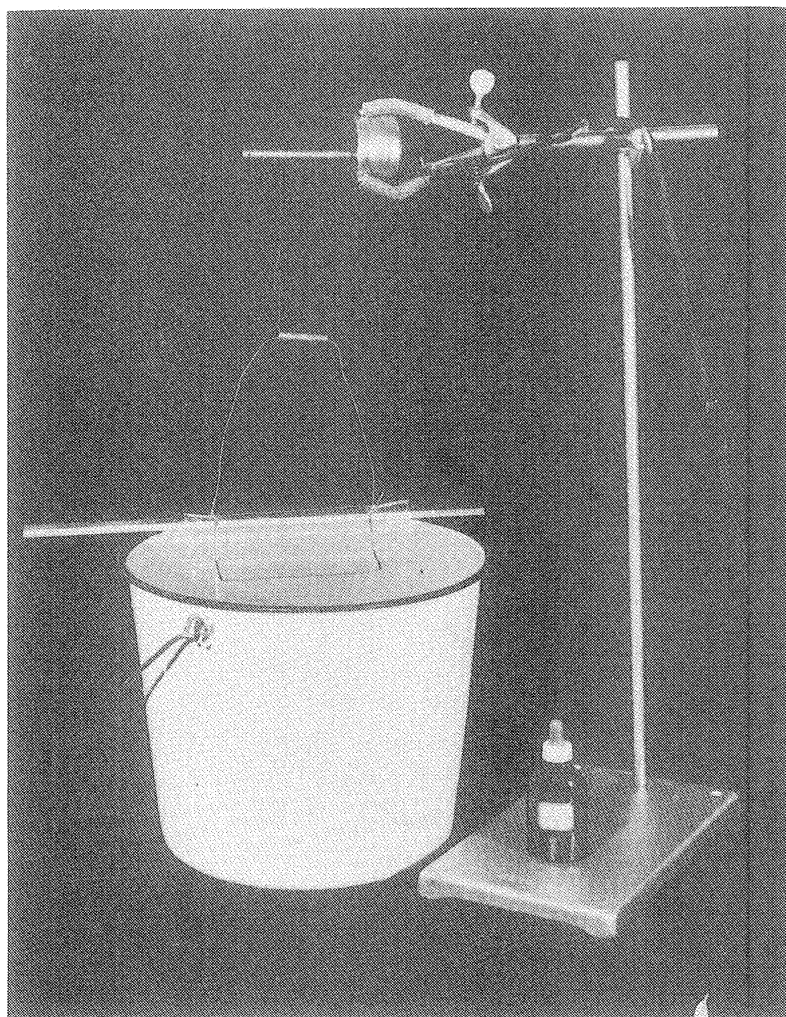


Fig. 25 Apparatus for Making Thin Plastic Films.

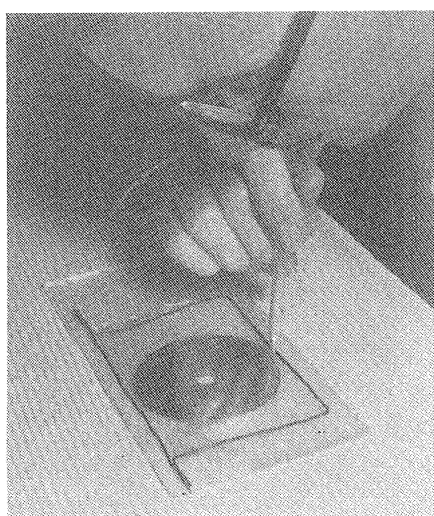


Fig. 26 Mounting the Film on a 4 pi Counting Plate.

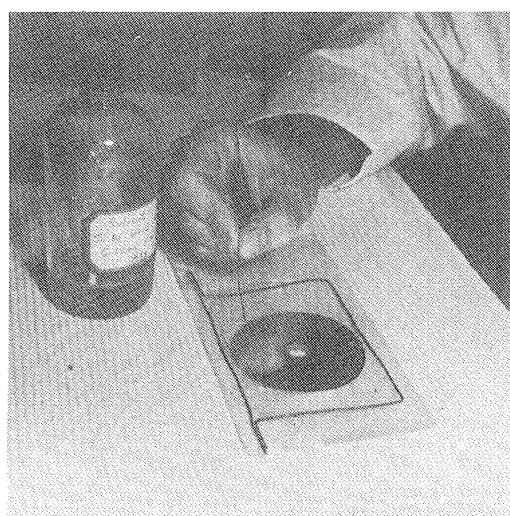


Fig. 27 Trimming the Mounted Film.

Several plastics may be used to make the films. These have been listed by Slätis (153) along with references on their fabrication into thin films. New techniques for use with VYNS resin (a polyvinylchloride-acetate copolymer obtainable from Canadian Resins and Chemicals Limited, Montreal, Quebec) have been developed by Pate and Yaffe. (147) Formvar E (a polyvinyl acetal obtainable from Shawinigan Products, New York) may be made into films by floating a 1 per cent solution in ethylene dichloride on water. Although these films are very strong mechanically, acidic solution attacks them. For this reason Zapon films (pyroxylin lacquer obtainable from Arthur S. LaPine and Company, Chicago, Illinois) were used for routine absolute counting. A solution of Zapon, Zapon thinner, and amyl acetate in a volume ratio of either 1:1:1 (33 per cent Zapon) or 2:1:1 (50 per cent Zapon) was used in this case.

The thickness of the film can be varied by using a solution of different concentration or changing the number of drops to form a film. A more practical expedient was to laminate several layers together to make thicker films. One layer was added at a time. Care must be exercised to prevent air pockets from forming between successive layers especially in the center.

2. Film Thickness Measurement. Pate and Yaffe (147) have summarized several ways of determining the film

thickness. Optical methods (33,154-156) both by interference of reflected light and by light absorption, were the subject of a few trials. Since the optical equipment was not readily available in this laboratory, this method was not exploited. The obvious procedure of weighing a given area of a uniform film was found difficult to apply due to the very small mass (as low as  $20\mu\text{g}$ ) of the films. The absorption of weak  $\beta$  particles, such as from  $\text{Ni}^{63}$ , described by Pate and Yaffe (147) is the easiest and quickest of the techniques to apply and was finally adopted for routine use.

The surface density of a few films was measured gravimetrically using an Ainsworth type FDJ microbalance. The films were mounted on a weighed sample plate and the weight of the film found by difference. At first great difficulty was encountered establishing rest points to better than  $\pm 10\mu\text{g}$ . Finally a procedure was evolved, based upon the work of Hillig (157) and Hull (158), wherein a weighing can be made in a period of about 40 minutes to a precision of  $\pm 3\mu\text{g}$ . Results of these determinations are shown in Table IV. Films belonging to the same batch number were made under identical conditions. The  $\text{Ni}^{63}$   $\beta$ -ray transmissions of the weighed films are also presented in the table. Films 8-18 show the effect of improved technique. Note that the surface densities of film 8-13 may be averaged to give  $18.0 \pm 1.5\mu\text{g}/\text{cm}^2$ , and films 14-18 show that the surface density per layer is

$19.4 \pm 1.3 \mu\text{g}/\text{cm}^2$ . Thus individual films may be made of the same thickness to within 7 - 8 per cent as determined gravimetrically. It will be shown in the next section that even an 8 per cent difference introduces no appreciable error in the film absorption correction.

In the application of the  $\text{Ni}^{63}$   $\beta$ -ray absorption technique the output of the lower half of the Borkowski  $4\pi$  chamber was connected to the proportional counter rather than employing a "conventional hemispherical  $2\pi$ -proportional counter," as Pate and Yaffe (147) did. The  $\text{Ni}^{63}$ , deposited on a one inch aluminum disk and covered with two layers of Zapon films, was placed face down on the film to be measured, and the  $2\pi$  counting rate determined. Since the beta transmission is determined over a small area in the center of the film it is not subject to peripheral irregularities and changes in support weight, and should be a much better estimate of the reproducibility of films from the same batch.

The results of the  $\text{Ni}^{63}$  absorption measurements are presented in figure 2. The points shown as squares were obtained from films whose thicknesses had been determined gravimetrically. For instance, the thickness of film numbers 8-13 were averaged to give an x-coordinate of  $18.0 \pm 1.5 \mu\text{g}/\text{cm}^2$  and their transmissions were averaged to give a y-coordinate of  $0.830 \pm 0.004$ . The weights of films 14, 15, and 16 were the averages of two sets of weighings which took place nine months apart. The uncertainties

Table IV. Surface Density Data for Films made from  
33 per cent Zapon Solution

Film Batch No.	Number of Layers	Weight ( $\mu\text{g}$ )	Area ( $\text{cm}^2$ )	Surface Density ( $\mu\text{g}/\text{cm}^2$ )	$\text{Ni}^{63}$ $\beta$ -ray transmission (fractional)
1	1	32	5.06	6.3	
2	1	20	5.06	4.0	
3	1	25	5.06	4.9	
4	2	42-72 <sup>a</sup>	5.06	8.3-14.2 <sup>a</sup>	
5	2	79-89 <sup>a</sup>	5.06	15.6-17.6 <sup>a</sup>	
6	2	69-90 <sup>a</sup>	5.06	13.6-17.8 <sup>a</sup>	
7	2	52-97 <sup>a</sup>	5.06	10.3-19.2 <sup>a</sup>	
8	3	878	45.60	19.3	0.832
9	3	661	45.60	14.5	0.836
10	3	867	45.60	19.0	0.827
11	3	772	45.60	16.9	0.832
12	3	869	45.60	19.1	0.821
13	3	872	45.60	19.1	0.831
14	4	1029-1028 <sup>a</sup>	45.60	22.6-22.6 <sup>a</sup>	0.843 $\pm$ 0.009
15	4	1648-1648 <sup>a</sup>	45.60	36.2-36.2 <sup>a</sup>	0.825 $\pm$ 0.022
16	4	2670-2664 <sup>a</sup>	45.60	58.6-58.5 <sup>a</sup>	0.792 $\pm$ 0.020
17	4	3366 <sup>a</sup>	45.60	72.5 <sup>a</sup>	0.760 $\pm$ 0.010
18	4	4251 <sup>a</sup>	45.60	93.2 <sup>a</sup>	0.754 $\pm$ 0.012

<sup>a</sup> The weight of the film plus aluminum plate was redetermined at a later date, giving the second number.

indicated in the y-coordinate represent the average deviation of two determinations. The points shown as circles in figure 28 correspond to the upper x-axis which displays the number of layers of films made by lamination using 50 per cent (2:1:1 volume ratio) Zapon solution. The uncertainties indicated in the y-coordinate represent the average deviation of at least two different films. Note that the films made from equal numbers of layers give the same Ni<sup>63</sup> transmission to within less than 2 per cent (average deviation). The adjustment of the scales of the x-axes is a more or less arbitrary normalization of the upper, relative scale to the lower, absolute scale. Figure 28 may thus be used to obtain the approximate thickness from a measurement of the Ni<sup>63</sup>  $\beta$ -transmission.

3. Film Absorption Correction. A certain fraction of the beta particles emitted from the source will be absorbed in the film between the source and the bottom half of the chamber. Whether or not this fraction is significant depends on the backing thickness and the shape and endpoint of the beta spectrum. The correction can be assessed in several different ways.

Seliger and coworkers (47, 159) at the National Bureau of Standards have treated this subject by a consideration of the number of particles detected in the top and bottom halves of the 4 $\pi$  chamber both separately and together. From the resulting analysis they have derived an expression

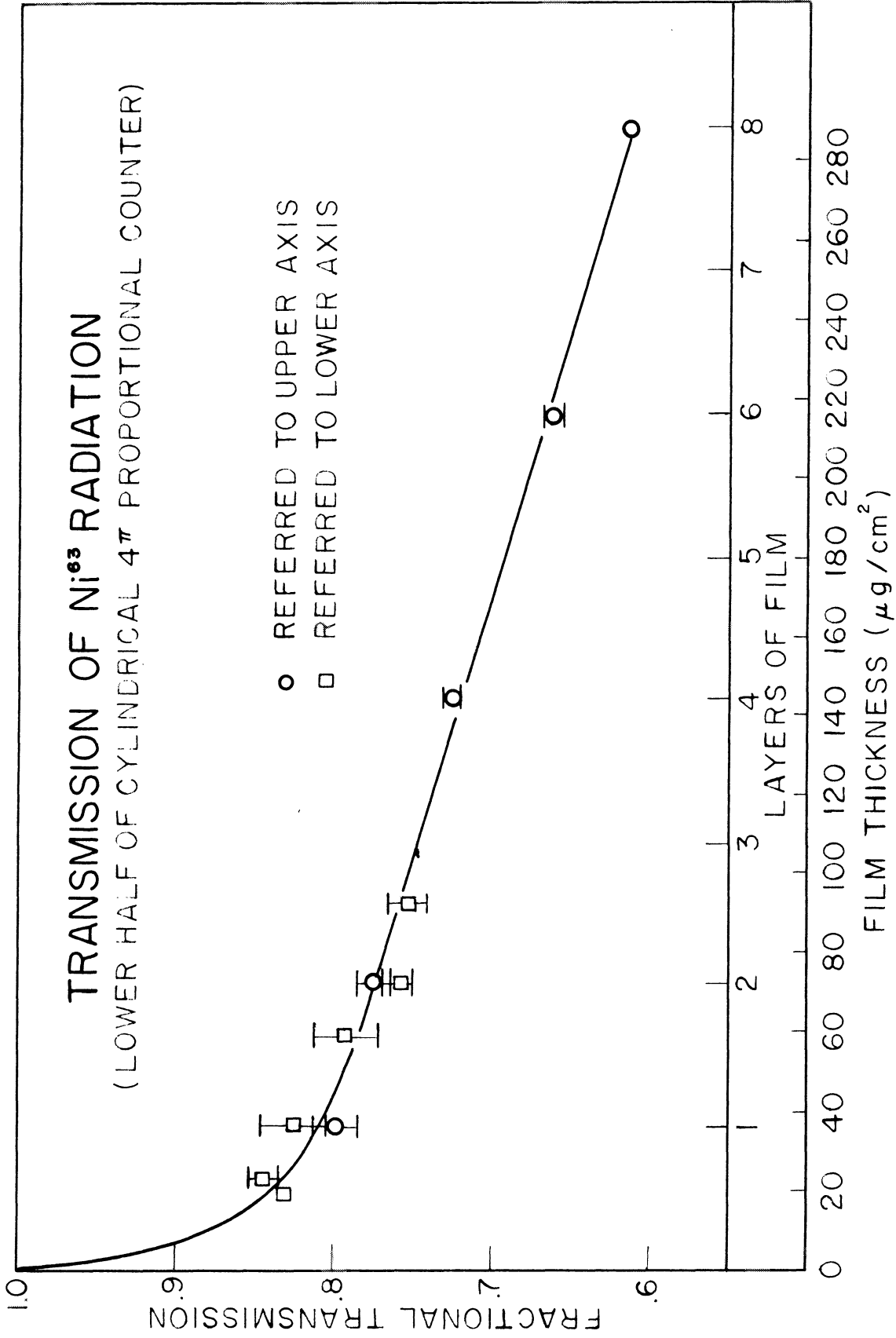


Fig. 28. Transmission of Ni<sup>63</sup> β-ray radiation in thin Zapon films. The upper x-axis gives the number of layers of film and the lower x-axis shows the surface density as determined gravimetrically.



for the fractional absorption in the film which is related to the absolute disintegration rate. The analytical treatment is complicated by the many energy-dependent scattering and absorption considerations. Thus they had to make certain assumptions which cast doubt as to the validity of their treatment.

Hawkins, et al. (52) at Chalk River made the correction by placing a film on top of the source in such a manner as to sandwich the source between two identical films. Their films consisted of  $100 \mu\text{g}/\text{cm}^2$  of plastic coated with  $50 \mu\text{g}/\text{cm}^2$  of gold. No account was taken of the radiation scattered from the walls of the chambers. The reduction in counting rate which occurs when the second film is placed on top of the source was considered to be the correction. This is equivalent to extrapolating a plot of the counting rate vs film thickness to zero.

Cohen (45) did essentially the same thing as Hawkins except that he used much thicker films. A  $7.76 \text{ mg}/\text{cm}^2$  thickness of aluminum was placed over the source (which itself was approximately  $6 \text{ mg}/\text{cm}^2$  thick) and the counting rate was determined. Next another sheet of aluminum was placed under the source and the counting rate redetermined. Assuming linearity of the resulting absorption curve the appropriate correction was made.

Smith (46) showed that this "sandwich" technique is unreliable. He states that the true correction is closer

to that obtained from a linear extrapolation of a plot of activity vs thickness of the source backing. Increasing numbers of aluminum films, each  $260 \mu\text{g}/\text{cm}^2$  thick, were used to vary the thickness of the source backing. He also gives a more complex mathematical treatment of the "sandwich" technique, which if applied should give results in agreement with the linear extrapolation technique.

In determining half lives by measuring specific activity, MacGregor (144) and Sawyer (145) corrected for film absorption at the same time as self absorption. They made up a series of samples varying both the source and surface density of the film. The specific activity was determined for each of these samples and was plotted vs the total thickness (sample plus backing). A linear extrapolation was then made to zero thickness to determine the true specific activity. MacGregor's film varied from 15 to  $65 \mu\text{g}/\text{cm}^2$ .

Houtermans and coworkers (43 - 44) followed a similar procedure. The source deposited on a film  $30 - 40 \mu\text{g}/\text{cm}^2$  thick, was covered with aluminum foils of varying thicknesses. The resulting absorption curve was extrapolated to zero absorber. The thinnest aluminum foil they used was  $240 \mu\text{g}/\text{cm}^2$ , however, and whether the slope of the curve remains unchanged below this value is open to question.

A consideration of these different methods led to the conclusion that the best way to make the source mounting correction is by the absorption curve technique. If the

thickness increments are of the order of  $15 \mu\text{g}/\text{cm}^2$  the extrapolation is only over that thickness which is the range of  $\sim 2$  kev electrons. (33) During the course of this work a paper appeared by Pate and Yaffe (147) in which they arrive at essentially the same conclusion. They present data demonstrating the validity of the absorption curve method and the erroneous results obtained when either the sandwich technique or the method of Seliger is used.

The procedure used in this work was the following. A series of sample plates was made up bearing different numbers of layers of Zapon films. Equal aliquots of the radioactive solution were pipetted onto each. After evaporation of the solution all the samples except one were covered with an additional Zapon layer to prevent loss of activity. The one uncovered sample had only one layer of source backing. The samples were then counted several times during their decay in order to detect any changes in the absorption curve as different components decay out of a complex mixture. Decay corrections were applied (using the effective half-life during the period of measurement) to normalize each absorption curve to one particular time.

Figure 29 shows an absorption curve obtained in this laboratory from  $\text{P}^{32}$  previously standardized at the National Bureau of Standards. Here, as in the rest of this work, the number of layers of Zapon film is plotted along the x-axis. This is justified by the fact that successive

layers of films can be made equal in thickness to within ~8 per cent as discussed previously. Since the curves so obtained are very nearly flat, a fairly large error - certainly more than 8 per cent - in the value of the thickness can be tolerated. The points represent averages of two determinations taken four weeks apart. As can be seen from the figure there is no evidence of a significant slope.

It will be noted that an aliquoting error is inherent in each point of the absorption curve. A separate experiment was done to evaluate the magnitude of this error. Aliquots of a  $\text{Co}^{60}$  solution were taken with micro pipettes which had been coated with dimethyl-dichloro silane (variously called Silgon, Drifilm, Desicote, etc.). (160-161) (These specially treated pipettes were used throughout this research.) The pipettes were rinsed with water after each filling and the

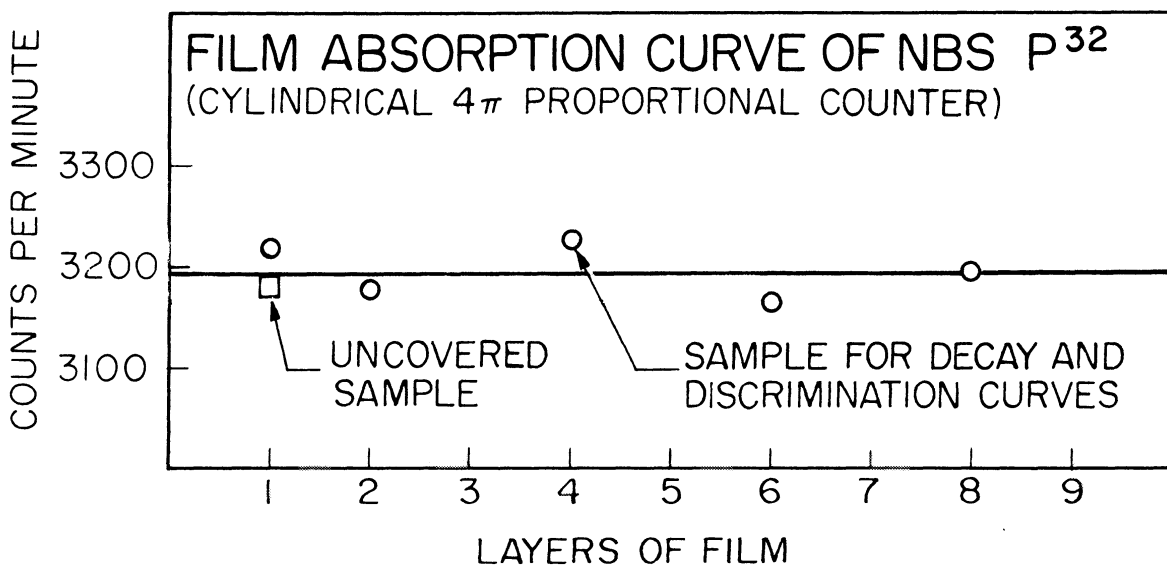


Fig. 29. Film absorption curve of  $\text{P}^{32}$  standardized at the National Bureau of Standards.

rinse was added to the sample. The counting was done with the scintillation well counter. The results are given in Table V. The first part of the table shows that essentially all of the active solution is removed in the initial transfer. However, for the rest of the work, one or two rinses were used to be on the safe side. The second part of the table shows the reproducibility to be better than  $\pm 2$  per cent, even for multiple fillings in which there was no rinse until after all of the  $\text{Co}^{60}$  solution had been transferred.

Table V. Aliquot Reproducibility

Pipette Vol. ( $\mu\text{l}$ )	Vol. taken ( $\mu\text{l}$ )	No. Rinses	Activity (c/m)
100	100	2	1202
100	100	1	1201
100	100	0	1164
250	250	2	2490
250	250	1	2532
250	250	0	2531
500	500	2	4557
500	500	1	4762
500	500	0	4806
100	100	1	722
100	100	1	713
100	100	1	688
100	200	1	1414
100	300	1	2094

4. Self Absorption. Chemical procedures in which the element in question is separated in a carrier free state possess obvious advantages with respect to the problem of absorption of very weak  $\beta$  particles in the sample itself. This is a goal which is advocated for cross section measurements in bombardment work in conjunction with  $4\pi$   $\beta$ -ray counting.

Even with carrier free separations there may be small amounts of foreign material, such as sodium chloride, picked up during the chemical processing. A quick check was made to find out roughly how much matter can be tolerated without absorbing an appreciable number of  $\beta$ -particles. Cobalt-60 was chosen for this purpose as its 0.32 Mev  $\beta$  ray represents a lower limit to the  $\beta$  energies encountered in the present work. Equal aliquots of  $\text{Co}^{60}$  were pipetted onto thin Zapon films. Varying amounts of a very dilute sodium chloride solution were pipetted on top of the activity. No particular care was taken to assure an even deposit, although insulin was tried without success. After evaporation of the solution, the deposits were covered with another Zapon film and counted. The resulting self absorption curve is depicted in figure 30. The errors indicated are the statistical errors of counting (standard deviation). From this crude experiment it was felt that a lower tolerance limit may be set at  $\sim 1/2 \mu\text{g}$  from an inspection of the curve.

This amount of inert material can be observed visually. Therefore if a visible deposit is present on a sample plate for absolute counting, one must suspect a significant self absorption correction for weak  $\beta$ -emitters.

5. Effect of a Conducting Coating. If the plastic film used for the source mount is not conducting, there will be a small field-free space in the center of the chamber. Thus some very weak particles may expend their energy in this region without producing a pulse. There are two ways of taking care of the situation: the film may be made conducting, or the size of the hole in the aluminum sample plate may be made small enough so that the effect is negligible.

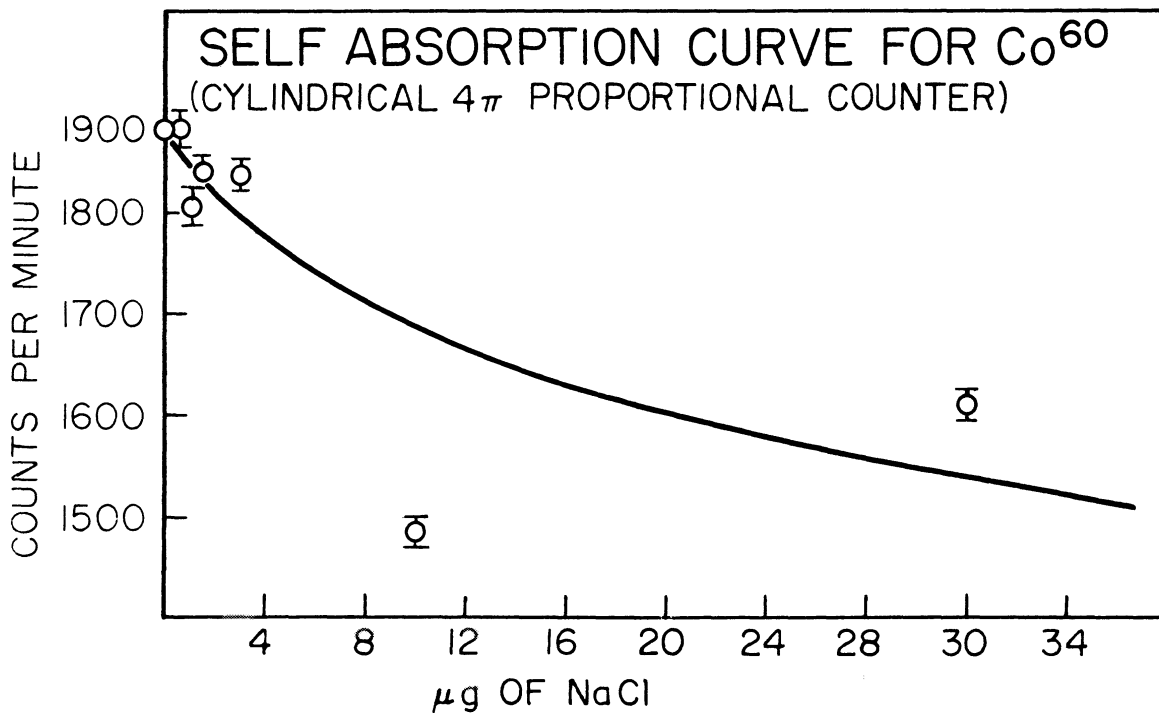


Fig. 30. Self absorption curve of  $\text{Co}^{60}$ .

Hawkins et al. (52) state that a minimum of  $25 \mu\text{g}/\text{cm}^2$  of gold must be evaporated on thin plastic films covering a 2 inch diameter hole. Mann and Seliger (159) at the National Bureau of Standards found that a low-field correction is necessary for  $\text{Co}^{60}$  but not for  $\text{P}^{32}$  using ~0.8 inch diameter hole. However, the Bureau's standardizations are now all made with  $15 \mu\text{g}/\text{cm}^2$  of gold evaporated on the plastic. (159) With a 1 1/2 inch opening, Smith (46) used  $260 \mu\text{g}/\text{cm}^2$  aluminum foils for strong beta rays, and thin aluminized plastic films for weak emitters. Meyer-Schützmeister and Vincent (44) employed 5 -  $15 \mu\text{g}/\text{cm}^2$  of copper evaporated onto plastic films over a 0.4 inch diameter aperture. (Their purpose in using the conducting coating was other than the elimination of the low-field effect.) Pate and Yaffe (151) recently made a study of the minimum thickness of gold necessary for correct operation. They conclude that for  $\text{Ni}^{63}$  and  $\text{P}^{32}$  alike at least  $2 \mu\text{g}/\text{cm}^2$  gold is needed for their 1 and 2 inch apertures. Borkowski (48) states that as long as the opening in the sample plate is less than 1/2 inch no conducting coating is necessary.

Since the sample plates used in this work had center holes 1/2 inch in diameter, it was thought that no conducting coating would be necessary. This point was checked in two ways. First, samples were counted that were obtained from the National Bureau of Standards where the  $4\pi$  standardization is done with the conducting film, and excellent agreement was obtained (better than 1 per cent -



the details are given later). Secondly, voltage plateau curves were taken of  $\text{Co}^{60}$  (the weakest  $\beta$ -emitter encountered in the present work) mounted both on two layers of Zapon and one layer of Zapon coated with an evaporated layer of gold. Pate and Yaffe (51) considered the existence of a voltage plateau as a criterion of the proper functioning of their  $4\pi$  counter. Although it was felt that discrimination plateaus (see next section) constitute a better measure, the data presented in figure 31 demonstrates that a voltage plateau is obtained with the cylindrical chambers for  $\text{Co}^{60}$  either with or without the conducting film of gold.

(Pate and Yaffe's data do not extend to anode potentials greater than 3400 volts and their sample plates had either 1 or 2 inch apertures. These differences may explain why they do not obtain voltage plateaus without the conducting film whereas such plateaus are obtained in the present work.) Figure 31 also includes a curve of a  $\text{Sr-Y}^{90}$  sample for comparison, mounted on 1/4 mil Teflon, which was used as a standard throughout this work to check on the day-to-day performance of the counter. The three curves are not normalized to the same counting rate on the plateau because of the confusion of the individual points that would result.

In the later experiments (Titanium bombardments) gold was evaporated onto Zapon films just to be on the safe side. The optimum arrangement, for the various

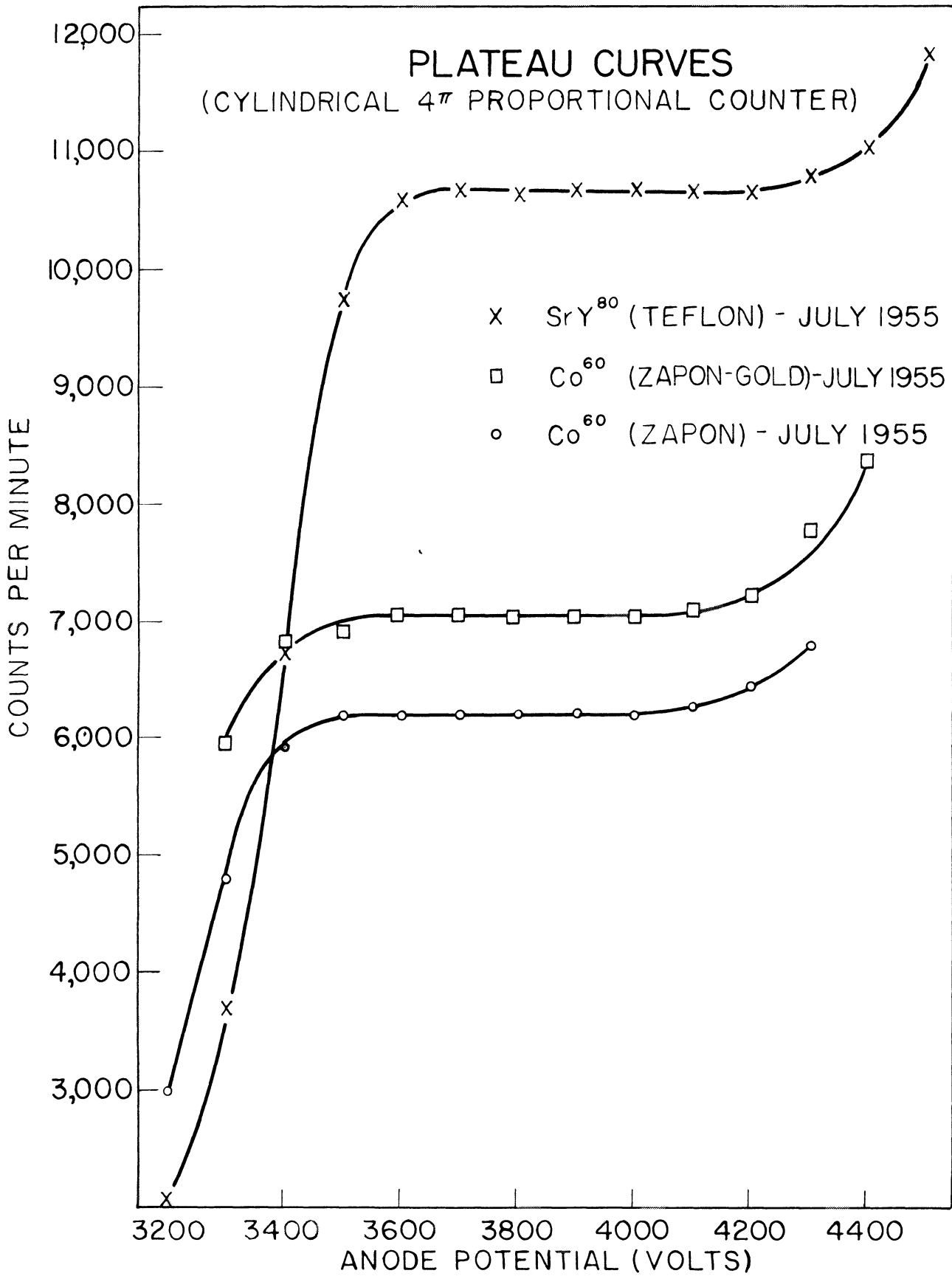


Fig. 31. Voltage plateau curves with various samples.

layers is depicted in figure 32 as determined by trial and error. The gold is first evaporated onto one film covering only the central part of the sample plate.

(Pate found it makes no difference to which side the gold is applied.) Additional layers of Zapon and the activity are then applied to the opposite side.

#### 6. Effect of Gain, Trigger and Voltage Settings.

In both of the instruments used (see the section on  $4\pi$  Counters, page 35) the amplifier gain is variable as is the trigger (discrimination) level. The latter defines the minimum pulse height necessary to trigger the scaler and hence permits one to eliminate electronic noise. Voltage plateau curves of Sr-Y<sup>90</sup> were taken covering the full range of gain and trigger settings. For routine counting a point was chosen on the best plateau. For absolute  $\beta$ -ray counting Seliger (47) has shown that it is necessary to take discrimination curves, i.e., a plot of counting rate vs trigger setting for a given gain and voltage, to determine the position of a discrimination plateau. This is necessary for each  $\beta$  emitter measured because each one may yield characteristic curves which look quite different depending on the shape and end-point of the beta spectrum, complications from conversion electrons, etc. This necessitates taking discrimination curves at intervals during the decay of samples containing more than one nuclide, because as one component decays away the radiations coming from the sample change. Moreover

electronic changes may shift the plateau or otherwise alter the settings for "absolute" counting over a period of several months.

These curves may be expected to exhibit a linear portion, or plateau, which may be extrapolated to zero discrimination level to arrive at the true counting rate. The idea behind this is that in the region of the  $\beta$ -ray distribution in the neighborhood of zero energy, the noise level will cover up the true counts as is evidenced by a sharp rise in the counting rate near zero discrimination level. This noise is cut out by increasing the discrimination setting to a point above the noise level. But in so doing some of the weakest  $\beta$  particles will also have been lost. It is reasonable to suppose that some relation exists between the pulse height and the probability of emission of beta particles with that height. It follows that the discrimination curve will assume a definite form

### SAMPLE FOR $4\pi$ COUNTER

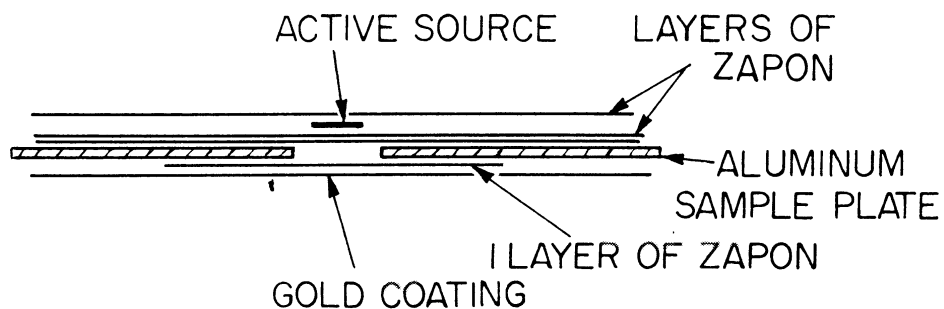


Fig. 32. Preparation of the  $4\pi$  counting plate showing the arrangement of the various layers.

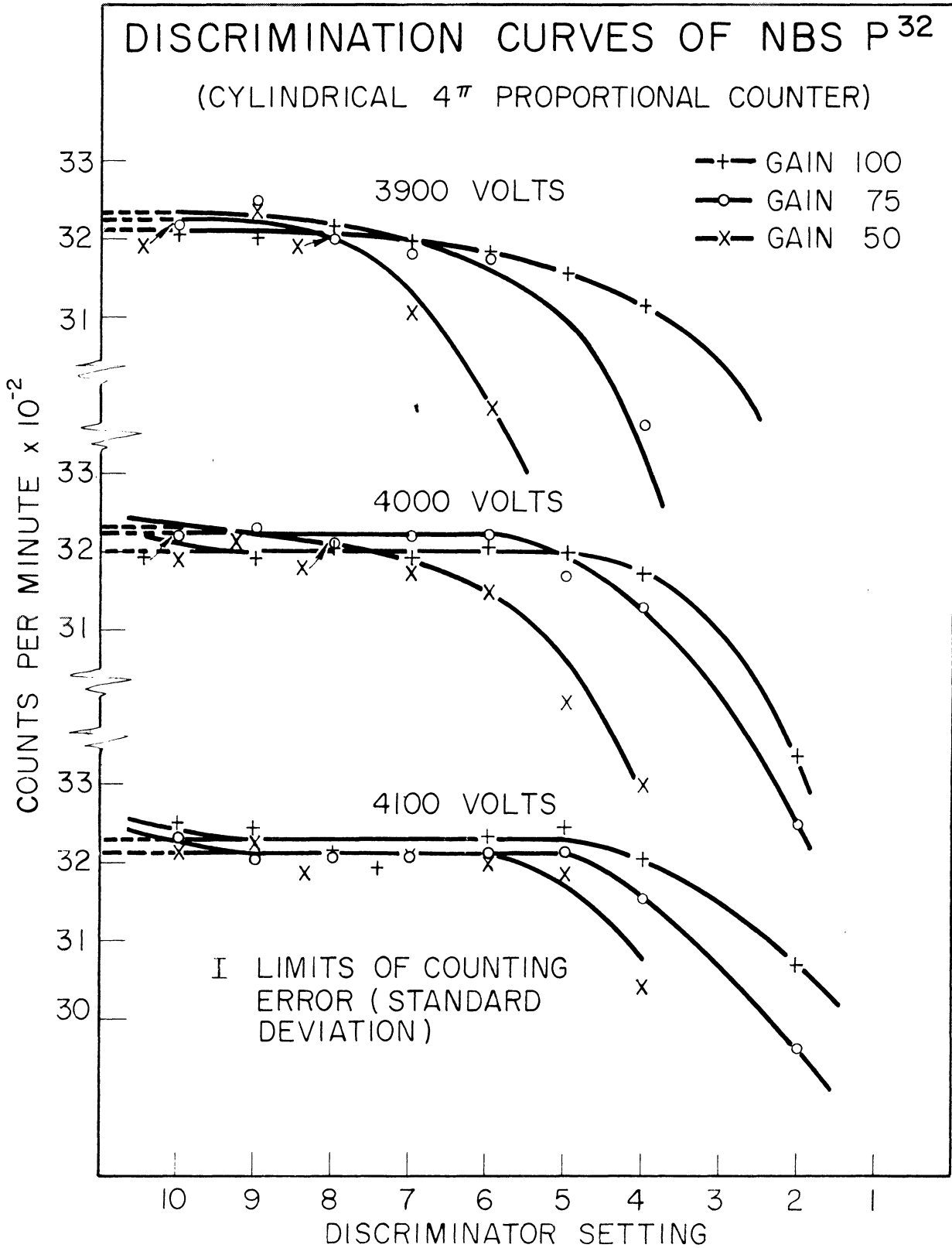


Fig. 33. Discrimination curves of P<sup>32</sup> standardized by the National Bureau of Standards. The limits of the counting error shown are twice the standard deviation of a single point.

in this low energy region, and it may be assumed to be linear to a first approximation.

In practice the flat portion of the discrimination curves showed no evidence of a slope for the  $\beta$  emitters studied covering an energy range of 0.36 - 4.2 Mev. An example of this is given in figure 33 which shows the curves for NBS P<sup>32</sup>. The sample selected for those measurements was the one mounted on 4 layers and covered with one layer of Zapon (see figure 29). The experimental points have been corrected for decay. The gain numbers merely indicate the dial setting on the Nuclear-Chicago Model 162 scaler. The x-axis is also an arbitrary scale showing the actual dial settings - the discrimination level increases to the right. Note that the disintegration rate is the same for the three voltages and the three amplifier gains shown, within the error due to counting statistics of about 1 per cent for the individual points. The limits of this error (twice the standard deviation) are indicated on the figure which applies to all of the points - this avoids the confusion which would result if the error of each point were plotted. This error could, of course, be reduced by increasing the number of disintegrations counted for an individual counting rate measurement, but limitations of time available for these curves dictated the duration of each measurement.

7. Dead Time Correction. Another possible source of error arises from the fact that an event which produces a

pulse will render the counter insensitive for a finite period called the dead time. In proportional counters this dead time is relatively short - typically of the order of  $5\mu\text{sec}$  - which means that it is possible to record very high counting rates without significant coincidence losses. Since the present work involves following the decay of samples over large variations in counting rate, this small dead time is of particular advantage.

The determination of the dead time has been adequately treated in the literature. (162-166) The available methods of measurement group themselves into three classifications. First, there are the paired sample techniques developed by Kohman (163-164) which involve counting two samples of approximately the same strength separately and then again simultaneously. The sum of the two separate counting rates will in general be greater than the counting rate taken together, and from this is deduced the fractional coincidence loss. Secondly, one may measure the minimum time between two discernable pulses at the various stages of the scaling circuit with an oscilloscope and take the longest dead time observed to determine the coincidence correction. Thirdly, the correction can be found by the measurement of sources of known relative intensities, in particular the observation of the decay of a source which is decaying with a moderate half-life. Here the decay is followed for several half-

lives to a low counting rate at which there is assumed to be no loss of counts. The theoretical curve is drawn through these decay points using the known half-life and extrapolated to the high counting rates. The deviation of the observed points from the theoretical curve is interpreted as the correction term. This strictly empirical method involves no assumptions other than an accurate knowledge of the half-life of the activity observed, and quite closely parallels the actual operating conditions of the counter.

When the paired sample technique was tried in this work it invariably resulted in meaningless negative numbers appearing in the formula for the dead time. An analysis of the propagation of errors indicated that for such a short dead time as  $\sim 5 \mu\text{sec}$ , extremely accurate counting rates must be determined in order to result in an answer to which some significance can be attached. This possibly affords an explanation of the anomalous results, because the rates were determined only to within  $\sim 0.5$  per cent in these experiments.

The  $4\pi$  proportional counter was tested for coincidence losses at high counting rates by following the decay of the  $54$  minute  $\text{In}^{116}$ . This isotope was produced by bombarding  $5$  mil indium foil with neutrons which are available in abundance just outside the cyclotron vacuum tank near the window box B, figure 1. They are produced from (d,n) reactions of stray deuterons hitting the deflector,



paddle probe, etc. By bombarding for only about 5 minutes no observable amount of 50-day  $\text{In}^{114}$  is produced, while an adequate amount of the 54-minute  $\text{In}^{116}$  results from the 145 barn thermal neutron cross section of  $\text{In}^{115}$ . The 4.5-hour  $\text{In}^{115m}$  is produced only by fast neutrons, (170-172) so paraffin was placed around the indium foil to moderate the neutrons. Actually, the first bombardment of indium foil resulted in an activity of the order of 5 hours and a long-lived component in addition to the 54-minute period. By decreasing the bombardment time from 45 to 5 minutes and increasing the thickness of paraffin surrounding the target foil from 1 to 6 inches, these two extraneous activities were not observed. (They were less by factors of at least 700 and 5,000 respectively for the 5-hour and the long-lived components.)

The results of the second bombardment are depicted in figure 34. The experimental points have been corrected for background. A single activity due to the 54-minute  $\text{In}^{116}$  is seen to remain after the short-lived impurities have died out. The decay curve is straight for a factor of  $10^4$  (13 half-lives) to  $\sim 10$  counts/min (10 times less than background.) The observed half-life agrees well with the reported values of  $53.93 \pm 0.03$  minutes (173) and  $54.31 \pm 0.07$  minutes. (174) The results of a least squares analysis of the decay points from  $t = 4.5$  hours on, yields 54.26 as the half-life. (Above 4.5 hours the

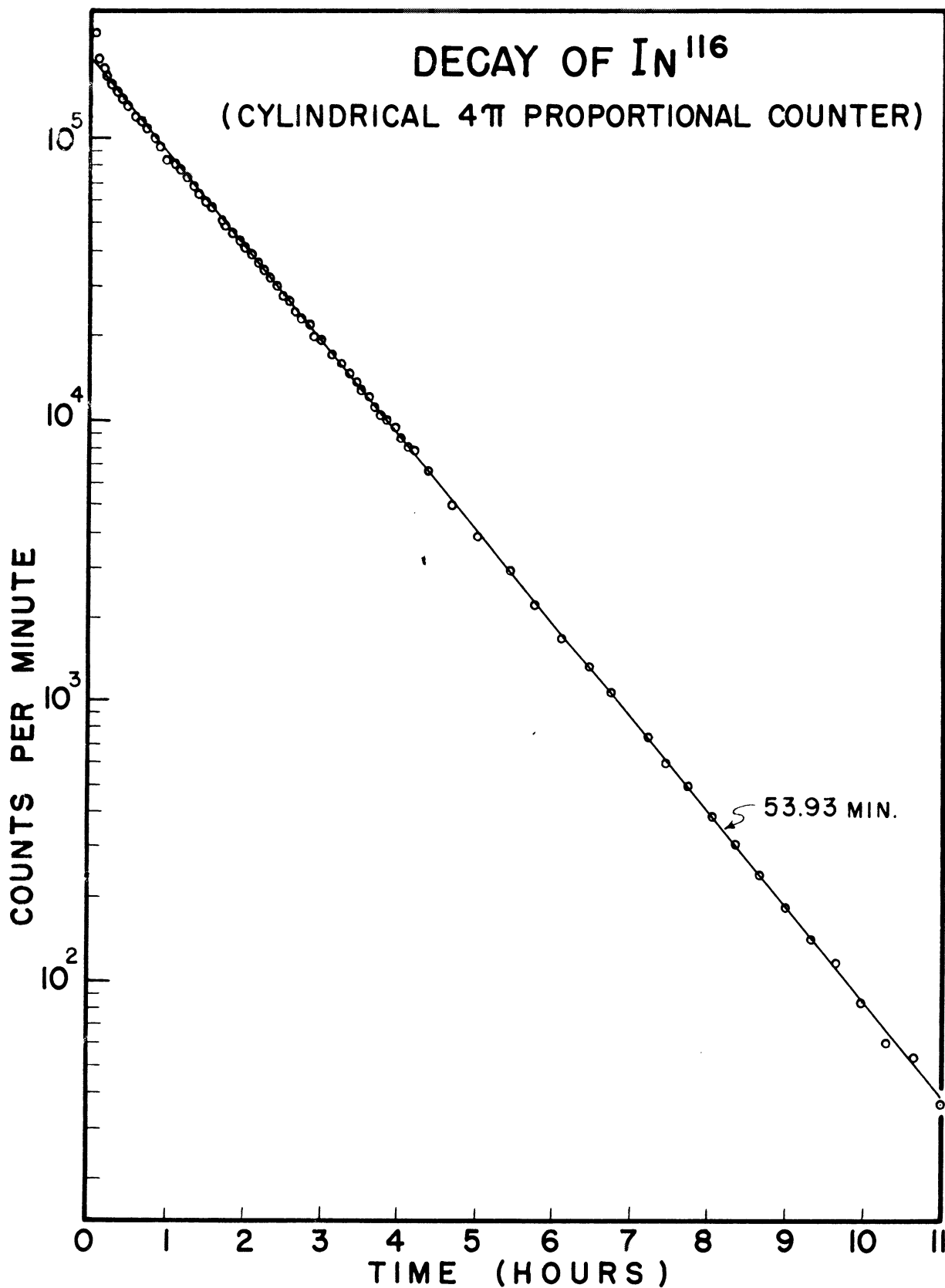


Fig. 34. Decay curve of  $\text{In}^{116}$  for use in determining the dead time of the  $4\pi$  proportional counter.

points start to deviate from linearity by ~0.1 per cent.) The first five points indicate the presence of an activity with a half-life of the order of three minutes. This dies down to less than one per cent of the 54 minutes activity by the time the latter is  $1.3 \times 10^5$  cpm.

These data were treated according to the method of T. P. Kohman as outlined by Calvin, et al. (165) The provisional corrections,  $\underline{C}'$ , were calculated from

$$C' = \frac{N_0 e^{-\lambda t} - R - b}{R} \quad (11)$$

where  $\underline{R}$  is the observed counting rate,  $\underline{b}$  is the background rate,  $\underline{N_0}$  is the true rate when  $t = 0$ , and  $\underline{N_0}$  is a tentative value of  $\underline{N_0}$ . The value of the half-life was taken as 53.93 minutes for these calculations. Figure 35 shows a plot of  $\underline{C}'$  vs  $\underline{R}$ , and the solid line drawn through the points by means of a least squares analysis. Note that assuming the formulas

$$N = R + \tau R^2, \quad (12)$$

where  $\underline{N}$  is the true counting rate and  $\underline{\tau}$  the dead time, it follows that

$$C = \tau R. \quad (13)$$

This is the justification for drawing a straight line through the points with a slope equal to  $\underline{\tau}$ . The

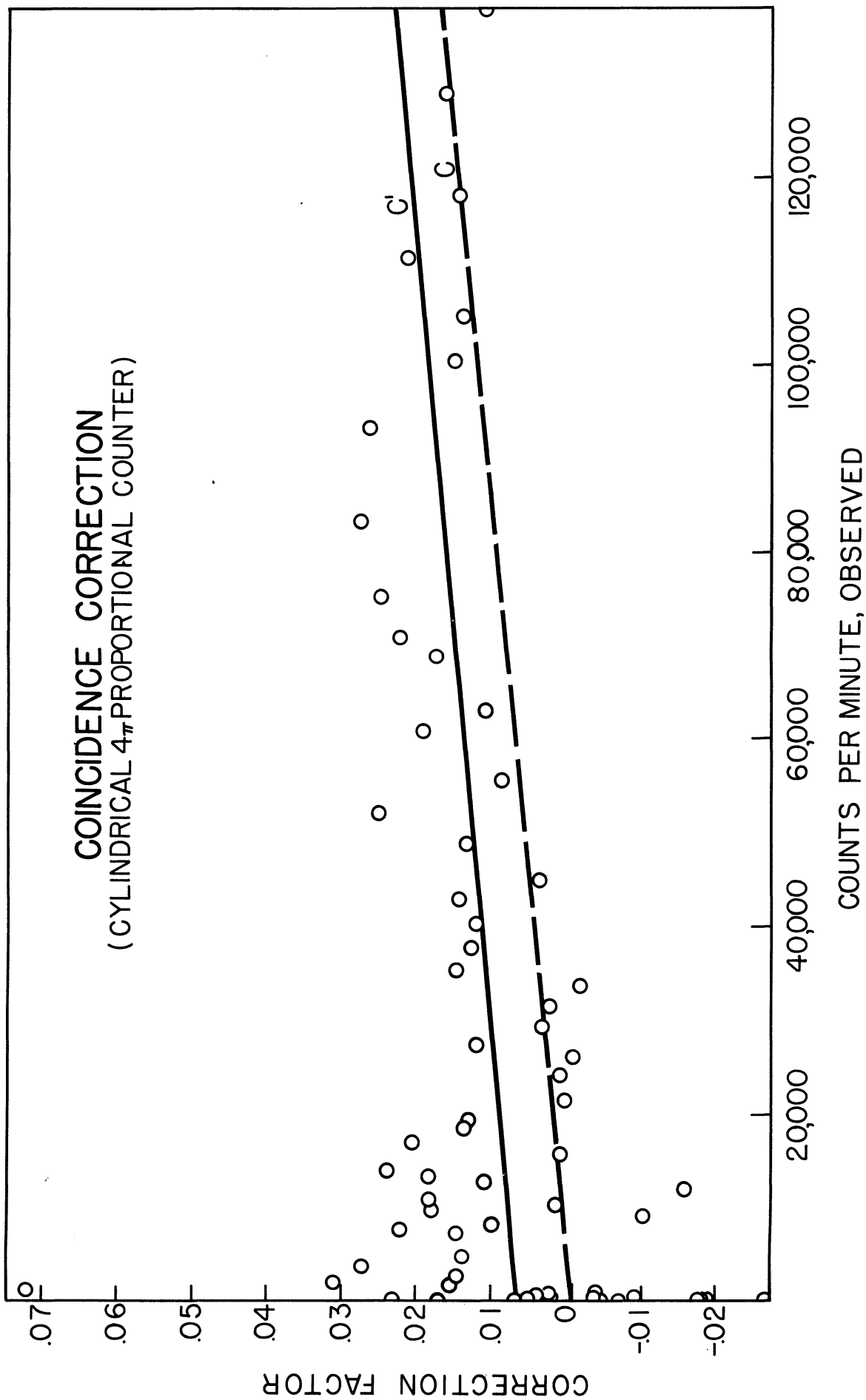


Fig. 35. Coincidence (dead time) correction curve for the 4 $\pi$  proportional counter, based upon the decay of In116. The solid line is the provisional curve, and the dotted line is the true curve.

intercept of the curve at  $R = 0$  is taken to be  $N_0$ , from which the correct values of  $C$  can be calculated by the method outlined by Calvin. The curve of  $C$  vs  $R$  is also shown in figure 35.

The results of the second bombardment of indium gives  $7.1 \mu\text{sec}$  as the dead time. A third indium bombardment was followed from  $1.2 \times 10^6$  counts/min to below background and the dead time from this was calculated to be  $8.6 \mu\text{sec}$ . These two values agreed well within the standard error of each determination. The average,  $7.9 \mu\text{sec}$  (corresponding to a correction of 1.2 per cent/thousand counts/min), was used to obtain a working curve of the percentage correction vs the gross counting rate similar to the solid line in figure 35.

#### 8. Counting of National Bureau of Standards Samples.

A solution of  $P^{32}$  with  $0.001 \text{ M H}_3\text{PO}_4$  carrier was obtained from the National Bureau of Standards. It had been standardized in a  $2\pi$  ionization chamber previously calibrated by  $4\pi$  proportional counting. (49) Micropipettes, calibrated with mercury and coated with Silgon, were used to transfer aliquots of the solution to a series of sample plates bearing varying numbers of non-conducting Zapon films (made from 33 per cent Zapon solution). Water from one rinse was added to the sample plate. Drying was accomplished in an atmosphere of ammonia to prevent the Zapon from being attacked. All the samples but one (on one layer) were

covered with an additional layer of Zapon.

The samples were counted to give the film absorption curve already discussed (figure 29). The discrimination curves (figure 33) taken with the sample which was deposited on four layers of Zapon have also been treated above.

The decay was followed on the four layer sample at the gain and trigger settings determined from the discrimination curves. The decay curve is presented in figure 36. The solid line was calculated assuming 1.4 per cent of  $P^{33}$  contaminant at the time of the standardization. Values of 1.4 and 1.9 per cent (175-176 ) have been reported for the percentage of  $P^{33}$  in pile-produced  $P^{32}$ , and Westermarck (177 ) reports this number varies with the amount of fast neutrons contaminating the thermal neutron flux. The present choice of 1.4 per cent was more or less arbitrary, and a variation in this number by a factor of two does not make a significant change in the following calculation. The half-lives used were 14.30 days for  $P^{32}$  ( 95, 178 ) and 24.4 days for  $P^{33}$  ( 179 ) which were deemed to be the best values available in the literature. The calculated curve fits the experimental points well, and the graphical analysis leads to  $159 \times 10^3$  disintegrations/sec/ml as the initial activity normalized to the average of the points of the film absorption curve. If the effective half-life is taken as 14.4 days as recommended by Seliger, (49) the initial activity turns out to be  $160 \times 10^3$  disintegrations/sec/ml. Either of these

values agree well with the Bureau's value of  $160 \times 10^3 \pm 2$   
per cent disintegrations/sec/ml.

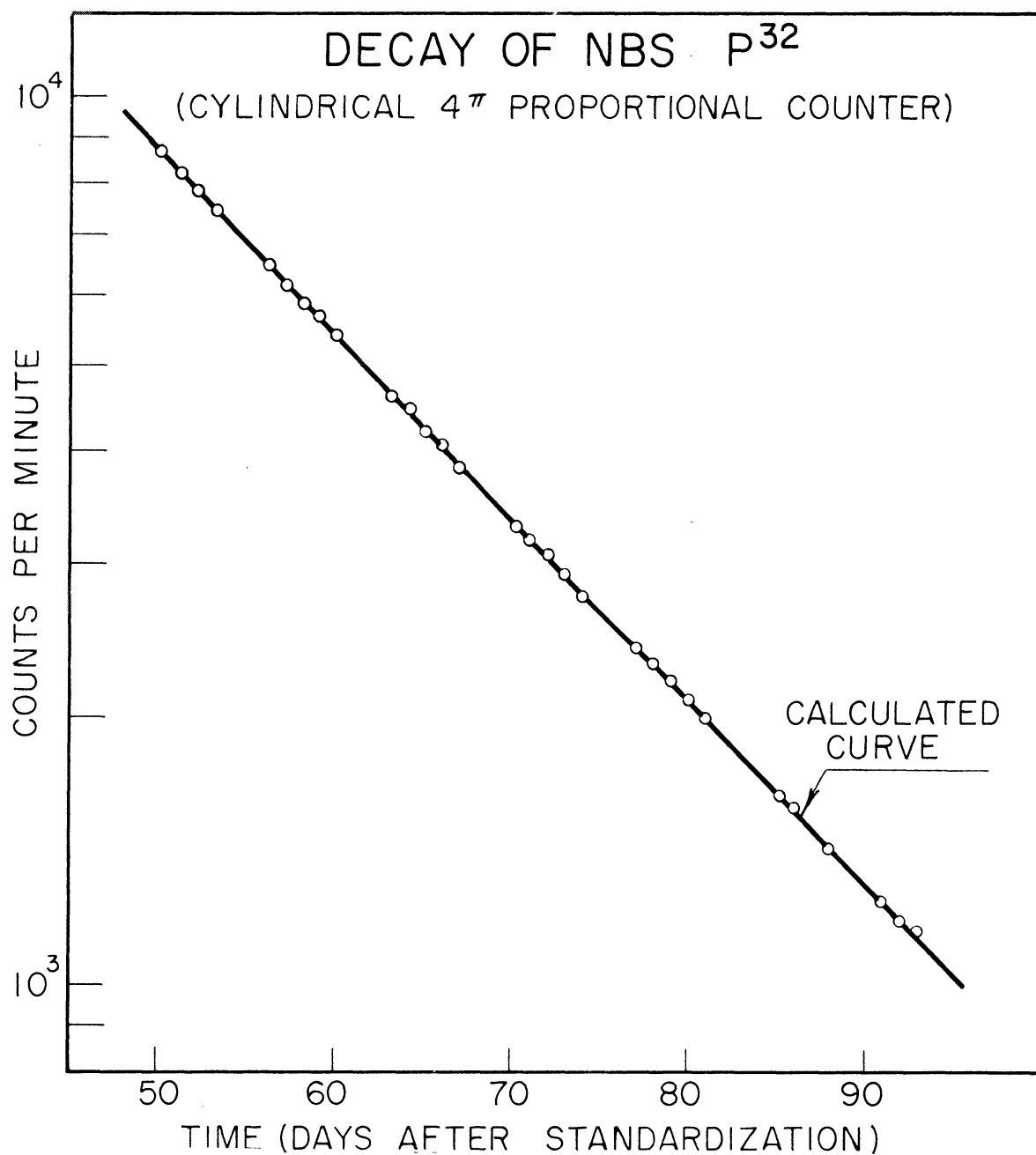


Fig. 36. Decay curve of P<sup>32</sup> standardized at the National Bureau of Standards. The calculated curve is based upon 1.4 per cent of P<sup>33</sup> present in the original sample.



## EXPERIMENTAL RESULTS

In the foregoing sections the discussion has been of a rather general nature describing the various pieces of apparatus and the techniques and procedure used in the measurement of absolute cross sections. In the material to follow the application of these experimental techniques to the specific yield-determining bombardments will be treated. First of all the equations will be derived which are used to transform the experimental data into cross sections. A short discussion of the steps followed in the course of a bombardment will then be given. Next the data from the four different elements studied will be annotated and the values of the cross sections so obtained will be discussed in the light of the experimental errors associated with each of the component factors entering into the calculation. Finally a few additional considerations in the measurement of reaction yields will be treated.

### A. Derivation of Equations

The cross section equations will be treated first, followed by the equations used to calculate the chemical yield by the technique of adding a radioactive tracer. The symbols used are listed at the end of this section.

#### Cross Section

The cross section of a nuclear reaction is defined as the probability that a given nuclear reaction will occur when a nucleus is exposed to a beam or flux of bombarding

particles. The term cross section originates from the simple picture that the reaction probability is proportional to the area which the target nucleus presents to the incident beam. One assumes that the nucleus is a small sphere suspended in a medium composed mainly of empty space. The cross section,  $\sigma$ , multiplied by the number of nuclei per square centimeter of target,  $n$ , gives the ratio of the area of the target nuclei to the total area (including both the empty space and the target nuclei.) If  $I$  is the number of bombarding particles per second, the total number of reactions  $N_T$  which occur will be given by

$$N_T = \sigma InT, \quad (14)$$

where  $T$  is the duration of the bombardment in seconds.

Note that  $\sigma$  may be thought of as an experimentally determined proportionality constant with the dimensions of  $\text{cm}^2$ . In order to apply equation (14) to the calculation of cross sections from experimental data it must be modified somewhat.

In the first place account must be taken of the fact that the radioactive product decays at the same time that it is being produced. Thus

$$\frac{dN}{dt} = \sigma In - \lambda N \quad (15)$$

where  $\lambda$  is the decay constant of the product nuclei. If the beam does not change in intensity during the course of the bombardment, i.e. if  $I$  remains constant, equation (15)

may be integrated to give the number of nuclei present at any time, t, after the beginning of the bombardment:

$$N = \frac{I\sigma n}{\lambda}(1-e^{-\lambda t}). \quad (16)$$

It is the total number of product nuclei formed  $N_T$ , which is needed to substitute into equation (14). If  $N_0$  is the number of nuclei at the end of a bombardment of duration T seconds,

$$N_0 = \frac{I\sigma n}{\lambda}(1-e^{-\lambda T}). \quad (17)$$

This equation may be solved immediately for  $\sigma$ , or combined with equation (14) to obtain

$$N_T = \frac{N_0 \lambda T}{(1-e^{-\lambda T})}. \quad (18)$$

If the cyclotron beam drifts appreciably in intensity during the course of the bombardment, equation (17) may be modified further. As pointed out in the Beam Integrator Section, page 18, the integrator output can be fed into a traffic counter which prints out the number of counts collected at equal intervals. Since equation (17) expresses the number of nuclei at the end of bombardment for I constant, it may be applied to each interval of duration  $\Delta t_i$  seconds during which the beam current is assumed to be practically constant. Then

$$\begin{aligned}
 N_0 &= \sum_{i=1}^m \frac{I_i \sigma n}{\lambda} (1 - e^{-\lambda \Delta t_i}) e^{-\lambda t_i} + \frac{I_j \sigma n}{\lambda} (1 - e^{-\lambda \Delta t_j}) e^{-\lambda t_j} \\
 &= \frac{\sigma n \cdot f(I_{ij})}{\lambda} \quad (19)
 \end{aligned}$$

where the function  $f(I_{ij})$  is defined as

$$f(I_{ij}) = (1 - e^{-\lambda \Delta t_i}) \sum_{i=1}^m I_i e^{-\lambda t_i} + (1 - e^{-\lambda \Delta t_j}) I_j. \quad (20)$$

The summation is carried out over all of the  $m$  equal intervals, and  $t_i$  is the time from the end of the  $i$ th interval to the end of bombardment. The term involving  $j$  is added separately because the traffic counter record cannot in general be divided into an integral number of equal intervals, i.e.  $\Delta t_i \neq \Delta t_j$ , so  $\Delta t_j$  is just the length of the last interval. Thus equation (19) merely adds up the number of nuclei formed at the end of each interval with allowance for decay from the end of that interval to the end of bombardment. The result, of rearranging equation (19) and combining with equation (14) is

$$N_T = \frac{N_0 \lambda I T}{f(I_{ij})}. \quad (21)$$

This reduces to equation (18) for the case in which  $I_i = I_j = I$ . Equation (21) will be used later to figure the

total number of nuclei of one nuclide formed relative to some other nuclide of a different half-life, which in turn is needed to calculate the chemical yield by the tracer technique.

In order to relate  $I_i$  (or  $I$ ) to the number of counts collected on the beam integrator, the calibration curve, figure 21, is consulted. The slope of this curve,  $K$ , gives the number of counts per minute equivalent to one microampere. For deuterons (one charge per particle),

$$I_i = \frac{B_i}{K\Delta t_i} \cdot \frac{60 \times 10^{-6}}{1.60203 \times 10^{-13}} \quad (22)$$

where  $B_i$  is the number of counts recorded by the beam integrator in the time interval  $\Delta t_i$ .

The number of target atoms per square centimeter  $n$ , is obtained from the weight of the target  $w$ , the target area  $A$ , the atomic weight  $M$ , and the (fractional) isotopic abundance  $a$ , as follows:

$$n = \frac{wa}{AM} \cdot \frac{6.0228 \times 10^{23}}{10^3} \quad (23)$$

The observed absolute counting rate extrapolated to the end of bombardment,  $C_0$ , may be converted to  $N_0$  as follows:

$$N_0 = \frac{C_0}{\lambda Y} \cdot \frac{1}{60} \quad (24)$$

where  $Y$  is the (fractional) chemical yield.

Finally the cross section is derived by combining equations (14), (21), (22), (23) and (24). Thus

$$\sigma = \frac{C_0 AMK}{waY \cdot f(B_{ij})} \cdot 7.3887 \times 10^{-38} \quad (25)$$

where

$$f(B_{ij}) = \frac{1 - e^{-\lambda \Delta t_i}}{\Delta t_i} \sum_{i=1}^m B_i e^{-\lambda t_i} + \frac{1 - e^{-\lambda \Delta t_j}}{\Delta t_j} B_j$$

$$= K \cdot f(I_{ij}) \cdot 2.667 \times 10^{-9}. \quad (26)$$

In some cases the correction for non-constant beam was not made, in which case equation (25) reduces to

$$\sigma = \frac{C_0 AMKT}{waYB(1 - e^{-\lambda T})} \cdot 7.3887 \times 10^{-38}. \quad (27)$$

### Chemical Yield

For those cases in which the chemical yield is determined by adding a known amount of radioactive isotopic tracer, the chemical yield,  $\underline{Y}$ , is the ratio of the amount of recovered tracer to the amount added:

$$Y = \frac{N'_{T2}(\text{recovered})}{N'_{T2}(\text{added})} . \quad (28)$$

The primes refer to the tracer, and the subscript 2 refers to a particular nuclide. Sometimes the nuclide which is added as tracer will not be produced in the bombardment in sufficient quantities to be observed, but in most instances there will be a contribution to the total activity of this nuclide from the (d,a) product of the nuclear reaction.

Then it is necessary to perform a separate experiment in which the bombarded target is worked up without the addition of the isotopic tracer. The number of atoms of the tracer isotope formed by nuclear reaction is then related to the number of some other isotopic species also produced in the reaction. Thus the ratio of the two activities,

$$Q = \frac{N_{T2}}{N_{T1}} \quad (29)$$

is determined, where subscript 1 refers to the other activity chosen as a reference. Note that this experiment amounts to measuring the relative cross sections for formation of the two activities. Thus

$$\frac{\sigma_2}{\sigma_1} = Q \frac{a_1}{a_2} . \quad (30)$$

With a knowledge of  $Q$  the bombardments can be carried out to determine the absolute cross section. Then  $N_{T2}^i$  (added) atoms of tracer are added to a solution of the target, and the chemical yield becomes

$$Y = \frac{\Sigma N_{T2} - N_{T2}}{N_{T2}^i(\text{added})} \quad (31)$$

where

$$\Sigma N_{T2} = N_{T2} + N_{T2}^i(\text{recovered}), \quad (32)$$

that is,  $\Sigma N_{T2}$  includes both the tracer and the (d,  $\alpha$ ) reaction product. In equations (29), (31) and (32) the values of  $N_{T1}$  are calculated from

$$N_{T1} = \frac{C_{01}B}{60 \cdot f(B_{1j})} \quad (33)$$

which is the result of substituting equations (22), (24) and (26) into equation (21) neglecting the fractional chemical yield  $Y$ . Assuming a constant beam, the formula for  $N_{T2}$  is

$$N_{T2} = \frac{C_{02}T}{60(1 - e^{-\lambda_2 T})} \quad (34)$$

Since component 2 is long-lived the correction for non-constant bombardment is negligible and equation (34) is valid.



The maximum error introduced by applying equation (34) to calculate  $\underline{N}_{T2}$  for the tracer may be seen from the following consideration. In effect, these equations extrapolate  $\underline{N}_0$  back to an effective midpoint,  $\underline{T}$ , of the bombardment, the midpoint being governed by the amount of decay occurring during the bombardment. If  $\lambda \ll T$ , then  $N_T \approx N_0$ . This can be seen from the equation defining  $\underline{T}$ :

$$N_0 e^{-\lambda \underline{T}} = N_T = I \alpha n T . \quad (35)$$

From equations (35), (22) and (19) it follows that

$$\underline{T} = \frac{1}{\lambda} \ln \frac{\lambda B}{f(B_{ij})} . \quad (36)$$

Thus the difference between  $\underline{N}_0$  and  $\underline{N}_T$  will be fixed by the half-life of the isotope in question, the amount of beam hitting the target, and the time distribution of the beam. Since the tracers used have long half-lives, the error introduced by using equation (34) for  $\underline{N}_{T2}$  and  $\underline{\Sigma N}_{T2}$  is negligible. As an illustration, the decay of 25.4-day  $P^{33}$  during one hour (a typical bombardment time) amounts to only 0.1 per cent which represents the maximum possible error in the calculation of  $\underline{N}_{T2}$  and  $\underline{\Sigma N}_{T2}$  ! The error is reduced much further by the extrapolation to  $\underline{T}$  via equation (34).

The chemical yield  $\underline{Y}$  is finally expressed in terms of observable quantities by substituting equations (29), (33)

and (34) into (31), making use of the relation

$$\Sigma C_{T2} = \lambda_2 \Sigma N_{T2} \quad (37)$$

where  $\Sigma C_{T2}$  is the total observed activity of component 2 in counts per minute. Thus

$$Y = \frac{\frac{T\Sigma C_{O2}}{(1-e^{-\lambda_2 T})} - \frac{QBC_{O1}}{f(B_{1j})_1}}{\frac{TC_{O2}(\text{added})}{(1-e^{-\lambda_2 T})}} \quad (38)$$

In case the correction for non-constant bombardment is not made for component 1, the chemical yield becomes

$$Y = \frac{\frac{\Sigma C_{O2}}{(1-e^{-\lambda_2 T})} - \frac{QC_{O1}}{(1-e^{-\lambda_1 T})}}{\frac{C_{O2}(\text{added})}{(1-e^{-\lambda_2 T})}} \quad (39)$$

The following is a list of symbols used in the preceding section:

- a = fractional isotopic abundance
- A = area of the target in square centimeters
- B = total number of counts recorded by beam integrator
- $B_i$  = number of counts recorded by beam integrator during the ith interval
- $C_0$  = absolute counting rate at the end of bombardment

- $C_{01}$  = absolute counting rate of component 1 at end of bombardment
- $C_{02}$  = absolute counting rate of component 2 at end of bombardment
- $\Sigma C_{T2}$  = total observed activity of component 2 in count/min
- $\Delta t_i$  = duration of the ith interval (sec)
- $f(B_{ij})$  = a function of  $B_i$  and  $B_j$  defined by equation (26)
- $f(I_{ij})$  = a function of  $I_i$  and  $I_j$  defined by equation (20)
- $I$  = number of bombarding particles/sec
- $I_i$  = number of bombarding particles/sec during the ith interval
- $K$  = slope of integrator calibration curve, i.e., counts/min/ma
- $\lambda$  = decay constant
- $M$  = atomic weight
- $n$  = number of target nuclei per square centimeter
- $N$  = number of nuclei at time t
- $N_0$  = number of nuclei at the end of bombardment
- $N_T$  = total number of nuclei formed
- $N_{T1}$  = total number of nuclei of component 1 formed by nuclear reaction
- $N_{T2}$  = total number of nuclei of component 2 formed by nuclear reaction
- $\Sigma N_{T2}$  = total number of nuclei of component 2 formed by nuclear reaction plus recovered tracer
- $N'_{T2}$  = total number of nuclei of tracer of component 2

- $N_{T2}'$ (added) = total number of nuclei of tracer of component 2 added before chemical separation
- $N_{T2}'$ (recovered) = total number of nuclei of tracer of component 2 recovered in the counting sample
- Q = the ratio  $N_{T2}:N_{T1}$  from a bombardment in which no tracer was added
- $\sigma$  = cross section
- t = time after beginning of bombardment
- $t_i$  = time from the end of the ith interval to the end of bombardment in seconds
- T = duration of bombardment in seconds
- $\bar{T}$  = effective midpoint of bombardment defined in equation (35)
- w = weight of the target in milligrams
- Y = fractional chemical yield

## B. Bombardment Procedure

Targets of magnesium, sulfur, titanium, and cadmium were prepared as indicated in the Target Preparation Section, page 63, and placed in the slots of the target probe head, figure 3. Any of the several positions could have been used for the bombardments, but usually the target was bombarded in position 7, leaving position 8 for a collimator. Thus the effect of secondary electron emission from the target was diminished by the geometry (see figure 19). The collimator in position 8 was merely an additional aluminum target support frame without a film across the 2 1/4 inch hole. The 1/16 inch thickness of the aluminum was calculated to be sufficient to stop the deuteron beam plus any secondary protons produced in the aluminum.

The current integrator was warmed up for several hours and tested to see that it was functioning normally. A calibration check was made either before or after each bombardment following the secondary standardization method discussed in the Beam Determination Section, page 44. The "background" (charge collected or lost with no input current) was also checked to make sure it was not unduly high.

A scattering target of 1/4 mil Mylar was usually kept in the beam path (N of figure 1) during bombardment to assist in keeping the deuterons focused on the Faraday cup target. The scattered radiation from this foil was detected by the monitor counters (O of figure 1) and an audible signal was produced as well as a deflection on a meter located at the cyclotron control panel.

After bombardment, the target was dissolved and the chemical separation of the (d, $\alpha$ ) product performed (see Chemical Separation Section, page 72). The substrate was dissolved along with the target because it contained some product nuclei which had recoiled out of the target. The final counting sample was prepared on thin Zapon films as described in the Absolute Beta Counting Section, page 87. The decay was followed in the  $4\pi$  counter and the absolute value of  $C_0$  determined for each component of the decay curve.

### C. Magnesium Bombardments

The chart of the nuclides for the magnesium region is shown in figure 37. The products of the (d, $\alpha$ ) reaction on magnesium include two activities in sodium, the 15-hour  $\text{Na}^{24}$  and the 2.6-year  $\text{Na}^{22}$ . Sodium-24 decays with the emission of a 1.390 Mev  $\beta$ -ray, followed by two  $\gamma$ -rays in cascade. (180) Sodium-22 is a positron emitter of 0.542 Mev maximum energy, followed by a 1.277 Mev  $\gamma$  ray. (180) Recently electron-capture branching amounting to 7-11 per cent has been reported for  $\text{Na}^{22}$ . (181 - 183) No other activities were observed in the deuteron bombardments carried out in this work.

Five magnesium bombardments were obtained, the first of which was for the purpose of evaluating the chemical procedure (see Chemical Separation Section, page 75). The experimental data and the various derived quantities used in the determination of the cross section are pre-

## NUCLIDE CHART OF THE MAGNESIUM REGION

		Al <sup>23</sup> .13s	Al <sup>24</sup> 2.1s β <sup>+</sup> , γ	Al <sup>25</sup> 7.4s β <sup>+</sup>	Al <sup>26</sup> 67s   10 <sup>6</sup> y β <sup>+</sup>   β, γ	Al <sup>27</sup> 100	Al <sup>28</sup> 2.27m β <sup>-</sup> , γ	Al <sup>29</sup> 6.56m β <sup>-</sup> , γ
		Mg <sup>22</sup> .13s	Mg <sup>23</sup> 12s β <sup>+</sup>	Mg <sup>24</sup> 78.60	Mg <sup>25</sup> 10.11	Mg <sup>26</sup> 11.29	Mg <sup>27</sup> 9.5m β <sup>-</sup> , γ	Mg <sup>28</sup> 21h β <sup>-</sup> , γ
Na <sup>20</sup> .385s β <sup>+</sup>	Na <sup>21</sup> β <sup>+</sup>	Na <sup>22</sup> 2.6y β <sup>+</sup> , EC, γ	Na <sup>23</sup> 100	Na <sup>24</sup> 15h β <sup>-</sup> , γ	Na <sup>25</sup>			

Fig. 37. Chart of the nuclides showing possible products of deuteron reactions on magnesium.

sented in Table VI for the last four bombardments. The following additional factors are needed for the calculation of the cross section:

$$\begin{aligned}M &= 24.32 \\K_D &= 9.9 \pm 0.1 \text{ counts/min}/\mu\text{a} \\a(\text{Mg}^{26}) &= 0.1129 \\a(\text{Mg}^{24}) &= 0.7860\end{aligned}$$

The errors shown are standard deviations. Bombardments 2 and 3 were exploratory in nature but are included for the sake of completeness. The following paragraphs deal with the distinctive features of the individual bombardments.

#### Target Preparation

The preparation of the magnesium target has been discussed on page 66. In all but one of the targets, the magnesium covered a circular area just matching the 2 1/4 inch hole in the aluminum target support. Target No. 3 covered a rectangular area larger than the circular opening. This target (and to a lesser extent, target no. 5) was also peculiar in that it had the whitish cast referred to before on page 66. Target No. 3 was weighed before and after bombardment to estimate the amount of material lost from magnesium targets either in the cyclotron or in transit. This ~~did~~ not yield conclusive information, as the weight was 9.6796 g before compared to 9.7804 g after. The gain in weight may have been due to adsorption of moisture onto the plastic substrate.



Table VI. Summary of Bombardment Data for Mg(d,a)Na

Bombardment No.	2	3	4	5
Suppressor ring(volts) floating		1110	1113	1110
D. C. supply ( $\mu$ a)		5	5	10
Slits J(in.) vertical		0.250	0.500	0.500
horizontal	0.250	1.000	1.000	1.000
Slits L(in.) vertical	none	0.25	0.25	0.25
horizontal	none	0.50	0.50	0.50
Target N(mils of Mylar)	0.50	0.25	0.25	0.25
Target R position	1	7	7	7
w(mg)	27.1	21.8	16.0	18.5
A(cm <sup>2</sup> )	25.7	40.2	25.7	25.7
substrate	Teflon	Mylar	Mylar	Mylar
Integrator range	C	D	D	D
B(counts)	385.0	82.0	164.0	154.0
f(B <sub>ij</sub> ) (counts/sec)		0.001017	0.001998	0.001916
T(sec)	3600	5160	7817	4814
Number of Zapon layers on counting sample	1	4	4	4
Zapon soln. used (%)	33	50	50	50
C <sub>O1</sub> (Na <sup>24</sup> ) (counts/min)	68881 $\pm$ 366	162130 $\pm$ 1050	40398 $\pm$ 175	35885 $\pm$ 916
$\Sigma$ C <sub>O2</sub> (Na <sup>22</sup> ) (counts/min)	483.7 $\pm$ 1.5	1646 $\pm$ 6	300.5 $\pm$ 2.3	546.4 $\pm$ 4.2
Q	10.4 <sub>3</sub>	---	10.7 <sub>3</sub>	---
Na <sup>22</sup> tracer added ( $\mu$ l)	0	10	0	30
C <sub>O2</sub> '(added)(for 10 $\mu$ l)	0	1352 $\pm$ 4	0	21822 $\pm$ 1.9
Y		0.341		0.0435

### Chemical Procedure

The chemical procedure has been presented in figure 22. A noticeable residue was present in the counting sample prepared for  $4\pi$  counting in bombardments 2 and 3, so doubly distilled water was used to make up the eluting agent in bombardment 4, while the use of conductivity water ( $1 \times 10^{-6}$  ohm<sup>-1</sup>cm<sup>-1</sup>) reduced the residue even more in bombardment 5. A quick estimate of the amount of residue (from ~10 ml of eluate) present in the counting sample of bombardment 4 showed it to be below the detection limit (0.0001 g) of the Ainsworth type DLB balance.

The chemical yield was determined in bombardment 3 and 5 by adding tracer Na<sup>22</sup> produced in bombardment 1. The stock solution was stored in a polyethylene bottle, and 10  $\mu$ l aliquots were transferred to the Phillips beaker just prior to dissolving the target in bombardment 5, and about an hour before in bombardment 3. After the chemical separation was under way, 10  $\mu$ l aliquots were transferred to  $4\pi$  counting plates to determine the amount of Na<sup>22</sup> added as tracer. One 10  $\mu$ l sample was prepared in this way in bombardment 3 and three 10  $\mu$ l samples in bombardment 5. The aliquoting error was assessed in the latter case from the average of the three Na<sup>22</sup> counting rates. The  $4\pi$  plates used in each case were prepared identically to the ones used for the sample of the sodium separated from the target.

### Absolute Beta Counting

Discrimination curves were taken for the decay samples of bombardments 4 and 5. Curves obtained at various times after bombardment corresponding to 3 and 100 per cent of  $\text{Na}^{22}$  in the mixture of  $\text{Na}^{22}$  and  $\text{Na}^{24}$  are presented in figures 38 and 39 respectively. Each point has been corrected for the small amount of decay of the  $\text{Na}^{22}$  -  $\text{Na}^{24}$  mixture that occurs during the time in which the data were obtained. It can be seen that the discrimination plateau exhibits no evidence for a slope within the experimental error due to the counting statistics. The limits of this error are indicated at the bottom of the graphs; the length of the line represents twice the standard deviation of a single point. As seen from figure 38 and 39, altering the  $\text{Na}^{22}$  -  $\text{Na}^{24}$  ratio has no effect on shifting the plateau. Thus the error in the absolute counting rate due to inaccuracies in the gain, voltage, and discriminator settings is represented by the standard deviation of  $\pm 0.74$  per cent obtained from the average deviation in the points on the plateau of figure 38.

The effect of absorption of weak beta particles in the Zapon film was studied by a series of samples made with different numbers of backing films. Three typical absorption curves, taken from bombardment 4 are shown in figure 40. Each point has been corrected for decay which occurred during the time that the six samples were being counted. The points exhibit a scatter about a line drawn arbitrarily through the points and show no evidence for a slope. The errors indicated in

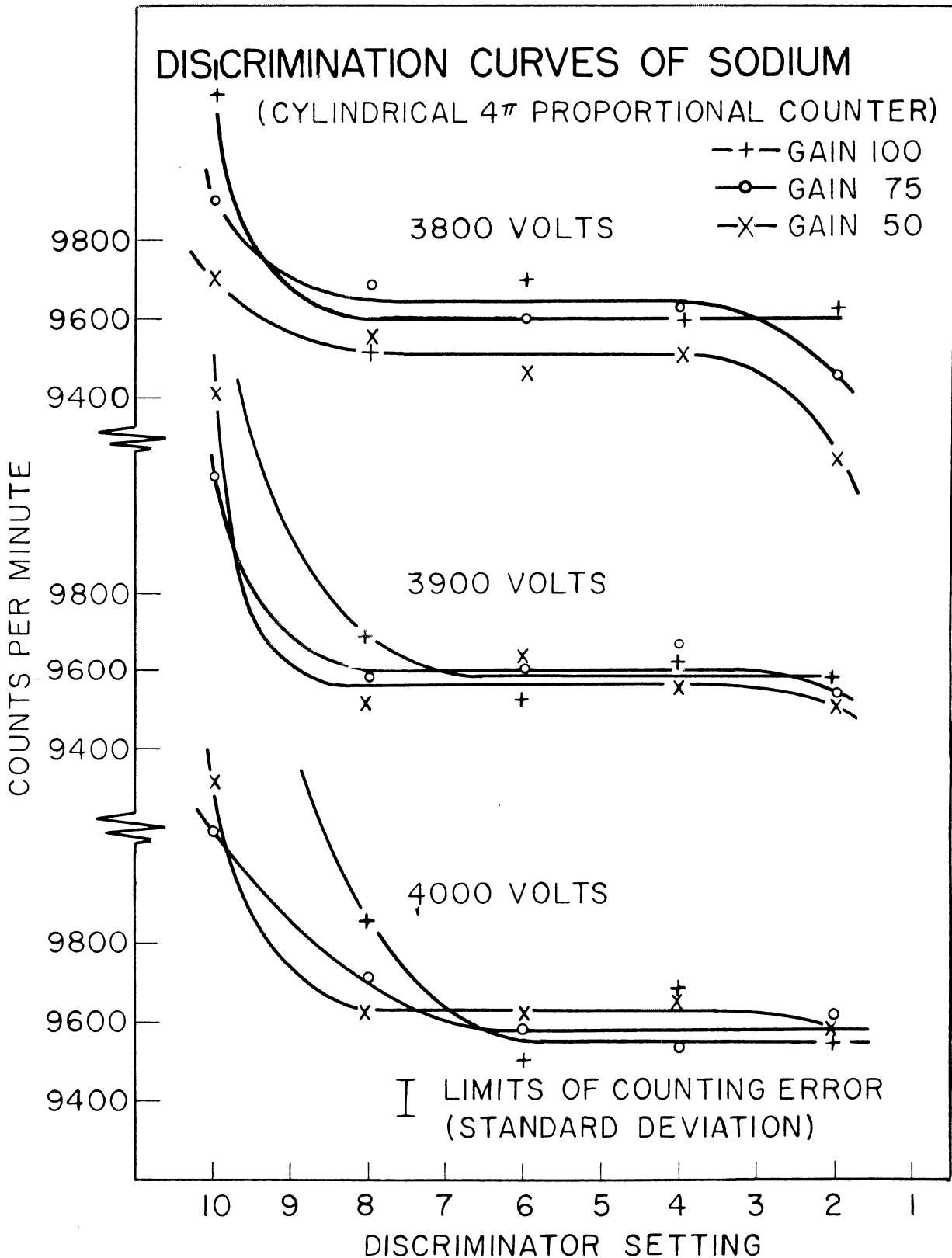


Fig. 38. Discrimination curves of a mixture of 3 per cent  $\text{Na}^{22}$  and 97 per cent  $\text{Na}^{24}$  taken from magnesium bombardment 4. The limits of counting error shown are twice the standard deviation of a single point.

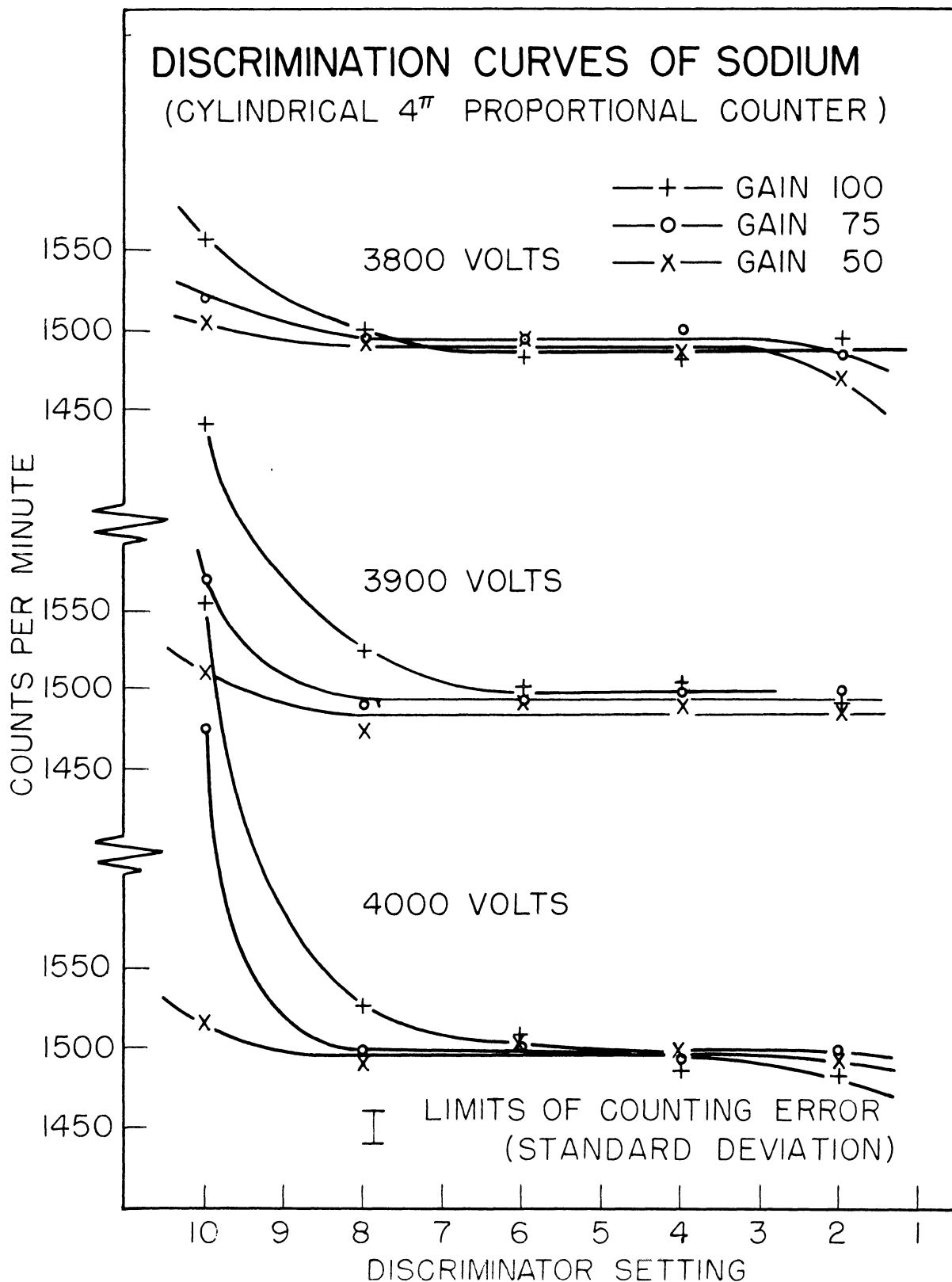


Fig. 39. Discrimination curves of 100 per cent Na<sup>22</sup> taken from magnesium bombardment 3. The limits of the counting error shown are twice the standard deviation of a single point.

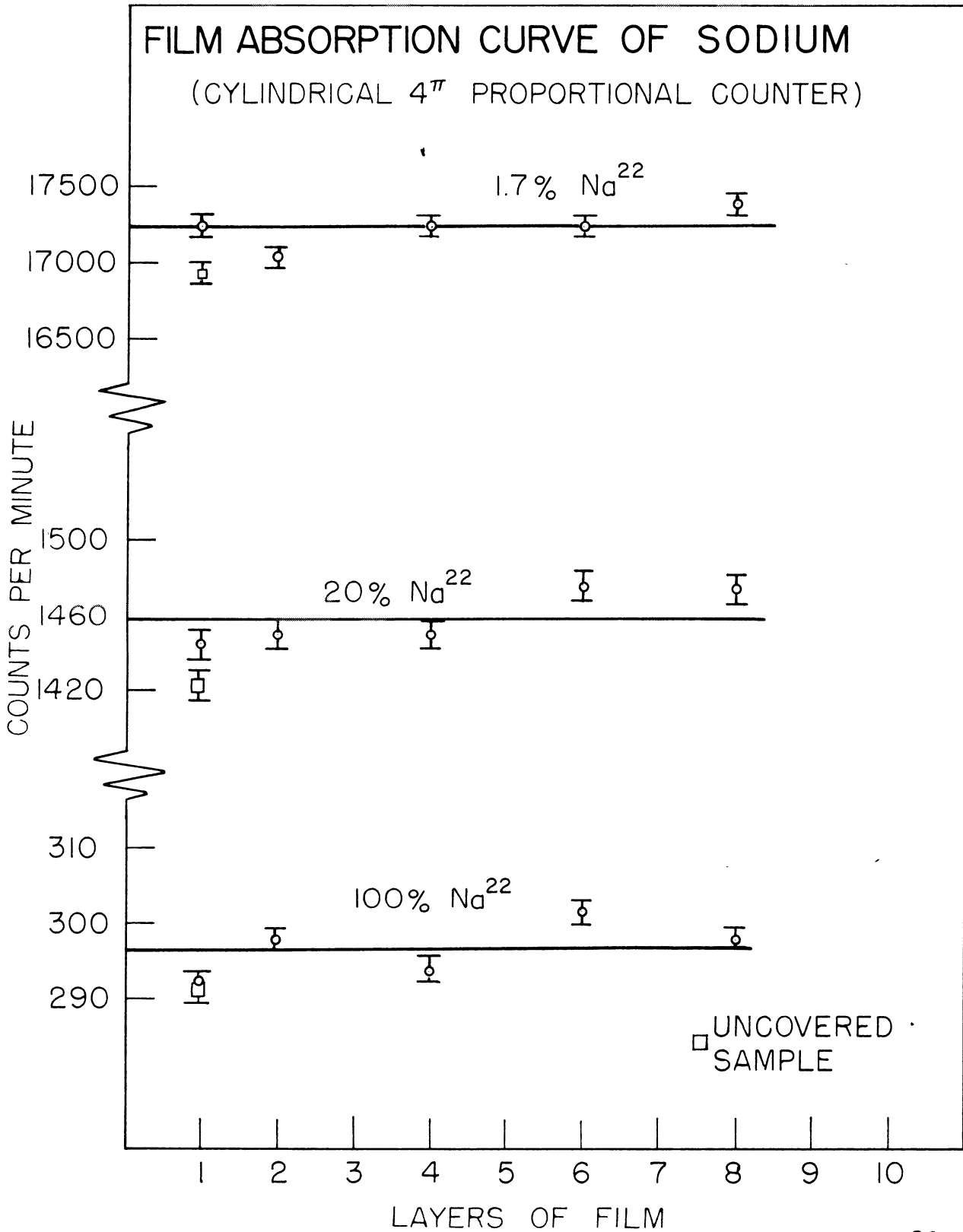


Fig. 40. Film absorption curve of various mixtures of Na<sup>22</sup> and Na<sup>24</sup> taken from magnesium bombardment 4. The errors shown are standard deviations due to counting statistics.

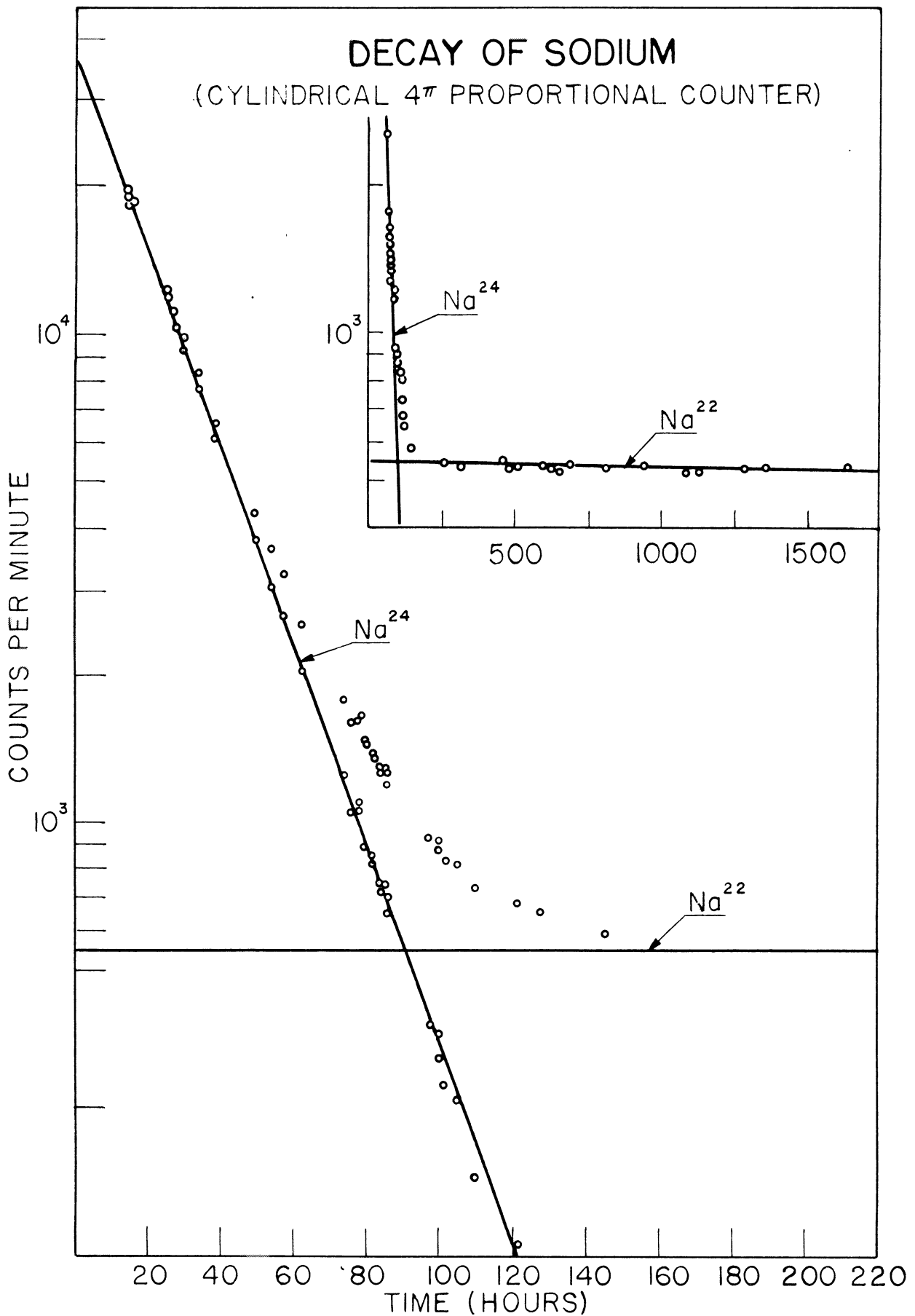


Fig. 41. Decay curve of sodium separated from magnesium resolved into the 2.6-year  $\text{Na}^{22}$  and 15-hour  $\text{Na}^{24}$  components by the method of least squares. The data were taken from magnesium bombardment 5.

figure 40 are standard deviations of the individual counts. The points, corresponding to different samples, do not fall on the curve because of the aliquoting error which has already been shown to be of the order of 2 per cent (see Table V). Figure 40 also shows that changing the  $\text{Na}^{22}$  -  $\text{Na}^{24}$  ratio produces no noticeable effect. The average of the points representing the covered samples was taken for each of the absorption curves, the average deviation in the points computed, and the corresponding standard deviation was calculated to be 0.43, 1.15, and 1.23 per cent, which is of the same order as the counting error.

#### Analysis of Decay Curves

It was felt that the decay data warranted treatment by the method of least squares, since the two nuclides encountered in the magnesium bombardments possess vastly different half-lives (15 hours compared 2.6 years), and can be produced in sufficient quantity to make it possible to obtain good counting statistics. A typical decay curve obtained from bombardment 5 is pictured in figure 41 showing the resolution into the two components.

The procedure followed for the least squares analysis was to set up "machine equations" (184) that facilitate the computation of the sums by use of a calculator. Computational errors were avoided by obtaining agreement between two persons as to the value of a summation before accepting it. Similar checking went into the conversion of calendar time to the number of hours after the end of bombardment. It was



decided to weight each of the points equally in spite of the fact that some were obviously better than others.

Half-Life of Na<sup>24</sup>. The gross decay curve was thus resolved by first finding the least squares line of best fit for the 2.6-year Na<sup>22</sup> component and then subtracting it from the gross curve to produce the points through which a line of best fit was computed by the same method as for the 15-hour Na<sup>24</sup>. Since the long-lived activity could not be followed for a time long enough to determine its half-life experimentally, the value of 2.60 years obtained by Laslett (135) was assumed for the purposes of this calculation. Laslett did not quote an error, but one may assume the uncertainty to be ~0.4 per cent. This will not affect the present decay curve analysis because of the relatively large difference in the Na<sup>22</sup> and Na<sup>24</sup> half-lives. The short-lived component, however, exhibited an exponential decay over factors of 150-4000, so that the half-life could be determined by least squares.

The decay curves were first analyzed graphically to determine which points should be included in the Na<sup>22</sup> analysis. In Table VII the half-life and intercept of the Na<sup>22</sup> and Na<sup>24</sup> obtained by the method of least squares are given together with the graphical resolution for comparison.

In bombardment 2 the Zapon film broke after most of the Na<sup>24</sup> had decayed, so the sample was repaired by sandwiching it between two additional Zapon films. Apparently some activity was lost in this operation as the Na<sup>24</sup> decay points deviated markedly from linearity after this happened and were

therefore neglected in calculating the half-life and intercept of the Na<sup>24</sup> component for bombardment 2.

Table VII. Analysis of Decay Curves of Sodium

	Bbdt. No.	Method of analysis	Half-life	Period of observation	CO (counts/min)
Na <sup>22</sup>	2	l. s.	2.60 <sup>a</sup> yr	0.64 yr	483.7±1.5
		graph.	"		485
	3	l. s.	"	0.21 yr	1646±6
		graph.	"		1650
	4	l. s.	"	0.18 yr	300.5±2.3
		graph.	"		298
	5	l. s.	"	0.16 yr	546.4±4.2
		graph.	"		545
Na <sup>24</sup>	2	l. s.	14.813±.025hr	100hr	68,881±366
		graph.	15.1 <sup>b</sup>		66,000
	3	l. s.	14.910±.025	144hr	162,130±1050
		graph.	15.1 <sup>b</sup>		157,000
	4	l. s.	15.002±.017	166hr	40,398±175
		graph.	15.1 <sup>b</sup>		40,000
	5	l. s.	14.946±.101	146hr	35,885±916
		graph.	15.1 <sup>b</sup>		36,000

a See reference (185)

b See reference (186)

The resolved lines, computed by least squares analysis have been depicted in figure 41 for bombardment 5. They are seen to pass through the points, as do for the points obtained by graphical resolution. The weighted average of the Na<sup>24</sup> half-life is compared with the values present in the literature in Table VIII. The value obtained in this work compares favorably with those of Solomon (188) and Tobailem (193) which seem to be the best values available.

Table VIII: Summary of Half-Lives of Na<sup>24</sup>

t 1/2 (Hours)	Authors	Reference	Period of Observation
14.97 <sub>±</sub> 0.01	Lockett and Thomas	187	5 Half-Lives
15.06 <sub>±</sub> 0.04	Sreb	186	
15.04 <sub>±</sub> 0.06 <sup>a</sup>	Solomon	188	13 Half-Lives
15.10 <sub>±</sub> 0.04	Cobble and Attleberry	189	
15.1 <sub>±</sub> 0.1	Wilson and Bishop (recalculated by Sreb)	190	2 Half-Lives
15.0 <sub>±</sub> 0.1 <sup>b</sup>	Sinclair and Holloway	191	
14.8 <sub>±</sub> ~1%	Van Voorhis	192	10 Half-Lives
14.90 <sub>±</sub> 0.05	Tobailem	193	(Differential Method)
14.93 <sub>±</sub> 0.04 <sup>a</sup>	This work		7-12 Half-Lives

<sup>a</sup> Standard Deviation

<sup>b</sup> Probable Error

Cross Section for Na<sup>22</sup> and Na<sup>24</sup>

As mentioned above, bombardments 2 and 3 were exploratory in nature, and the measurement procedures had not been developed to their fullest, whereas bombardments 4 and 5 were performed with much more refined techniques. Bombardments 2 and 4 were used to determine relative values, and 3 and 5 were used to determine absolute values of the cross section.

In bombardment 2 the traffic counter was not used with the integrator and hence  $f(B_{ij})$  could not be calculated. The residue on the  $4\pi$  plates was relatively large which could have resulted in an unknown amount of self absorption.

In bombardment 3 one circumstance which may have resulted in too low a value for  $\sigma$  was that the target was suspected of having some oxide impurity. Another unknown error acting in the same direction was the possible self absorption due to the residue on the  $4\pi$  plate. There were three sources of error in this bombardment acting to give too high a value of  $\sigma$ . First, the magnesium target extended beyond the area defined by the 2 1/4 inch collimator (spare target mount), and the possibility exists that a contribution to the yield of Na<sup>24</sup> was made by the reaction  $Mg^{24}(n,p) Na^{24}$  resulting from neutrons produced in the collimator. Secondly, by adding the tracer an hour before dissolution of the target, some Na<sup>22</sup> may have exchanged with the sodium of the Pyrex beaker. Thirdly, the aliquots made for determining  $C'_{O_2}$  (added) were taken several hours after adding the tracer to the Phillips

beaker. Since the volume of the  $\text{Na}^{22}$  solution was only ~2 ml, evaporation from the solution may have produced a significant change in concentration which would have resulted in too high a value of  $C'_{\text{O}_2}$  (added). Moreover only one sample of the tracer was prepared to determine  $C'_{\text{O}_2}$  (added).

In bombardment 5 the target may have had a slight amount of oxide impurity, and the aliquots of the tracer were taken several hours after adding the tracer to the Phillips beaker.

The results of bombardments 4 and 5 were obtained using much better techniques than bombardments 2 and 3, as seen from the above considerations, and therefore the cross sections are based upon bombardments 4 and 5 only. The values are

$$\begin{aligned}\sigma(\text{Na}^{22}) &= 0.151 \pm 0.006 \text{ barns at } 7.8 \pm 0.1 \text{ Mev} \\ \sigma(\text{Na}^{24}) &= 0.094 \pm 0.004 \text{ barns at } 7.8 \pm 0.1 \text{ Mev,}\end{aligned}$$

calculated with the aid of equations (25) and (38).

The cross section for the formation of  $\text{Na}^{22}$  has been corrected for electron-capture branching as follows. The branching ratio has been reported variously as 7.1 per cent, (181) 11.0 per cent, (182) and 6.5 per cent. (183) Assuming a value of 8 per cent, and the counting efficiency of the  $4\pi$  counter to be 5 per cent for electron-capture events, the overall counting efficiency of the  $4\pi$  counter for  $\text{Na}^{22}$  becomes 96 per cent. This is the value which Sherr and Liller (182) determined experimentally for the Borkowski  $4\pi$  counter, and was used to calculate the cross section for  $\text{Na}^{22}$  quoted above.

The errors in the cross sections quoted above are based upon the errors associated with each of the factors of equations (25) and (38), and may be considered to be an estimate of the standard deviation. The component errors which were assumed in the propagation are listed in Table IX.

Table IX. Propagation of Errors  
in Cross Section for  $\text{Hg}(d,\alpha)\text{Na}$

Factor	Estimated Standard Deviation (per cent)	
	Bombardment No.4	Bombardment No.5
$C_{02}$	0.77	0.77
T	0.01	0.01
$(1-e^{-\lambda_2 T})$	0.19	0.19
$C_{01}$	0.43	2.55
B	0.03	0.03
$f(B_{ij})$	0.03	0.03
Q, eqn.(29)	0.91	
$C'_{02}$ (added)		0.09
Y, eqn.(38)		2.93
$A/w$		0.47
M		.02
$K_D$		1.01
$a(\text{Mg}^{26})$		.05
$a(\text{Mg}^{24})$		.01
$\sigma(\text{Na}^{24})$ , eqn.(25)		4.04
$\sigma(\text{Na}^{22})$ , eqn.(30)	4.15	

Excitation functions of the Mg(d,  $\alpha$ ) Na reactions have been previously reported by Irvine and Clarke (194) and Bartell and Softky.(195). Reading the cross section values at 7.8 Mev from their published graphs, 0.092 and 0.147 barns were obtained for Na<sup>24</sup> and Na<sup>22</sup> yields from Irvine and Clarke's work, and 0.009 barns was obtained for the Na<sup>22</sup> yield from Bartell and Softky's results. The results of the present investigation are seen to duplicate those of Irvine and Clarke quite closely.

#### D. Sulfur Bombardments

The chart of the nuclides for the sulfur region is shown in figure 42. There is only one (d,  $\alpha$ ) reaction product of sulfur that is long-lived enough to observe conveniently. This is the 14.3-day P<sup>32</sup> which decays by the emission of a 1.701 Mev  $\beta$  ray. (180) It was the only activity observed in the bombardments of sulfur.

Five sulfur bombardments were obtained, the first of which was for the purpose of evaluating the chemical procedure (see Chemical Separations Section, page 78).

Bombardments 2 and 5 were worthless, as the sulfur was vaporized by the cyclotron beam. The experimental data and derived quantities for bombardments 3 and 4 are presented in Table K. The following additional factors are needed for calculation of the cross section:

$$M = 32.066$$

$$K_D = 9.9 \pm 0.1 \text{ counts/min}/\mu\text{a}$$

$$a(S^{34}) = 0.04215$$

## NUCLIDE CHART OF THE SULFUR REGION

			Cl <sup>33</sup> 2.8s $\beta^+$	Cl <sup>34</sup> 33.2m $\beta^+, \gamma$	Cl <sup>33</sup> 75.4	Cl <sup>36</sup> $4.4 \times 10^5$ y $\beta^-$	Cl <sup>37</sup> 246	Cl <sup>38</sup> 37.29m $\beta^-, \gamma$	Cl <sup>39</sup> 55.5m $\beta^-, \gamma$
		S <sup>31</sup> 3.18s $\beta^+$	S <sup>32</sup> 95.018	S <sup>33</sup> 0.750	S <sup>34</sup> 4.215	S <sup>35</sup> 87.1d $\beta^-$	S <sup>36</sup> 0.017	S <sup>37</sup> 5.04m $\beta^-, \gamma$	
P <sup>28</sup> .2s $\beta^+, \gamma$	P <sup>29</sup> 4.57s $\beta^+, \gamma$	P <sup>30</sup> 2.5m $\beta^+$	P <sup>31</sup> 100	P <sup>32</sup> 14.3d $\beta^-$	P <sup>33</sup> 24.4d $\beta^-$	P <sup>34</sup> 12.4s $\beta^-$			

Fig. 42. Chart of the nuclides showing possible products of deuteron reactions on sulfur.



The errors given are estimated standard deviations. The distinctive features of bombardments 3 and 4 are treated below.

#### Target Preparation

The preparation of the sulfur target has been described on page 67. Target No. 4 was weighed before and after bombardment and it was found to have lost 8.2 mg, or 11 per cent, during the irradiation. Inspection revealed that within the area struck by the beam there appeared to be less sulfur than was originally present. Thus it seemed that sealing the target between two layers of polystyrene was not 100 per cent effective in preventing vaporization of the sulfur by the beam.

#### Chemical Procedure

The chemical procedure has been presented as figure 23. Difficulty was experienced in dissolving target No. 4. It was finally found necessary to heat the mixture strongly for a few minutes after 7 hours of less vigorous treatment. Since sulfuric acid was present the possibility existed for some phosphorus to escape before the tracer had the opportunity to complete the interchange with the (d, a) product.

The tracer used for chemical yield determination in bombardment 4 was the 24.4-day  $P^{33}$ . This was obtained by allowing the 14.3-day  $P^{32}$  to decay from several old bottles of high specific activity  $P^{32}$  (Carbide and Carbon Chemicals Co., Oak Ridge National Laboratory, Oak Ridge, Tennessee, Catalog No. P-32-P-11). Two 100  $\mu$ l samples of the tracer

Table X. Summary of Bombardment Data for S(d, $\alpha$ )P

Bombardment No.	3	4
Suppressor ring (volts)	floating	1110
D. C. supply ( $\mu$ a)	25	10
Slits J (in.) vertical		0.500
horizontal		1.000
Slits L (in.) vertical	none	0.25
horizontal	none	0.50
Target N(mils of Mylar)		0.25
Target R position	3	7
w(mg)	74.1	73.7
A(cm <sup>2</sup> )	25.7	25.7
substrate	polystyrene	polystyrene
Integrator range	D	D
B(cnts)	324+	64
T(sec)	6060	4879
Number of Zapon layers	5	2
Zapon soln. used (%)	50	50
C <sub>O1</sub> (P <sup>32</sup> ) (cnts/min)	40,000	9700 $\pm$ 200
C <sub>O2</sub> (P <sup>33</sup> ) (cnts/min)	0	1750 $\pm$ 100
P <sup>33</sup> tracer added ( $\mu$ l)	0	750
C <sub>O2</sub> ' (added) (for 100 $\mu$ l)	0	1173 $\pm$ 33
Y		0.20

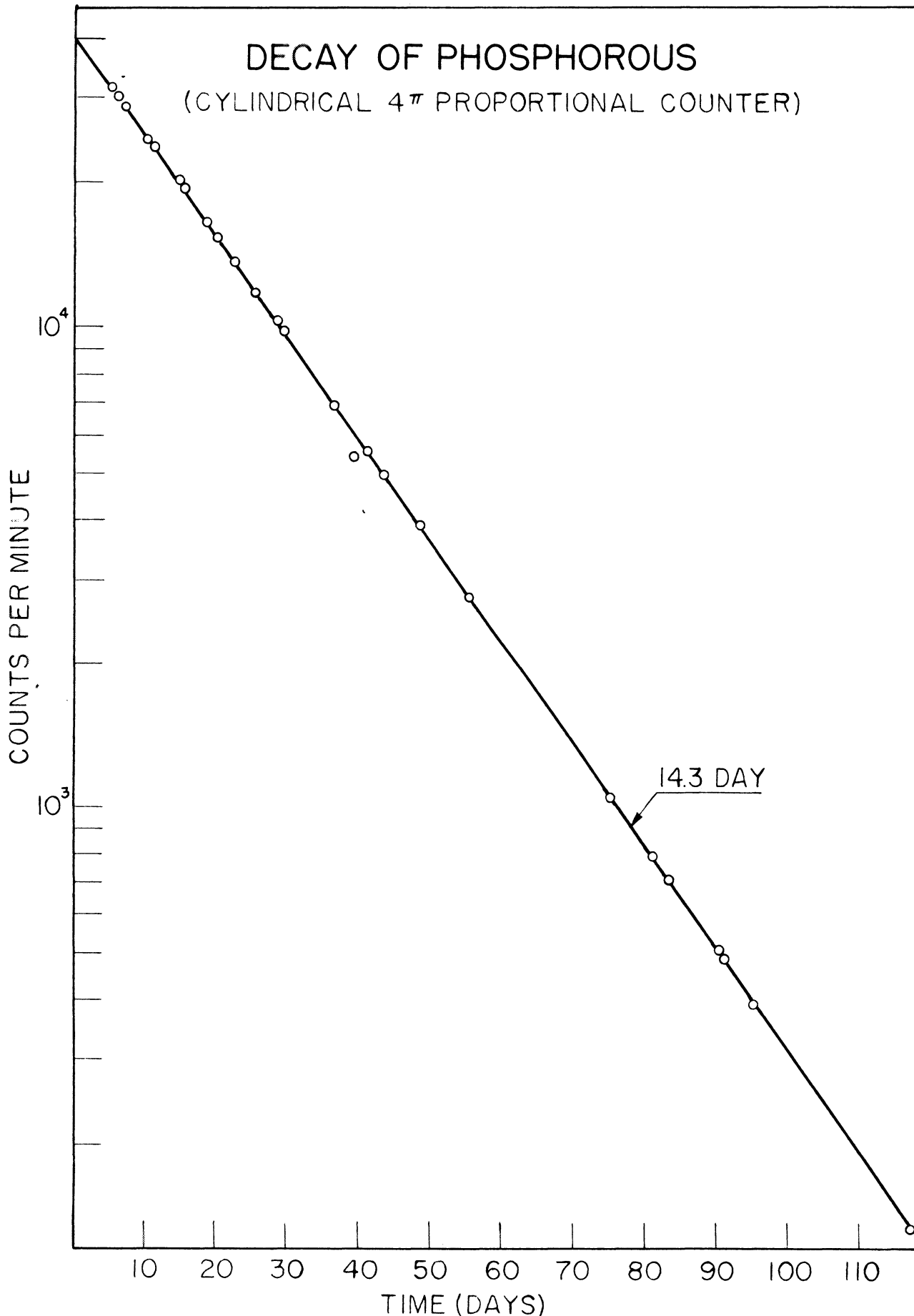


Fig. 43. Decay curve of phosphorus separated from sulfur showing the decay of 14.3-day  $P^{32}$ . The data were taken from sulfur bombardment 3.

were made to determine the amount of tracer added, one at the same time and one 30 minutes after adding 750  $\mu$ l of the tracer to the Phillips beaker. The  $4\pi$  counting plates used for the tracer and for the separated phosphorus were prepared under identical conditions.

An insignificant amount of  $P^{33}$  is produced in the bombardment from secondary neutrons as indicated by the absence of a significant amount of activity with a half-life greater than 14.3 days. This is shown in figure 43, taken from sulfur bombardment No. 3 in which no  $P^{33}$  tracer was added. An upper limit of 0.6 per cent of the initial activity could possibly be attributed to  $P^{33}$ .

#### Absolute Beta Counting

Discrimination curves had previously been taken of  $P^{32}$  when the work with the National Bureau of Standards  $P^{32}$  sample was done (see page 114), so only enough curves were taken with the (d, a) product to determine the voltage, gain, and discriminator settings to count the sample. These curves are shown in figure 44 and correspond to 77 per cent  $P^{32}$  in the mixture of  $P^{32}$  and  $P^{33}$ . Note that the characteristics of the counter have changed since the work was done on the NBS sample so that the discrimination plateau has shifted towards a higher bias potential. The magnitude of the error due to a possible slope should not be affected, so that the limits of this error can be taken to be the same as previously determined.

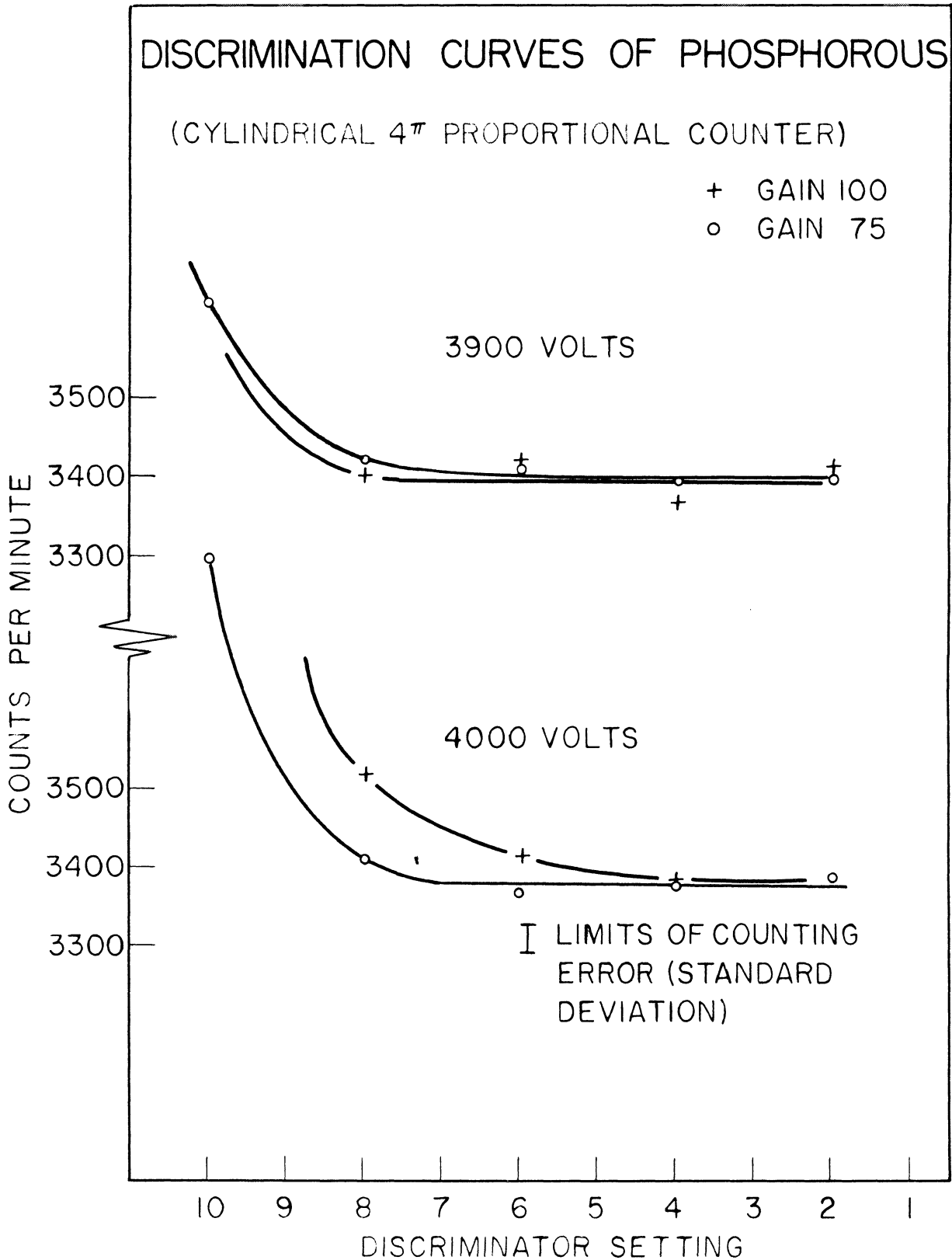


Fig. 44. Discrimination curves of a mixture of 77 per cent P<sup>32</sup> and 23 per cent P<sup>33</sup> taken from sulfur bombardment 4. The limits of counting error shown are twice the standard deviation of a single point.

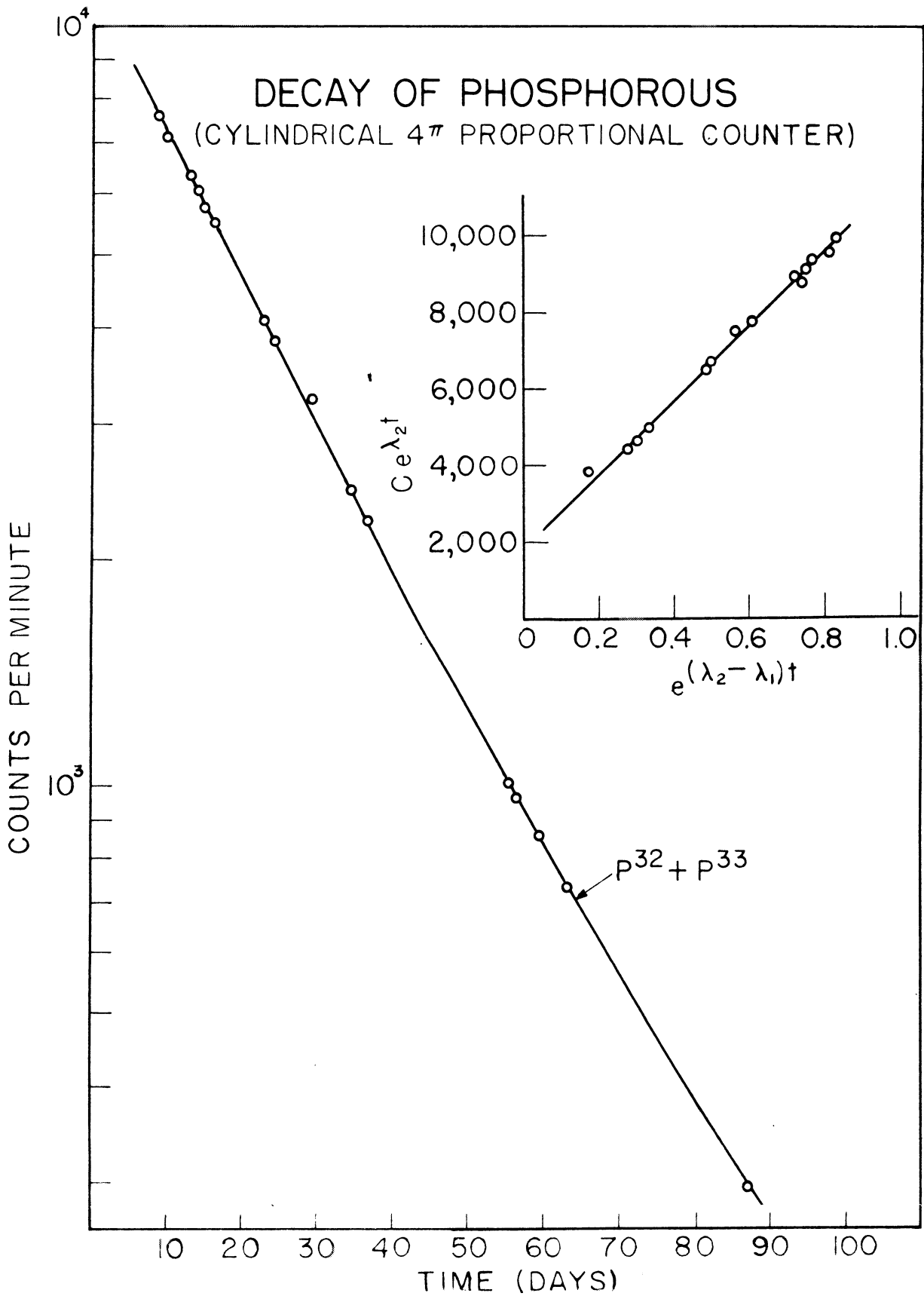


Fig. 45. Decay curve of phosphorus separated from sulfur. The resolution is shown in the insert, the slope and intercept giving the initial activities of the P<sup>32</sup> and P<sup>33</sup> respectively. The data were taken from sulfur bombardment 4.

Similarly, the film absorption problem had been investigated before (see page 1C2).

### Analysis of Decay Curves

The decay curve of the phosphorus sample from bombardment 4 is given in figure 45. Since the two component half-lives are so close together as to make ordinary graphical analysis extremely difficult, the data was treated by a method indicated by Worthing and Geffner (196) and applied by Biller (197). The gross decay curve given by

$$C = C_{01}e^{-\lambda_1 t} + C_{02}e^{-\lambda_2 t} \quad (40)$$

may be rearranged as follows:

$$C e^{\lambda_2 t} = C_{01} e^{(\lambda_2 - \lambda_1)t} + C_{02} \quad (41)$$

The left hand member of equation (41) is plotted against  $e^{(\lambda_2 - \lambda_1)t}$  to give a linear curve whose slope and intercept are respectively  $C_{01}$  and  $C_{02}$ . The insert of figure 45 shows such a plot when applied to  $P^{32}$  and  $P^{33}$  as components 1 and 2 of the gross decay curve, giving the values appearing in Table X.

The decay of the  $P^{33}$  tracer is shown in figure 46. Although most of the  $P^{32}$  had decayed, there is some longer-lived activity than the 24.4-day  $P^{33}$ . Unfortunately the tracer was not purified before use in bombardment 4, so for the purposes of calculation it was assumed that the contaminant was 87.1-day  $S^{35}$  which is also produced when sulfur is

irradiated with pile neutrons. The decay curve was resolved into the 24.4-day and 87.1-day components by application of equation (41). This is shown in the insert of figure 46 where the intercept is the initial activity of  $S^{35}$  and the slope is the initial activity of the  $P^{33}$ ,  $-C'_{O_2}(\text{added})$ , as given in Table X. In this graph the points corresponding to both samples are plotted, illustrating the aliquoting error.

#### Cross Section for $P^{32}$

The accuracy of these experiments is in doubt due to the several unknown errors associated with the sulfur bombardments.

As mentioned above, bombardments 2 and 5 yielded no results, and bombardment 3 was used to obtain relative yields (in this case,  $Q = 10$ ). Bombardment 4 was the only one in which the absolute cross section of  $P^{32}$  was measured, and unfortunately it was impossible to obtain another bombardment to determine the cross section more accurately. The loss of sulfur from the target when it was struck by the beam may have amounted to ~10 per cent, and possibly resulted in an error in  $\sigma$  of several times 10 per cent. This would be the case if the sulfur was lost from the one-half square inch area that was hit by the beam. Likewise any  $P^{33}$  tracer lost by the sulfuric acid treatment of the target would also lead to too low a result. The variation in target thickness was estimated at ~2 per cent, but may have been larger. The radioactive impurity in the  $P^{33}$  tracer and the difficulty in the resolution of the  $P^{32-33}$  decay curve led to sizable errors, but certainly small compared to the above unknown errors.



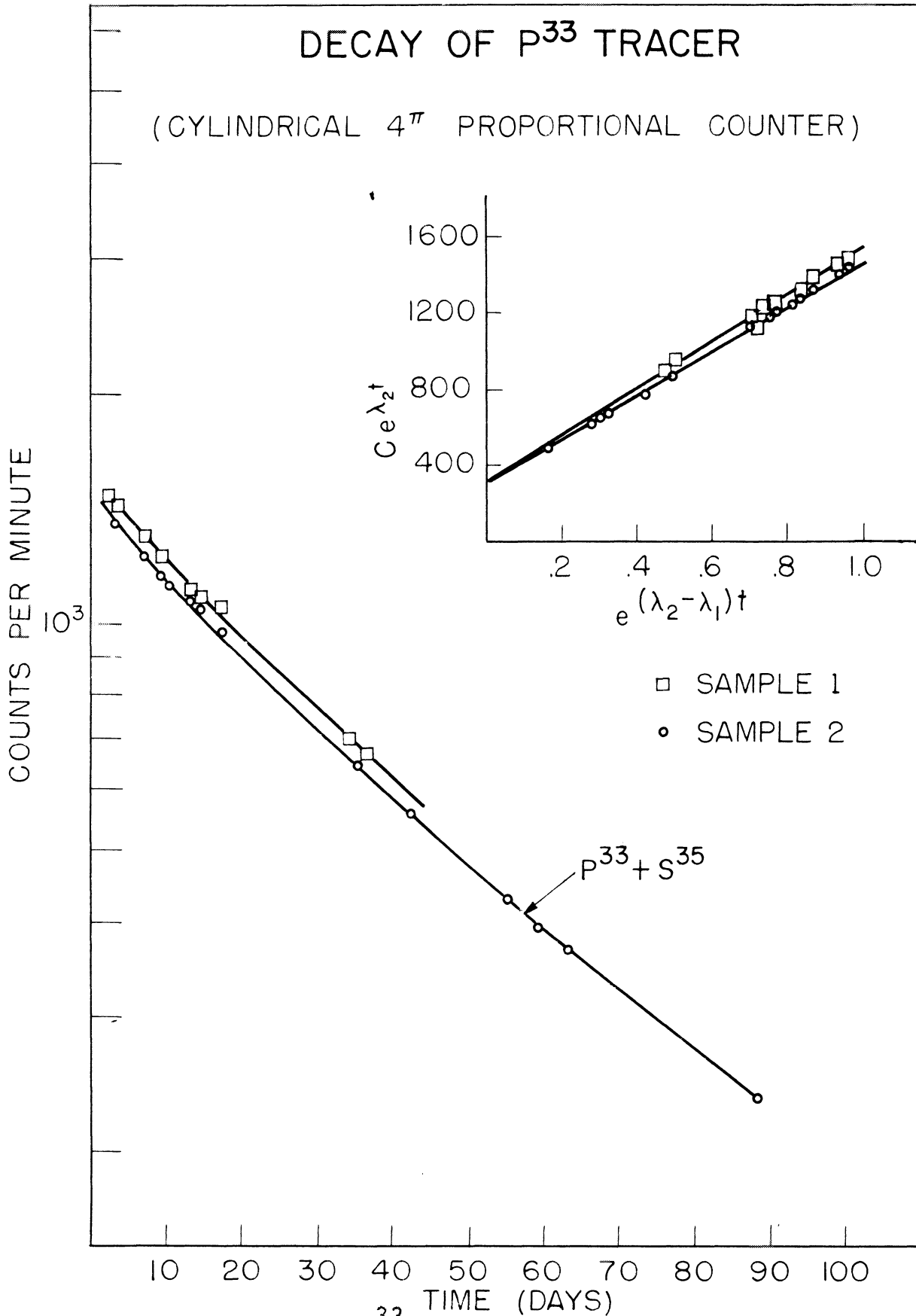


Fig. 46. Decay curve of P<sup>33</sup> tracer. The resolution into the P<sup>33</sup> and assumed S<sup>35</sup> components is shown in the insert, the slope and intercept giving the initial activities of p<sup>37</sup> and s<sup>35</sup> respectively. The data were taken from sulfur bombardment 4.

The cross section, calculated with the aid of equations (27) and (39) is

$$\sigma(P^{32}) = 0.3 \pm 0.2 \text{ barn at } 7.7 \pm 0.1 \text{ Mev.}$$

The uncertainties introduced by target vaporization and chemical yield determination were so large as to outweigh the errors inherent in the individual factors as outlined for magnesium, page 157 . Furthermore there was no way to assess the magnitude of these large errors, so that the error in the cross section quoted above is merely the writer's surmise of the standard deviation.

#### E. Titanium Bombardments

The chart of the nuclides for the titanium region is shown in figure 47. Three of the (d,  $\alpha$ ) reaction products of titanium possess half-lives of the same order of magnitude: 2.4-day  $Sc^{44}$ , 3.44-day  $Sc^{47}$ , and 44-hour  $Sc^{48}$ . The 2.4 day isomer decays by internal transition to 3.9-hour  $Sc^{44}$  which in turn decays with the emission of a 1.46 Mev  $\beta$  ray to stable  $Ca^{44}$ . Scandium 47 and 48 decay by the emission of 0.61 and 0.64 Mev  $\beta$  rays respectively accompanied by  $\gamma$  radiation. The fourth (d,  $\alpha$ ) product is  $Sc^{46}$ . The 19.5 second isomer decays to the 85-day ground state of  $Sc^{46}$  which emits a  $\gamma$  ray and a 0.36 Mev  $\beta$  ray. (180)

Five bombardments of titanium were obtained, the first of which was for the purpose of evaluating the chemical procedure (see Chemical Separations Section, page 80).

The experimental data and derived quantities for the other

NUCLIDE CHART OF THE TITANIUM REGION

$Sc^{40}$ ~3s $\beta^+, \gamma$	$Sc^{41}$ 873s $\beta^+$	$Ti^{44}$ >23y $\beta^-, \gamma$	$Ti^{45}$ 3.09h $\beta^+, \gamma$	$V^{47}$ 32m $\beta^+$	$V^{48}$ 16.3d $\beta^+, EC, \gamma$	$V^{49}$ 635d EC, $\gamma$	$V^{50}$ 0.24	$V^{51}$ 99.76	$V^{52}$ 3.75m $\beta^-, \gamma$	$V^{53}$ 23h $\beta^-, \gamma$
		$Ti^{46}$ 7.95	$Ti^{47}$ 7.75	$Ti^{48}$ 73.45	$Ti^{49}$ 5.51	$Ti^{50}$ 5.34	$Ti^{51}$ 5.8m $\beta^-, \gamma$			
		$Sc^{43}$ 3.9h $\beta^+, \gamma$	$Sc^{44}$ 2.4d; 39h IT   $\beta^-, EC, \gamma$	$Sc^{45}$ 100	$Sc^{46}$ 19.5s; 85d IT   $\beta^-, \beta^+, \gamma$	$Sc^{47}$ 3.44d $\beta^-, \gamma$	$Sc^{48}$ 44h $\beta^-, \gamma$	$Sc^{49}$ 57m $\beta^-$		

Fig. 47. Chart of the nuclides showing possible products of deuteron reactions on titanium.

Table XI. Summary of Bombardment Data for Ti(d, $\alpha$ )Sc

Bombardment No.	2	3	4	5
Suppressor ring (volts)	1100	1105	1095	1090
D. C. supply ( $\mu$ a)	2.5	48	30	38
Slits J(in.) vertical	0.250	none	none	none
horizontal	1.000	none	none	none
Slits L(in.) vertical	0.25	0.25	none	0.25
horizontal	0.50	0.50	none	0.50
Target N(mils of Mylar)	0.25	none	0.25	0.25
Target R position	8	7	7	7
w/A ( $\text{mg}/\text{cm}^2$ )	29	29	29	29
"substrate"			Mylar	Mylar
Integrator range	B	D	D	D
B(cnts)	1726	178	240	210
T(sec)	8340	4573	13051	6809
Number of Zapon layers	4	2	2	2
Zapon soln. used (%)	50	50	50	50
$C_{O1}(\text{Sc}^{44-47-48})$ (cnts/min)	253 $\pm$ 45	199 $\pm$ 100	574 $\pm$ 10	707 $\pm$ 15
Half-life of $\text{Sc}^{44-47-48}$ (days)	2.63	2.91	2.82	2.82
$\Sigma C_{O2}(\text{Sc}^{46})$ (cnts/min)	80 $\pm$ 10	510 $\pm$ 15	244 $\pm$ 6	277 $\pm$ 4
$Q$	10.09	7.72 $\pm$ .49		
$\text{Sc}^{46}$ tracer added ( $\mu$ l)	0	0	10	20
$C_{O2}'$ (added)	0	0	1581 $\pm$ 8	3055 $\pm$ 34
Y			0.060 $\pm$ .009	0.022 $\pm$ .004

four bombardments are presented in Table XI. In addition the following factors are needed for the cross section calculation:

$$\begin{aligned}M &= 47.90 \\K_D &= 9.9 \pm 0.1 \text{ counts/min}/\mu\text{a} \\a(\text{Ti}^{48}) &= 0.7345\end{aligned}$$

The errors given are estimated standard deviations. The distinctive features of the individual bombardments are treated below.

#### Beam Determination

It was noted that in bombardment 4 the traffic counter occasionally introduced extraneous charges into the current integrator. The check on the calibration factor showed that it may have been high by about 0.25 per cent for bombardments 4 and 5.

#### Target Preparation

The titanium foil used for the targets has been described on page 69. The metal was cut into pieces slightly larger than the opening in the target support which was specially made from 1/16 inch aluminum. The opening was a rectangular hole measuring 1/2 x 1 inch machined in the center of the target support. The target was Scotch-taped to the back of the support, so that the rectangular opening defined the area of the titanium hit by the deuterons. In the absolute determinations, 0.001 inch Mylar films were placed behind the foil to serve as catchers for recoil in the same way as the target substrates served for the other target elements.

### Chemical Procedure

The chemical procedure of figure 24 was followed except for minor changes. In bombardment 3, the scandium was carried through four cycles instead of the usual three. Conductivity water wasn't used for the preparation of reagents until bombardments 4 and 5, so that more solid matter was present on the  $4\pi$  samples in the earlier runs.

The tracer used was high specific activity 85-day  $\text{Sc}^{46}$  (Carbide and Carbon Chemicals Co., Oak Ridge National Laboratory, Oak Ridge, Tennessee, Catalogue No. Sc-46-P). The solution of  $\text{Sc}^{46}$  used in the chemical yield determination was processed through two cycles of the chemical separations procedure used in the titanium bombardments. About 20 ml of the purified  $\text{Sc}^{46}$  solution was stored in a polyethene bottle. Three samples of the  $\text{Sc}^{46}$  solution for the determination of the amount of tracer added were prepared at the same time as an equal aliquot was added to the Phillips beaker. In bombardment 4 this was done after a homogeneous solution was obtained, and in bombardment 5 before the target was dissolved. The  $4\pi$  plates used for the tracer were identical to those used for the chemically separated product.

### Absolute Beta Counting

Discrimination curves for scandium are shown in figures 48 and 49 corresponding to 70 and 100 per cent 85-day  $\text{Sc}^{46}$  respectively in the  $\text{Sc}^{44}$ - $\text{Sc}^{46}$ - $\text{Sc}^{47}$ - $\text{Sc}^{48}$  mixture. The data were taken on the sample from titanium bombardment 4 and were corrected for decay. The standard deviation

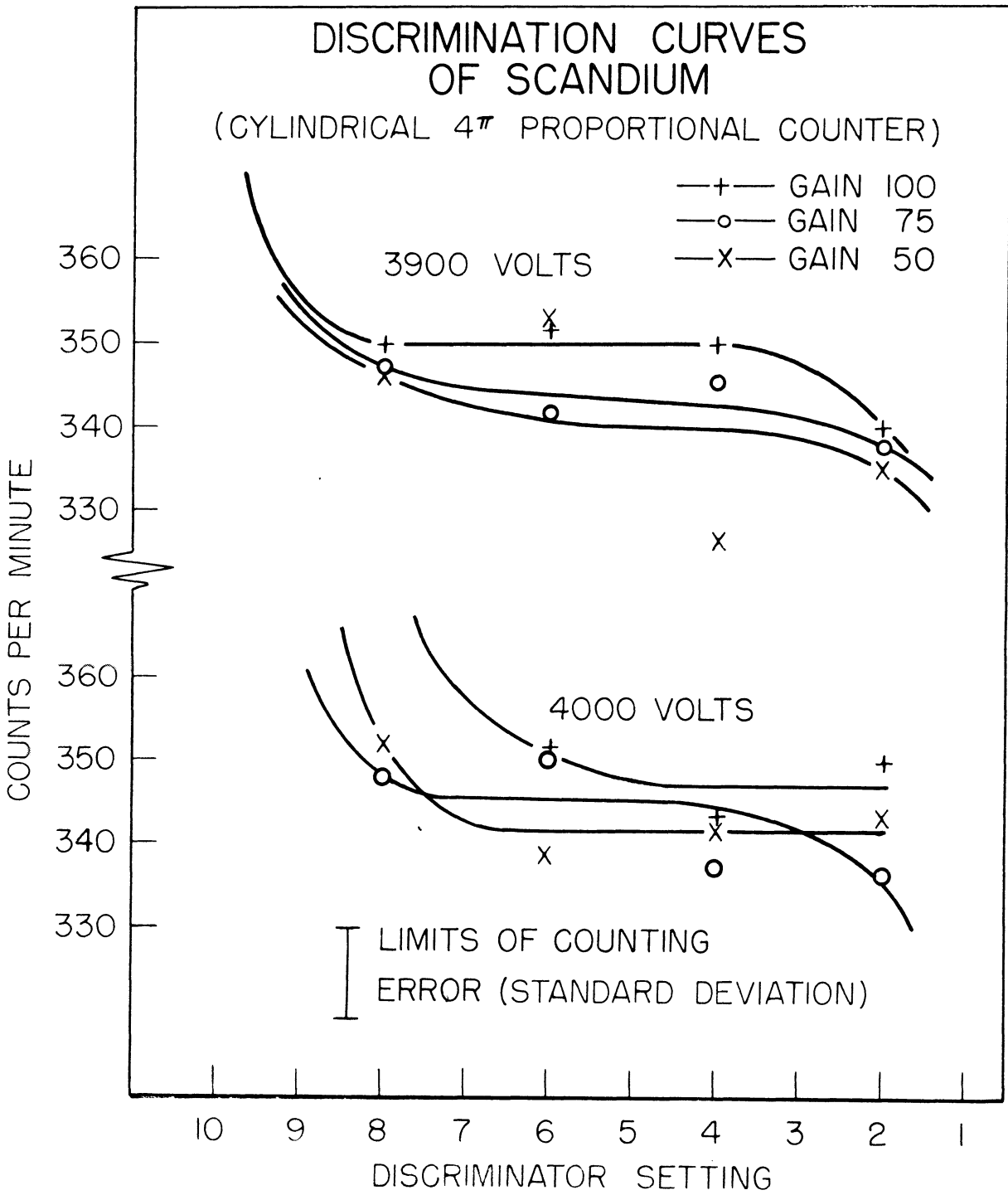


Fig. 48. Discrimination curves of a mixture of 70 per cent  $Sc^{46}$  and 30 per cent  $Sc^{44} + Sc^{47} + Sc^{48}$  taken from titanium bombardment 4. The limits of the counting error shown are twice the standard deviation of a single point.

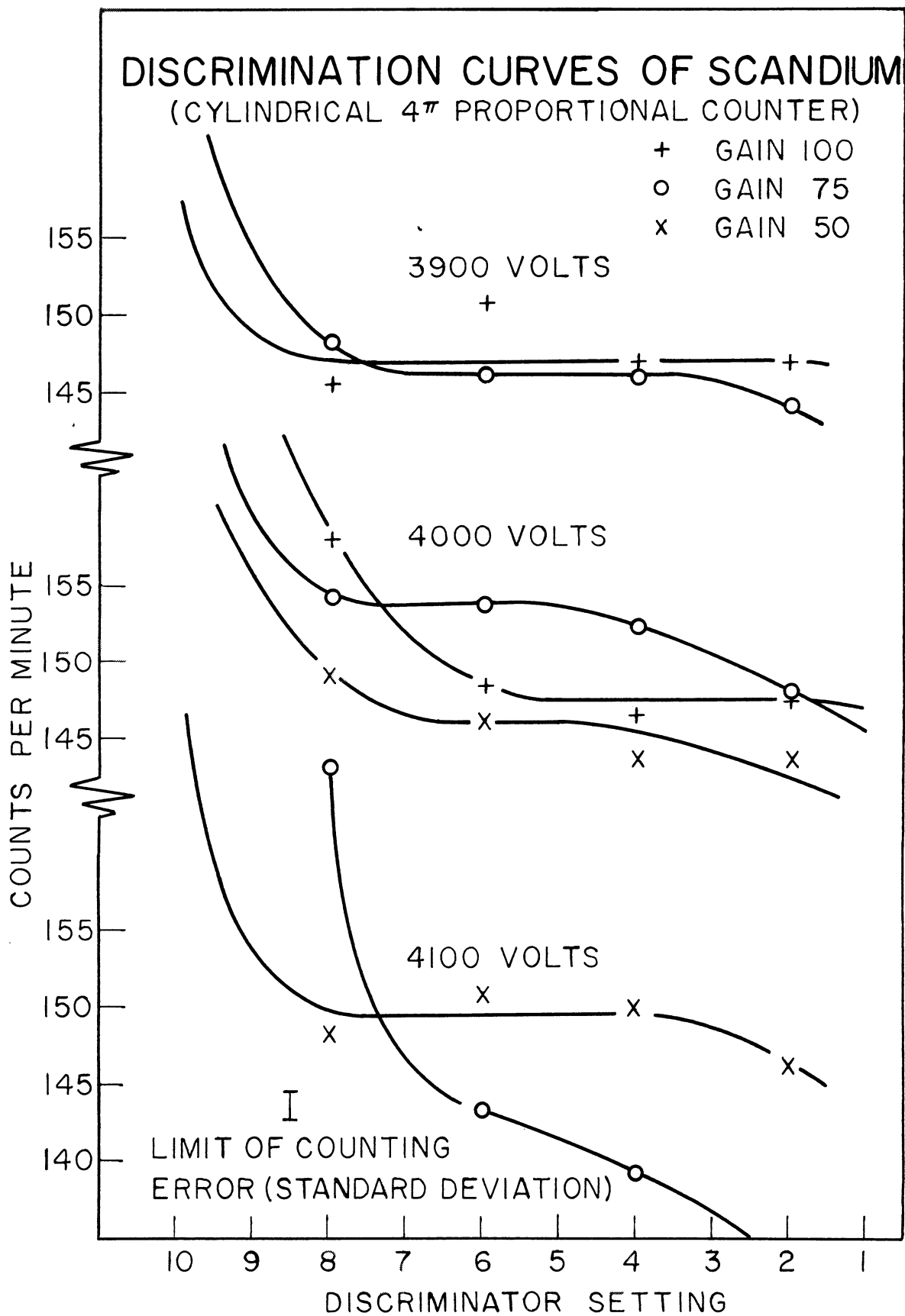


Fig. 49. Discrimination curves of 100 per cent  $Sc^{46}$  taken from titanium bombardment 4. The limits of the counting error shown are twice the standard deviation of a single point.



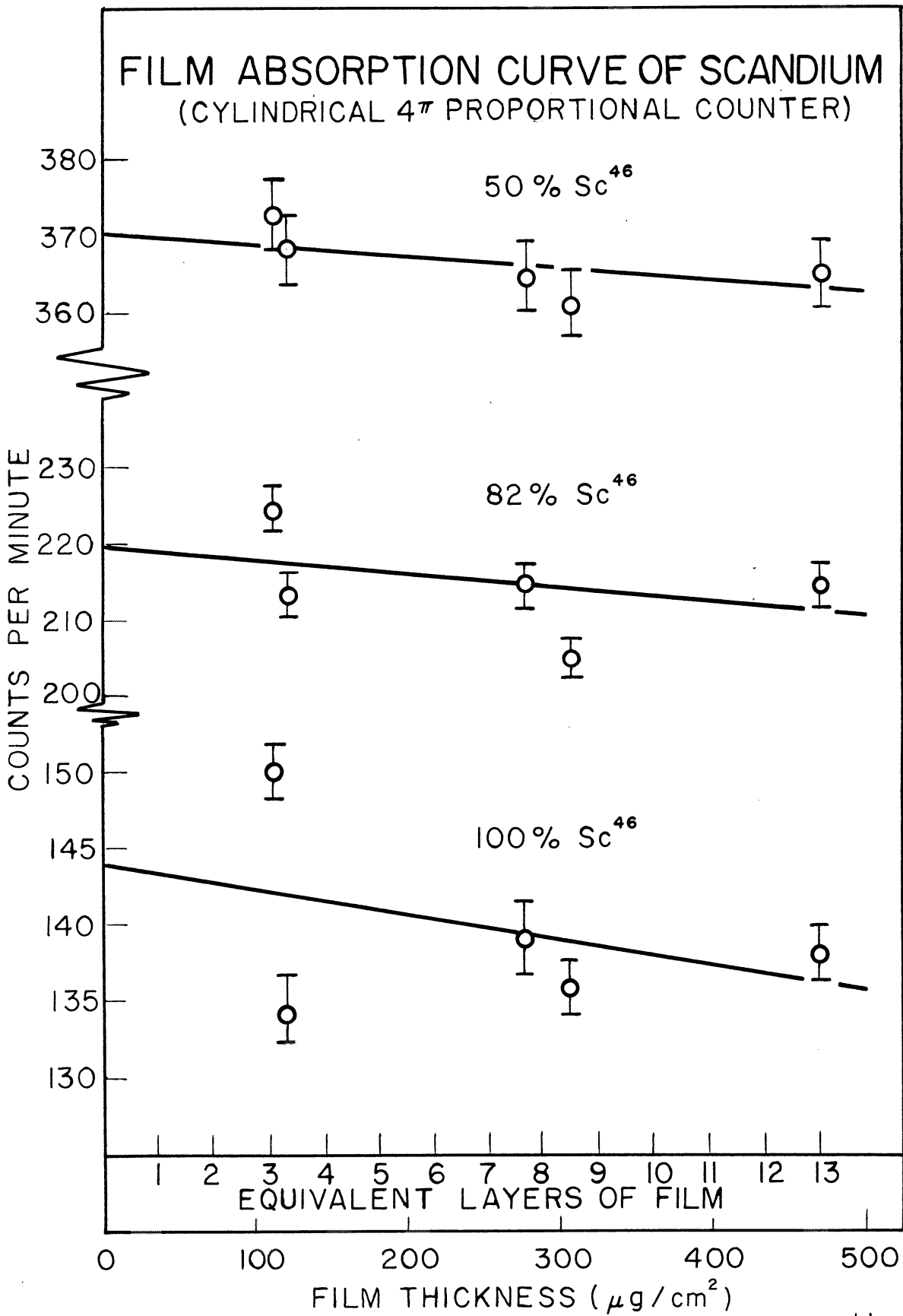


Fig. 50. Film absorption curve of various mixtures of Sc<sup>44</sup>, Sc<sup>46</sup>, Sc<sup>47</sup>, and Sc<sup>48</sup> taken from titanium bombardment 5. The errors shown are standard deviations due to counting statistics.

corresponding to the average deviation of the points on the discrimination plateau of figure 49 was found to be 2.0 per cent. This is larger than the error due to counting statistics, but it is reasonable considering that these data were collected over a period of eight days.

The film absorption curves are presented in figure 50. The sample plates were prepared as illustrated in figure 32 and consisted in different numbers of layers of Zapon coated with gold. The thickness of the films were determined by the  $\text{Ni}^{63}$   $\beta$ -ray absorption method discussed on page 100. The data were taken from bombardment 5 and each point was corrected for decay. Although the curve does exhibit a definite slope, the decay curves were taken of samples mounted on only two layers of Zapon, so the film absorption correction amounts to only about 1 per cent.

#### Analysis of Decay Curves

A typical decay curve is shown in figure 51 for titanium bombardment 4. When the 85-day  $\text{Sc}^{46}$  is graphically resolved from the gross curve, the resulting points define a straight line whose slope corresponds to a half-life of 2.63 - 2.91 days. This is, no doubt, the compound decay curve of the 2.4-day isomer of  $\text{Sc}^{44m}$ , the 3.44-day  $\text{Sc}^{47}$  and the 2.4-day  $\text{Sc}^{44}$ . If one assumes that these isotopes are produced in equal yield, that the electron-capture branching of the 3.9-hour  $\text{Sc}^{44}$  is negligible, and that the counting efficiency for the internal transition of  $\text{Sc}^{44m}$  is zero, the calculated decay curve is practically a straight line corresponding

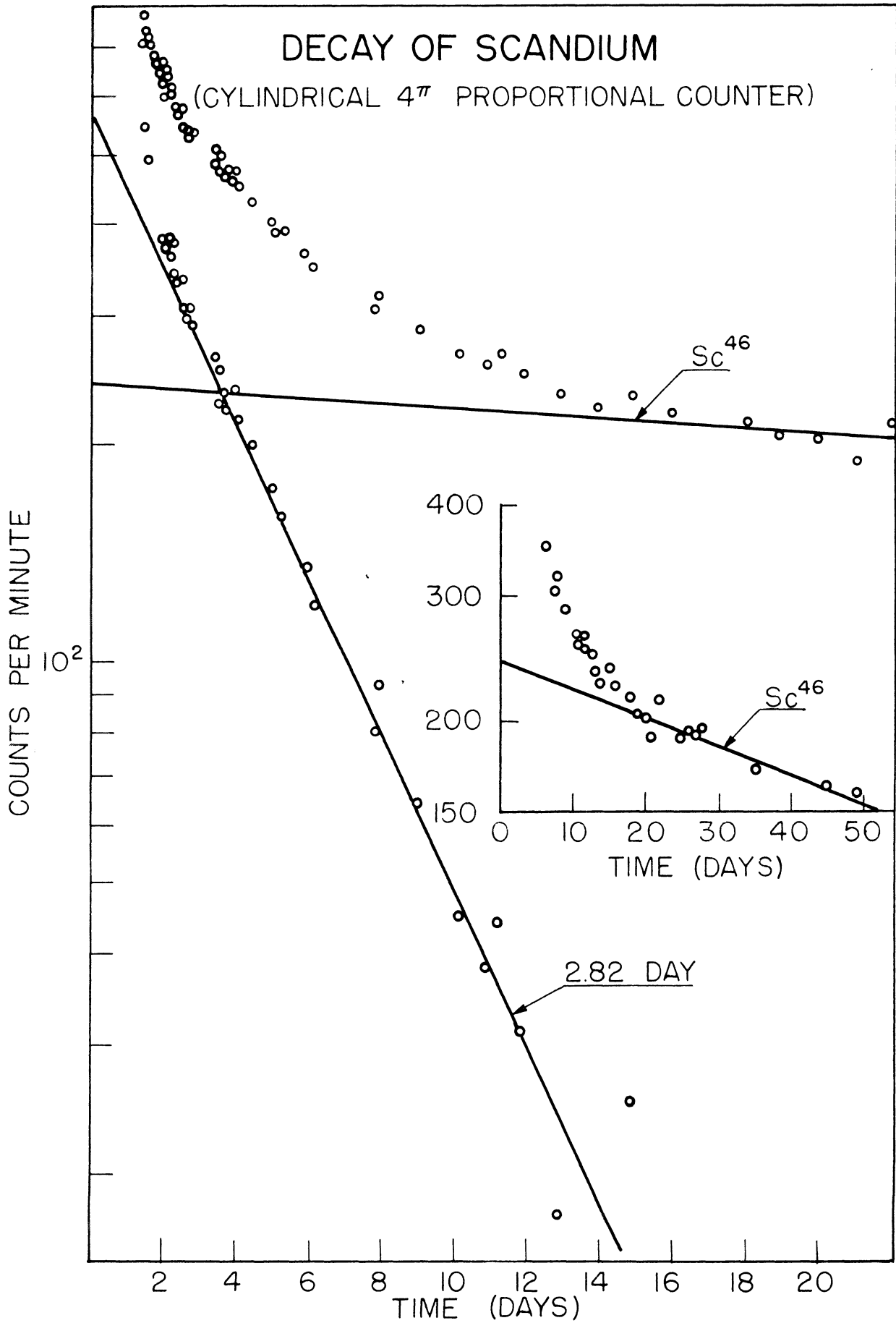


Fig. 51. Decay curve of scandium separated from titanium resolved into the 85-day Sc<sup>46</sup> and a 2.82-day component. The data were taken from titanium bombardment 4.

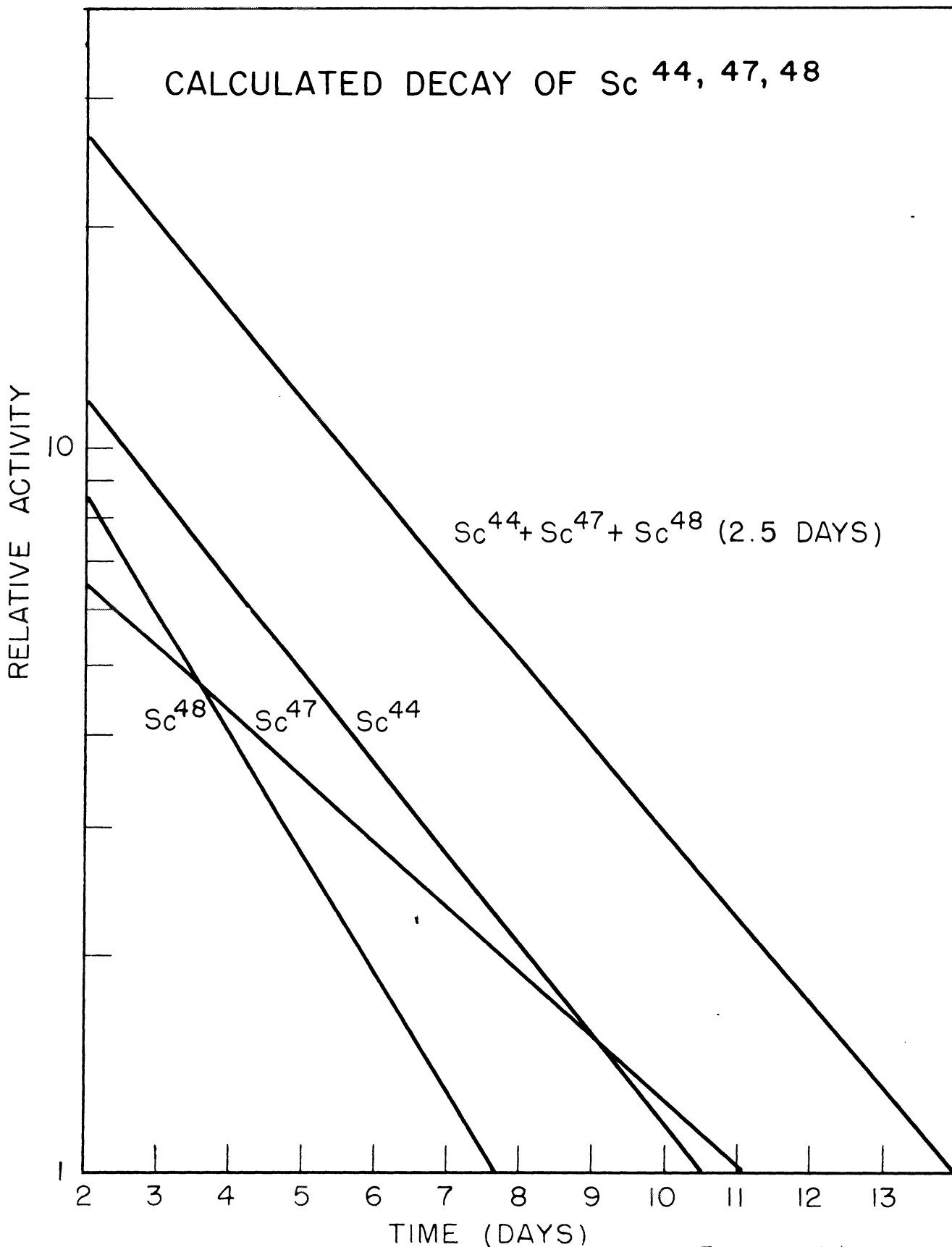


Fig. 52. Calculated decay curve of  $Sc^{44}$ ,  $Sc^{47}$  and  $Sc^{48}$ , assuming equal reaction yields, negligible electron-capture branching and zero counting efficiency for interval transition of  $Sc^{44}$ .

to a 2.6-day half-life. This is illustrated in figure 52, starting 2 days after bombardment to allow for the growth of the 3.9-hour positron emitting daughter of  $\text{Sc}^{44m}$ .

These assumptions are not completely valid, but it can be seen that the experimental decay curve is not in conflict with expectations, and furthermore that it is practically impossible to resolve the 2.63-2.91-day slope into its components.

### Cross Section for $\text{Sc}^{46}$

Bombardment 2 was obtained during the exploratory stage of the work. It resulted in a sample containing a sizable residue. The counting rate was very low, so that the resolution of the decay curve was not very accurate. Therefore the results of this bombardment were rejected in the calculation of cross sections. Bombardment 3 determined relative yields while bombardment 4 and 5 determined absolute cross sections.

Since part of the titanium target foils were behind the collimator in each case, the possibility existed that some scandium activities could have come from (n, p) reactions from fast secondary neutrons produced in the collimator. This resulted in an unknown systematic error.

Another error associated with bombardments 4 and 5 is in the determination of the number of incident deuterons. As mentioned above, the integrator recorded a small but unknown amount of beam in bombardment 4. A correction of 0.25 per cent was considered negligible in the integrator calibration

factor for bombardment 4 and 5, as determined by the calibration check.

Because of the uncertainties mentioned above and the difficulty in resolving the decay curves, the correction for non-constant bombardment was considered negligible. The experimental resolution of the decay curve of bombardment 3 into the 85-day  $\text{Sc}^{46}$  and the shorter component was the basis for calculating  $Q$ , i.e., the number of atoms of  $\text{Sc}^{46}$  produced by the (d,  $\alpha$ ) reaction was referred to the total number of atoms of the 2.4-day, 3.44-day, and 44-hour activities.

The standard deviations in the cross section of each of the bombardments, estimated as for the  $\text{Mg}(d, \alpha)\text{Na}$  yields, were smaller than the spread in the values from the two separate determinations. Since there was insufficient reason to reject either one of the bombardments 4 or 5, both results are presented below. The cross sections thus obtained with the aid of equations (27) and (30) are

$$\text{Bbdt 4: } \sigma(\text{Sc}^{46}) = .00018 \pm .00004 \text{ barn at } 7.0 \pm 0.8 \text{ Mev}$$

$$\text{Bbdt 5: } \sigma(\text{Sc}^{46}) = .00070 \pm .00012 \text{ barn at } 7.0 \pm 0.8 \text{ Mev}$$

where the errors are estimates of the standard deviation of bombardments 4 and 5 based upon the propagation of the errors in the individual factors as indicated in the magnesium bombardments.

#### F. Cadmium Bombardments

The chart of the nuclides for the cadmium region is shown in figure 53. Of the several possible (d,  $\alpha$ ) products

# NUCLIDE CHART OF THE CADMIUM REGION

	In <sup>107</sup>	In <sup>108</sup>	In <sup>109</sup>	In <sup>110</sup>	In <sup>111</sup>	In <sup>112</sup>	In <sup>113</sup>	In <sup>114</sup>	In <sup>115</sup>	In <sup>116</sup>	In <sup>117</sup>	In <sup>118</sup>	In <sup>119</sup>
	30m $\beta^+$	50m $\beta^+, \gamma$	4.3h $\beta^+, EC, \gamma$	50h   66m EC, IT   $\beta^+, EC, \gamma$	2.8d EC, $\gamma$	21m   4.5m IT   $\beta^+, \beta^+, EC$	104m   4.23 IT	49d   72s IT   $\beta^+, \beta^+, \gamma$	4.5h   95.77 $\beta^+, IT$	54m   13s $\beta^+, \gamma$	1.9h   1.1h $\beta^+, IT   \beta^+, \gamma$	4.5m $\beta^+, \gamma$	17.5m $\beta^-$
	Cd <sup>105</sup>	Cd <sup>106</sup>	Cd <sup>107</sup>	Cd <sup>108</sup>	Cd <sup>109</sup>	Cd <sup>110</sup>	Cd <sup>111</sup>	Cd <sup>112</sup>	Cd <sup>113</sup>	Cd <sup>114</sup>	Cd <sup>115</sup>	Cd <sup>116</sup>	Cd <sup>117</sup>
	57m $\beta^+, EC, \gamma$	1.215 $\beta^+, EC, \gamma$	6.7h $\beta^+, EC, \gamma$	0.875 EC	470d EC	12.39 IT	49   0.8   2.75 m   $\mu$ s   IT	24.07 IT	5.7y   12.26 $\beta^-$	28.86 IT	43d   53h $\beta^+, \gamma$	7.58 IT	3.0h   50m IT   $\beta^-$
	Ag <sup>103</sup>	Ag <sup>104</sup>	Ag <sup>105</sup>	Ag <sup>106</sup>	Ag <sup>107</sup>	Ag <sup>108</sup>	Ag <sup>109</sup>	Ag <sup>110</sup>	Ag <sup>111</sup>	Ag <sup>112</sup>	Ag <sup>113</sup>	Ag <sup>114</sup>	Ag <sup>115</sup>
	1.1h $\beta^+, \gamma$	1.2h   27m $\beta^+, EC   \beta^+, \gamma$	40d EC, $\gamma$	24m   8.2d $\beta^+, \beta^+, EC, \gamma$	445   51.35 IT	2.3m $\beta^+, EC, \gamma$	395   48.65 IT	270d   24s $\beta^+, \gamma   \beta^+, \gamma$	7.6d $\beta^+, \gamma$	3.2h $\beta^+, \gamma$	5.3h $\beta^-$	2m $\beta^-$	20m $\beta^-$

Fig. 53. Chart of the nuclides showing possible products of neutron reactions on cadmium.

only four were seen in the bombardments with 7.8 Mev deuterons. These were the 27-minute and "1.2-hour"  $\text{Ag}^{104}$  isomers, the 7.6-day  $\text{Ag}^{111}$  and the 3.2-hour  $\text{Ag}^{112}$ ; all  $\beta$  and  $\gamma$  emitters. The maximum  $\beta$ -ray energies of  $\text{Ag}^{111}$  are 1.04 and 4.2 Mev respectively. (180)

Ten bombardments of cadmium metal were obtained, most of which were for the purpose of developing the chemical procedure (see Chemical Separations Section, page 84). Only in bombardment 9 was it possible to determine absolute cross sections, with the chemical yield determined gravimetrically. The data and derived quantities from this bombardment are presented in Table XII. The errors are estimates of the standard deviations. The following paragraphs deal with the distinctive features of the bombardment.

#### Target Preparation

This has been adequately discussed on page 70.

#### Chemical Procedure

The chemical procedure has also been discussed previously on page 84. Using Sunderman and Meinke's procedure (89) in bombardment 9 the active silver did not completely exchange with the inactive silver chloride on the platinum gauze, because the gauze was dried in a  $110^{\circ}$  oven prior to use. This has the effect of deactivating the silver chloride surface. Therefore the target solution was scavenged later with ~10 mg of inactive silver carrier using the precipitation procedure (Part II of thesis). The chemical yield was finally



Table XII. Summary of Bombardment Data for Cd(d, $\alpha$ )Ag

Bombardment No.	9
Suppressor ring (volts)	1110
D. C. supply ( $\mu$ a)	40
Slits J (in.)	none
Slits L (in.) vertical	0.25
horizontal	0.50
Target N (mils of Mylar)	0.25
Target R position	7
W(mg)	47.9
A(cm <sup>2</sup> )	25.7
substrate	Reynolds Wrap
Integrator range	D
B(cnts)	279
T(sec)	4991
Number of Zapon layers	4
Zapon soln. used (%)	50
C <sub>01</sub> (Ag <sup>104</sup> )	6100 $\pm$ 500
C <sub>02</sub> (Ag <sup>112</sup> )	25000 $\pm$ 300
C <sub>03</sub> (Ag <sup>111</sup> )	372 $\pm$ 8
Y	0.54 $\pm$ .02
M	112.41
K <sub>D</sub> (cnts/min/ $\mu$ a)	9.9 $\pm$ 0.1
a <sub>1</sub> (Cd <sup>106</sup> )	0.01215
a <sub>2</sub> (Cd <sup>114</sup> )	0.2*86
a <sub>3</sub> (Cd <sup>113</sup> )	0.1226

calculated from the weight of AgCl recovered.

#### Absolute Beta Counting

Discrimination curves of the silver obtained at a time corresponding to 3 per cent of  $\text{Ag}^{111}$  in the  $\text{Ag}^{104}$  -  $\text{Ag}^{111}$  -  $\text{Ag}^{112}$  mixture are shown in figure 54, each point being corrected for decay. Once again there is no evidence for a slope in the plateau, and the average deviation of the points on the plateau corresponded was 0.85 per cent standard deviation. No measurement was made of the extent of self absorption, and it was felt that this unknown error was far greater than the film absorption correction, and hence the latter correction was not ascertained.

#### Analysis of Decay Curve

The decay curve is shown in figure 55. The resolution was done graphically. Three components were observed, the 27-minute  $\text{Ag}^{104}$  having decayed before the counting was started.

#### Cross Section for "1.2" hr $\text{Ag}^{104}$ , $\text{Ag}^{111}$ , and $\text{Ag}^{112}$

The uncertainties associated with bombardment 9 include the unknown error of self absorption. The decay curve resolution was handicapped because of the three components; two have comparable half-lives. The correction for non-constant bombardment was not made. Unfortunately, additional cyclotron time was not available to obtain more bombardments of cadmium for the purpose of measuring absolute cross sections.

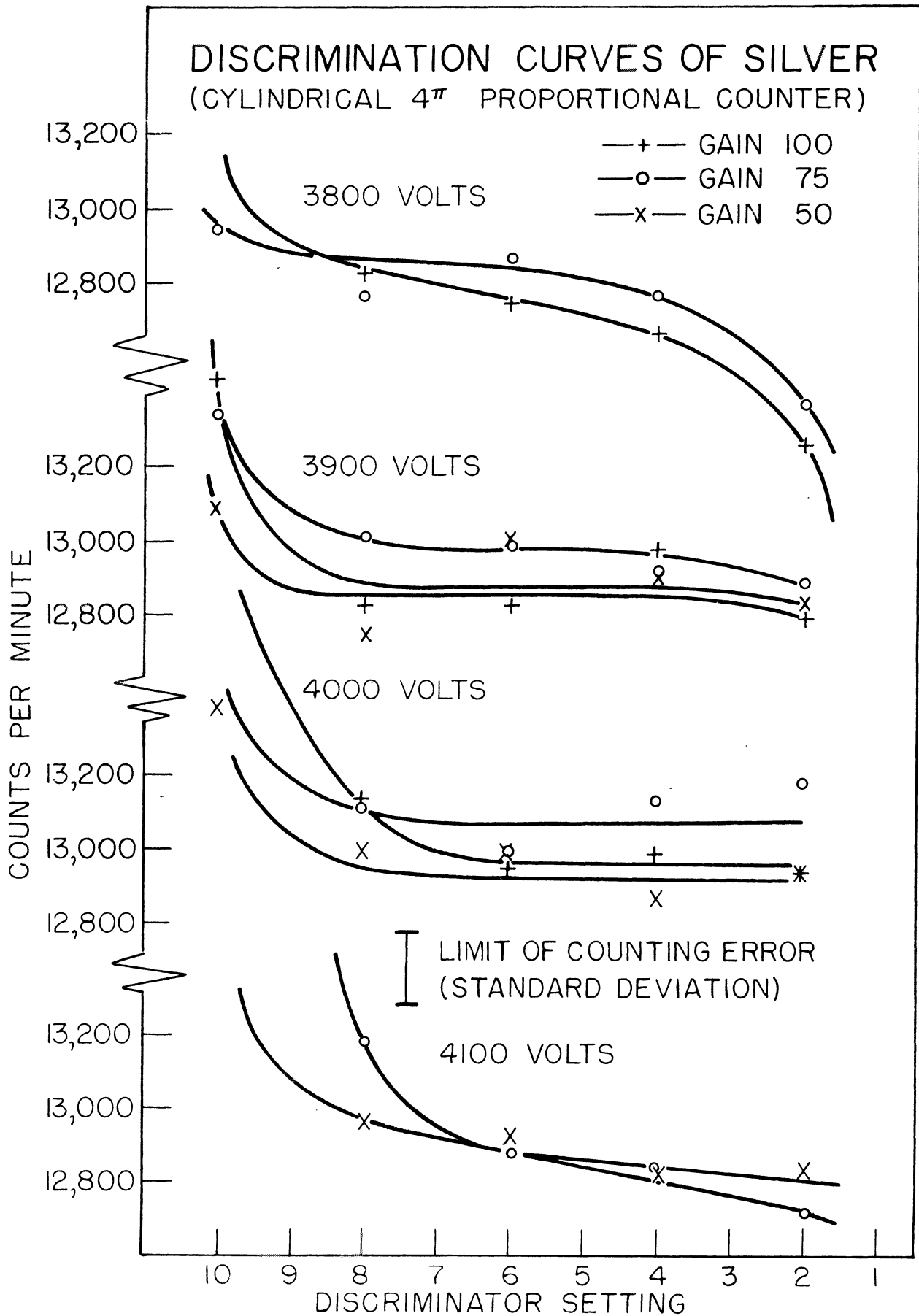


Fig. 54. Discrimination curves of a mixture of 3 per cent  $Ag^{111}$  and 97 per cent  $Ag^{112}$  taken from cadmium bombardment 9. The limits of counting error shown are twice the standard deviation of a single point.

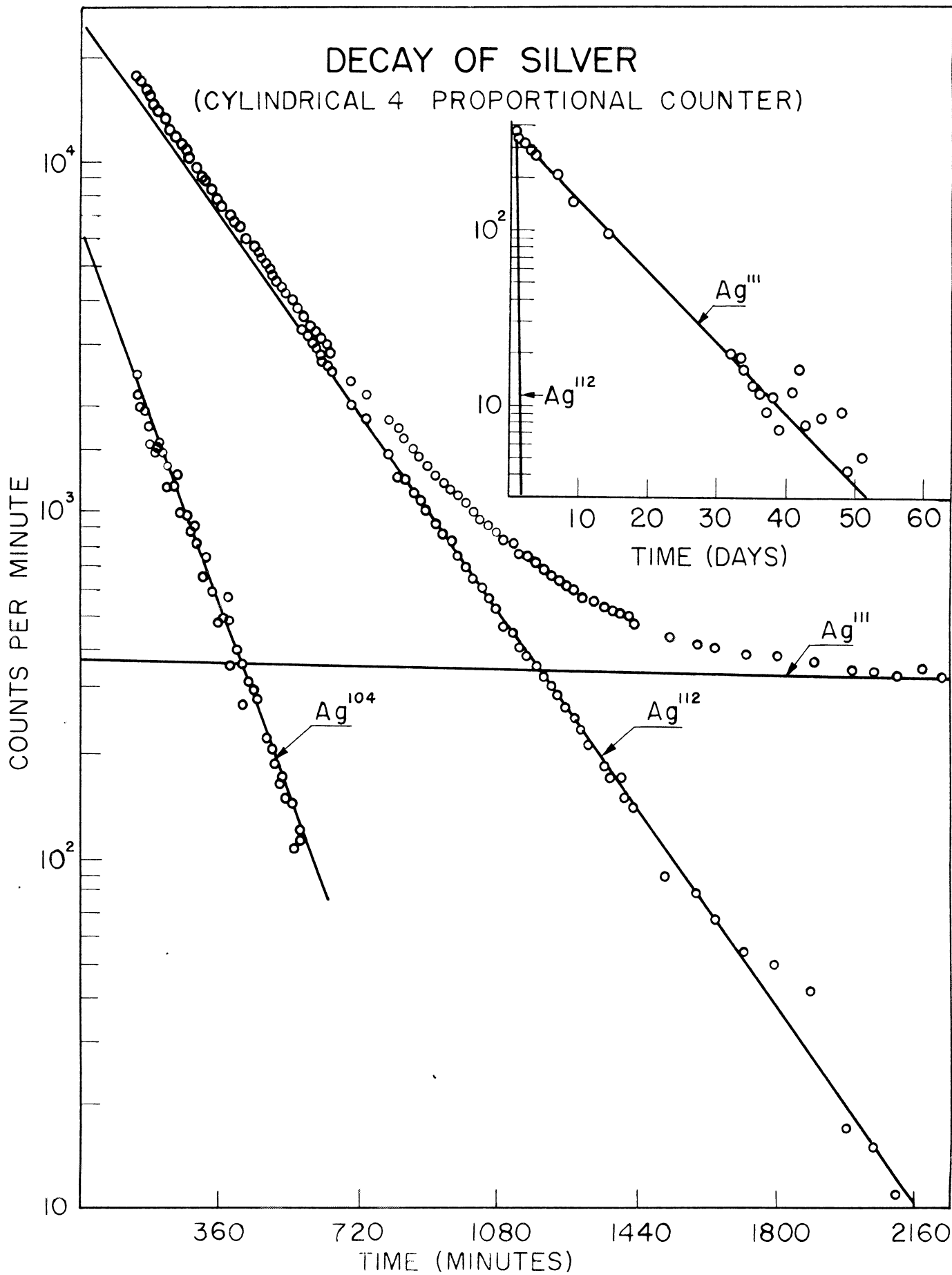


Fig. 55. Decay curve of silver separated from cadmium resolved into 101-minute  $Ag^{104}$ , 3.2-hour  $Ag^{112}$  and 7.6-day  $Ag^{111}$  components. The data were taken from cadmium bombardment 9.

The values calculated with the aid of equations (27) and (39) are

$$\sigma(1.2hAg^{104}) = 0.0017 \pm 0.0002 \text{ barn at } 7.8 \pm 0.1 \text{ Mev}$$

$$\sigma(Ag^{112}) = 0.00049 \pm 0.00002 \text{ barn at } 7.8 \pm 0.1 \text{ Mev}$$

$$\sigma(Ag^{111}) = 0.0004 \pm 0.00004 \text{ barn at } 7.8 \pm 0.1 \text{ Mev}$$

The errors are based upon the propagation of the individual errors in each of the factors, as indicated for the magnesium bombardments, and hence represent an estimate of the standard deviation.

### C. Loss of Recoil Nuclei

When a target nucleus is struck by a deuteron and undergoes a nuclear reaction, the product nucleus recoils with a certain amount of kinetic energy. Some nuclei will thus be ejected from the target itself, and if some provision is not made to catch these recoil nuclei, the apparent cross section will be too low. Fung (198) has studied the dependence of the recoil loss from thin (0.00025-0.001 inch) aluminum foils as a function of incident particle energy. He used protons, deuterons and alpha particles, and found losses ranging from 10 to 30 per cent for energies of 40-380 Mev.

In the present work it was necessary to determine the thickness of target backing which will stop all recoil nuclei. (Fung reported that little or no nuclei are caught by catcher foils placed in front of the target.) An experiment

was performed in which cadmium metal was bombarded with Mylar films serving as recoil catchers in front and behind the cadmium foil. The cadmium was evaporated onto a  $65 \mu\text{g}/\text{cm}^2$  Zapon film coated with aluminum. The cadmium was  $97 \mu\text{g}/\text{cm}^2$  in thickness. One 0.00025 inch Mylar film was placed in front of two 0.00025 inch films followed by one 0.001 inch film placed behind the target. The catcher films were counted after bombardment with a Geiger counter. All the films except the second film in back exhibited the same decay curve. This one film showed the presence of a ~10-hour period in addition to the 10-minute  $\text{N}^{13}$ . The amount of activity was too small to make any more accurate determination of the half-lives. It was concluded that the range of the recoil nuclei is such that they were stopped in the second 0.00025 inch film. Therefore all the targets used in the absolute cross section bombardments were all made with 0.001 inch thick substrates to be sure of stopping all the recoils.

#### H. Energy of the Deuteron Beam

The energy of the deuterons from the University of Michigan cyclotron has been measured by D. R. Bach. (60) On two separate occasions he found it to be 7.89 and 7.74 Mev. Thus a day-to-day variation of 0.15 Mev may be expected. The dispersion of the focusing magnet was 6.5 kev/min at 7.8 Mev, i.e., a point source of deuterons of various energies was spread out at the focal plane in a band of a width corresponding to the initial energy spread. For the 1/2 inch wide slit used in this work the energy

spread is 83 kev for a point source, and in practice it is greater due to the finite slit at the window box.

The Mylar scattering target (N of figure 1) was usually kept in the beam path during bombardment. The degradation in energy of the deuteron beam in passing through this 0.00025 film is negligible in comparison with the above energy spreads.

The targets bombarded in this work degrade the energy by approximately 0.08, 0.21, 1.6 and 0.08 Mev in the cases of magnesium, sulfur, titanium and cadmium respectively. (199) Thus the cross sections reported for these elements may be said to have been obtained at  $7.8 \pm 0.1$ ,  $7.7 \pm 0.1$ ,  $7.0 \pm 0.8$ , and  $7.8 \pm 0.1$  Mev respectively.

## DISCUSSION

The accuracy of the measurement of cross sections by the procedures evolved in this work is dependent on several factors. Large systematic errors due to lack of suppression of secondary electrons in the beam determination and loss of recoil nuclei from the target itself have been successfully overcome in the present work. The problem of fast secondary neutrons was eliminated by preparing targets of just the right area to match the collimator aperture. Since no observable (0.6 per cent of  $P^{32}$ )  $P^{33}$  was produced in the sulfur bombardments from a possible (n, p) reaction, it was concluded that stray neutrons contaminating the deuteron beam did not present a problem when the target area does not overlap the collimator.

One major source of error arose from the difficulties in resolving the decay curve of the (d,  $\alpha$ ) product. This has been overcome in the favorable case of the sodium from magnesium bombardments (15-hour and 2.6-year components) by the statistical analysis of a large number of decay points. The method of least squares was applied, but this method was found to be extremely time consuming. It is suggested that this method be coded for use with an electronic computer such as MDAC (Michigan Digital Automatic Computer). Once the initial coding were accomplished, for a general decay curve consisting of  $n$  components of  $m$  unknown half-lives, the resolution of complex decay curves could be accomplished in a minimum amount of time.



The present integrator is the other major source of error. This instrument was only linear at the very low counting rates and the calibration was only trusted to 1 per cent. A new unit is under construction, but no data have been obtained with it as yet. It is expected that with its completion 0.1 per cent accuracy can be achieved in the measurement of the cyclotron beam.

The metal evaporator is very useful for obtaining thin, even targets. It could be improved if a larger diffusion pump on the metal evaporator would make it possible to operate at lower pressures ( $\sim 10^{-6}$  mm mercury) without the possibility of introduction of air and other gases by small leaks and outgassing of the heater assembly. Thus the formation of oxides of the metal to be evaporated would be alleviated.

Two additional pieces of work could be done on the  $4\pi$  counting procedure. The effect of a conducting coating on the thin plastic films used in  $4\pi$  counting could be more precisely evaluated as there is still disagreement on this point in the literature. (51, 48) This could be done by preparing two series of samples of equal aliquots of a weak  $\beta$  emitter on plastic films of varying thickness. If one series had a conducting layer and the other did not, any discrepancy between the two absolute counting rates would be evidence for the effect. An improvement could also be made in the measurement of the thickness of the gold plus Zapon films by securing more absolute (gravimetrically

determined) points on the Ni<sup>63</sup>  $\beta$ -ray transmission curve, figure 27.

The maximum accuracy of the methods developed in this work is represented by the Mg(d,  $\alpha$ )Na cross sections in which 4 per cent accuracy (standard deviation) was achieved. Even this error could have been reduced if more points had been obtained on the decay curve. The accuracy of the other cross section measurements suffered from experimental difficulties which could be overcome as outlined below.

The accuracy of the P(d,  $\alpha$ )S cross section could be improved if a thin target of a salt such as Na<sub>2</sub>SO<sub>4</sub> could be prepared, an investigation of the exchange of phosphorous tracer and (d,  $\alpha$ ) product were made, and enough P<sup>33</sup> tracer obtained and purified. Another suggestion is to set up a counting apparatus near the cyclotron and attempt to measure the yield of the 2.55-minute P<sup>30</sup> relative to P<sup>32</sup> by counting the energetic (3.5 Mev)  $\beta$  rays without performing chemical separation.

The Ti(d,  $\alpha$ ) reactions could be studied to better advantage if separated isotopes were obtained and techniques developed for their fabrication into thin films without any loss. Thus the decay curves could be analyzed and the yields of Sc<sup>44</sup>, Sc<sup>47</sup>, and Sc<sup>48</sup> be determined.

As far as the Cd(d,  $\alpha$ )Ag cross sections are concerned, the principle extension of the present work would be to develop a carrier-free separation of the silver, perhaps using an ion-exchange procedure.

Finally, when enough accurate (d,  $\alpha$ ) reaction cross sections are obtained to give a general picture of the systematics of the reaction, a correlation with the existing theories should be attempted, e.g., the Bohr theory of the compound nucleus. The variation of the cross section as a function of atomic number should reflect the coulomb barrier. If absolute excitation functions were obtained, one could compare the cross sections at an energy corresponding to a certain percentage above the threshold. Schott and Meinke (200) report equal yields of (d,  $\alpha$ ) products from even-even zirconium target isotopes, while the results of the cadmium bombardments in this work indicate that the yields are not equal in the case of even-odd Cd<sup>113</sup> and the even-even Cd<sup>114</sup> target isotopes. Thus it would be interesting to note whether or not this odd-even effect is fortuituous. If a trend does exist the magnitude of this effect could be investigated.

## PART II: MASS ASSIGNMENT OF Ag<sup>104</sup>

### INTRODUCTION

A survey of the nuclide chart was made very early in this work to choose target elements best suited for study of the (d,  $\alpha$ ) reaction. One of the considerations in the choice was the possibility of obtaining new nuclear data by studying isotopes which heretofore had not been studied to any great extent. Thus information on the characterization of isotopes and absolute cross sections could be obtained at the same time..

Cadmium was one of the first elements to be bombarded. An inspection of the nuclide chart for the cadmium region figure 53 reveals that several isotopes of silver may result from the Cd(d,  $\alpha$ )Ag reactions. The 16-minute and 1.2-hour activities were of interest because little work had been done to assign mass numbers to these periods, and the (d,  $\alpha$ ) reaction would result in the production of Ag<sup>104</sup>. The opportunity thus presented itself to observe the periods associated with Ag<sup>104</sup>.

The radioisotope Ag<sup>104</sup> was first reported by Enns (201) as a product of a (p, n) reaction on palladium. He observed the 73-minute and a 16-minute activity which he assigned to Ag<sup>102</sup> and Ag<sup>104</sup> respectively. Lindner and Perlman (202) reported a 70-minute activity in a silver fraction separated from the spallation products of antimony bombarded with 190 Mev deuterons, but they were unable to make any mass assignment of this activity. Johnson (203) observed a

27 ± 1-minute positron activity as a daughter of  $Cd^{104}$ . Bendel and co-workers (204) bombarded palladium with 12-Mev deuterons and found a 1.1-hour activity in the silver fraction separated from the target. Recently Halder and Wiig (205) bombarded silver with high energy protons and purified the silver radiochemically. They noted a 25-minute and a 1.1-hour activity and attributed the former to  $Ag^{106}$  and/or  $Ag^{104}$ . The silver fraction was "milked" for palladium daughter activities, and they observed the 17-day  $Pd^{103}$  using an x-ray proportional counter. The yield of this daughter activity decreased with a half-life corresponding to the 1.1-hour period of silver, and hence they assigned the 1.1-hour activity to  $Ag^{103}$ . Additional radiation characterizations of  $Ag^{104}$  have been made by Cassatt (85) using silver produced by the (d, α) reaction on cadmium.

## EXPERIMENTAL PROCEDURES

### A. Target

In some of the work reported here natural cadmium oxide (Baker and Adams reagent grade) powder was used for the target material. It was wrapped in an envelope made of 1.5 mil aluminum (Reynolds Metal Co., Richmond, Virginia) and placed on the window box probe head (figure 7) for bombardment. Cadmium oxide electromagnetically enriched in  $Cd^{106}$  (Carbide and Carbon Chemical Co., Oak Ridge National Laboratory, Oak Ridge, Tennessee, Series AC Sample 88(a) ) was bombarded in a similar manner.

The mass analysis of these oxides are given in Table XIII.

Table XIII. Mass Analysis of Cadmium Oxide Target Materials

Cadmium Isotope	Atom per cent	
	Natural	Enriched
106	1.215	19.94
108	0.875	0.65
110	12.39	7.21
111	12.75	39.16
112	24.07	11.85
113	12.26	4.14
114	28.86	15.25
116	7.58	1.80

In other cases cadmium foil of unknown purity was rolled to 1-5 mils in thickness for bombardment on the window box probe.

#### B. Chemical Separations

Since cadmium is a bi-product of zinc ores or from copper and lead refining, these elements were suspected as impurities in the development of the chemical procedure. Aluminum was also present from the envelope containing the bombarded cadmium. Considering the activities produced in these metals encountered from (d, n), (d, p), and (d,  $\alpha$ ) reactions there is the possibility of finding interfering activities of the following elements present

in the target solution: copper, zinc, gallium, silver, cadmium, indium, thallium, lead and bismuth. The chemical separation must be fast enough to permit the observation of the 27-minute period, and one technique was found especially helpful in this respect. Filter tubes (Wilkens-Anderson Company, Chicago, Illinois, Catalogue No. 8480B) fitted with glass wool plugs for filters make it possible for a precipitate to be filtered, washed and dissolved in a matter of ~2 minutes.

The procedure adopted is shown in figure 56. To check the purity of the AgCl precipitate, the following procedure was tried. A portion of the final AgCl precipitate was subjected to further purification as follows. The precipitate was dissolved in 3 N HCl, Ag<sub>2</sub>S was precipitated with H<sub>2</sub>S, the precipitate washed and dissolved in 1 ml. of concentrated HNO<sub>3</sub>. The solution was diluted ca four fold and AgCl was reprecipitated with 1 ml. of 6 N HCl. A sample was prepared for counting and the remaining AgCl was subjected to a further repurification step. The chloride was converted to the oxide by digesting for 10 minutes with 2 ml of 6 N NaOH. This was dissolved in one drop of concentrated HNO<sub>3</sub>, diluted ca four fold with water, and AgCl precipitated as before with five drops of 1 N HCl, and a sample prepared for counting. Thus three separate samples were counted representing three different stages of chemical purification, and the resulting decay curves were compared. If any radioactive contaminant were present in the first silver sample (or in the silver sample repurified by the sulfide

CHEMICAL SEPARATIONS

Element separated: Silver

Procedure by: Hall

Target Material: Cadmium

Time for sep'n: 15 min

Type of bbd: 7.8 Mev deuterons

Equipment required:

Yield: ~70%

Barber filter tubes and suction bulbs (Wilkins-Anderson Co., cat. no. 8480B and 1686)

Degree of purification:  $\sim 10^4$

water bath  
micro bell jar  
Filtration apparatus (Tracer Lab, Boston, Mass.)

Advantages: Rapid separation

Test tubes, beakers, etc.

Procedure:

- (1) Place 1 ml con  $\text{HNO}_3$  in 100 ml high form beaker containing 20 mg of  $\text{Ag}^+$  and 10 mg each of  $\text{Tl}^+$ ,  $\text{Pd}^+$ ,  $\text{Bi}^{+++}$ ,  $\text{Cu}^+$ ,  $\text{Zn}^{++}$ ,  $\text{Ga}^{+++}$ ,  $\text{In}^{+++}$  carriers. Introduce the Cd target (~50 mg) and dissolve.
- (2) Dilute ca fourfold with hot water, add 2 drops 0.1% aerosol solution and 5 drops 1 N HCl.
- (3) Adjust ( $\text{Cl}^-$ ) to 0.0025 N and digest 1 min.
- (4) Filter through glass wool using filter tube and micro bell jar. Wash twice with hot 0.1 N  $\text{HNO}_3$ .
- (5) Dissolve precipitate off of filter by recycling 4 drops of 6 N  $\text{NH}_4\text{OH}$ , catching the solution in a 5 inch test tube.
- (6) Add 2.5 mg  $\text{Fe}^{+++}$ , filter and wash the precipitate twice with 6 N  $\text{NH}_4\text{OH}$ .
- (7) To the filtrate from (6) add 3 mg each of the original carriers, substituting  $\text{Cd}^{++}$  for  $\text{Ag}^+$ .
- (8) Add  $\text{HNO}_3$  and 2 drops 1 N  $\text{NH}_4\text{Cl}$  to precipitate  $\text{AgCl}$  and recycle if desired.
- (9) Filter the final  $\text{AgCl}$  precipitate on a 1 inch diameter filter paper using the filtration apparatus, wash with 0.1 N  $\text{HNO}_3$ , acetone, and ether.

Remarks: General references: W. W. Meinke, Chemical Procedures Used in Bombardment Work at Berkeley, AECD-2738(UCRL-432) (August 1949).

Fig. 56. Procedure for the chemical separation of silver from cadmium targets.



step) it is to be expected that further purification involving a different chemical method would result in the alteration of the ratio of the impurity to the silver. If this were the case the decay curves of the samples would not be identical. Since it was found that the three samples do, in fact, exhibit identical decays, it is concluded that the first silver sample (before repurification) is radiochemically pure.

### C. Counting

The samples were counted using two "pancake" end-window Geiger tubes (Anton Electronic Laboratories, Inc., Brooklyn, New York, Type 1001H) placed above and below the sample. The outputs of both tubes were connected in parallel and fed into a scale of 64 counting circuit (Nuclear-Chicago, Chicago, Illinois, Model 165). The sample was sandwiched between two copper absorbers of such a thickness as to stop the 1.04 Mev  $\beta$  rays of  $\text{Ag}^{111}$ .

A thin end-window chlorine quenched Geiger tube (Amperex Electronic Corporation, Hicksville, New York, Type 100C) mounted in a standard lead housing was also used in conjunction with a similar scaler. No absorber was used over the sample counted with this apparatus.

A survey beta-ray spectrometer (84) was used to distinguish between positrons and negatrons and to obtain rough beta spectra.

EXPERIMENTAL RESULTS

Five bombardments were obtained for the mass assignment work. The first 2 were of natural cadmium foil, numbers 3 and 4 were natural cadmium oxide, and number 5 was of cadmium oxide enriched in  $\text{Cd}^{106}$ . Bombardments 1, 2 and 3 were primarily used to evaluate the chemical procedure and develop the techniques, but some yield data were obtained from bombardment 1. The experimental results are summarized in Table XIV for bombardment 1, 4 and 5. The yields reported have been normalized to the 3.2-hour  $\text{Ag}^{111}$  acting as an internal standard. Numbers are given for the two different counting arrangements used.

The decay curves were quite similar to those obtained in Part I of this thesis, and the curve presented previously in figure 55 is typical except that the 27-minute silver activity does not appear there. In the mass assignment work, samples were counted as soon as 18 minutes after bombardment. This permitted the observation of the 27-minute period.

Table XIV. Relative Yields of Silver Isotope

Silver mass	Bbdt. 1 (Cd foil)		Bbdt. 4 (CdO)		Bbdt. 5 ( $\text{Cd}^{106}\text{O}$ )	
	No absorber		No abs.	Cu abs.	No abs.	Cu abs.
104(27m)			1.833	1.347	33.4	41.8
104(68m)	0.493		0.300	1.306 <sup>a</sup>	6.36	39.2
111	1		1	1	1	1
112	0.0178		0.020		0.0126	

<sup>a</sup> Half-life found to be 66 min.

The decay curves were resolved graphically with the assumption that the components were the 7.6-day  $\text{Ag}^{111}$  (206), the 3.2-hour  $\text{Ag}^{112}$  (207), the 27-minute  $\text{Ag}^{104}$  (203), and an isomer of  $\text{Ag}^{104}$  of unknown half-life. Thus the initial activity and slope of the unknown component was found by successive resolutions of the gross curve until three lines were obtained, possessing the assumed slopes.

The increase in the relative yield of the 27-minute and the 68-minute components which occurred when the enriched cadmium was bombarded shows that these periods arise from the  $\text{Cd}^{106}$  target isotope. In fact, the relative increases in yield approximates the value calculated if one assumes that the thin target formula is valid. The comparison of relative yields from enriched and natural cadmium targets is shown in Table XV.

Table XV: Ratio of the Relative Yields from Enriched (Bbdt.5) and Normal Cadmium Targets (Bbdts. 1 and 4)

Silver mass	Theoretical	Bbdt. 1 (Cd foil)		Bbdt. 4 (CdO)	
		no absorber		no abs.	Cu abs.
104(27m)	30.9			18.2	31.0
104(68m)	30.9	12.9		21.2	30.0
111	1	1		1	1
112	0.635	0.71		0.63	

For products of  $\text{Cd}^{106}$ , the ratio of the relative yield from the enriched target to the relative yield from the natural

target was calculated to be 30.9. Similarly the yield of reaction products from  $\text{Cd}^{113}$  was expected to decrease by a factor of 0.635. These theoretical values are duplicated in the table as well as can be expected.

Additional experiments using the beta-ray survey spectrometer indicated that the 68-minute activity decays by positron emission. The maximum energy of these positrons must be greater than about 1 Mev.

#### DISCUSSION

The assignment of the 68-minute and 27-minute activities of silver to mass number 104 was based upon the increased yield of these activities when cadmium enriched in  $\text{Cd}^{106}$  was bombarded with 7.8 Mev deuterons. The silver was produced by the (d,  $\alpha$ ) reaction.

The energy of the deuterons was low enough so that no (d,  $\text{an}$ ) reaction products were observed. Thus the 5.3-hour  $\text{Ag}^{113}$  was not present in the silver fraction.  $\text{Cd}^{116}$  is 7.58 per cent abundant and a 5.3-hour activity amounting to only 2 per cent of the initial activity of the 3.2-hour  $\text{Ag}^{112}$  or 8 per cent of the initial activity of 68-minute  $\text{Ag}^{104}$  would have been detected in the decay curve. Therefore the (d,  $\text{an}$ ) reaction must be only about 0.002-0.05 times less probable as the (d,  $\alpha$ ) reaction. Other work in this laboratory (200) has shown that no (d,  $\text{an}$ ) products are observed when yttrium is bombarded with 7.8 Mev deuterons. An attempt was made to show specifically that no  $\text{Ag}^{103}$  was produced by the (d,  $\text{an}$ )

reaction in which the 17-day  $\text{Pd}^{103}$  daughter was milked from the silver fraction. No activity was observed in the palladium fraction, when counted with a NaI scintillation crystal, although a lower detection limit could not be set.

The 68-minute activity is therefore  $\text{Ag}^{104}$ , an isomer of the 27-minute  $\text{Ag}^{104}$ . It seems that the 1.1-hour (66-minute) activity attributed by Halder and Wiig to  $\text{Ag}^{103}$  on the basis of "milking" experiments is due to a different nuclide from the one observed in this work, so that two similar half-lives belong to adjacent isotopes  $\text{Ag}^{103}$  and  $\text{Ag}^{104}$ .

## ACKNOWLEDGEMENTS

The author is truly grateful to Professor W. W. Meinke for the valuable aid, cooperation and guidance that he rendered throughout the course of this work.

The suggestions and advice of Professor W. C. Parkinson, Professor P. V. C. Hough, and Professor E. F. Westrum are sincerely appreciated.

The willing assistance of Harvey M. Nye in obtaining bombardments, of Walter E. Barrett, Almon G. Turner, Jr., Jerry L. Kochanny, Jr., and Mrs. Rosemary S. Maddock, in various phases of the problem was gratifying to the author. Thanks also go to Wayne A. Cassatt, Jr., for the many helpful discussions and to Mrs. Jacqueline Hall, Larry Hall, and Mrs. Oswald Anders for their painstaking help in preparing the manuscript.

The author is indebted to the U.S. Atomic Energy Commission for partial support of this research, to the memory of Florence Fenwick for the receipt of a Memorial Fellowship, and to the Regents of the University of Michigan for the two grants-in-aid received while engaged in this work. The help of the Isotopes Division of the U.S. Atomic Energy Commission for supplying both enriched and radioactive isotopes for use in this work is acknowledged.

## APPENDIX I

### Instructions for the Use of the Metal Evaporator

Refer to figures 10-14 for the valve numbers, pictures of the heater assembly, etc.

#### To Turn Pumps On

1. CLOSE valves 2 and 3 and open valve 1.
2. Turn water to diffusion pump ON.
3. Turn the fore pump ON.
4. Turn the diffusion pump ON.
5. After the oil is hot, feel the intake of pump to see if cooling coils are operating properly.

CAUTION: Do not tighten sylphon valves too tight-- just a sixteenth of a turn after the valve has seated itself is sufficient.

#### To install Filament and Catcher (Substrate)

1. Clamp the filament (Helix, basket, or foil or alundum crucible) between electrodes.
2. Check for short or open circuit.
3. Place the metal to be evaporated on filament.
4. Screw aluminum "ringstand" rod in spare hole in base plate and JUST BARELY tighten the hex lock nut.
5. Place substrate on aluminum frame and adjust its position on the "ringstand" rod.

To Evacuate Bell Jar

Wait until diffusion pump has been hot for about fifteen minutes, then

1. CLOSE valve 1 (3 is already closed).
2. CLOSE valve 4 (Hoke valve).
3. OPEN valve 2 for only five minutes at a time.
4. Turn ON vacuum gauge and adjust heater current to 70 ma.
5. CLOSE valve 2 and wait thirty seconds: then
6. OPEN valve 1 for one minute.
7. CLOSE valve 1 (3 is already closed).
8. OPEN valve 2 for an additional period of five minutes only.

Repeat steps 5, 6, 7, 8 until thermocouple gauge reads 1.5 mv.

9. OPEN valve 1 and continue pumping until thermocouple gauge indicates  $\sim 5 \times 10^{-2}$  mm.
10. OPEN valve 3 and CLOSE valve 2.

To Use Cold Trap

Wait until pumps have evacuated to about  $10^{-4}$  mm Hg, then

1. Fill dewar about 2/3 full and bring it up under the cold trap so that only the bottom quarter inch is immersed.
2. After about two minutes raise the trap higher.
3. In removing the trap, allow it to reach 0°C before opening the system to the atmosphere.



To Open up Bell Jar

1. Remove cold trap and allow to warm up with valves 1 and 2 open and 3 closed (while pumping on the system).
2. CLOSE valve 2.
3. OPEN valve 4 (Hoke valve) .
4. Remove bell jar and set it on a soft towel.

To Turn Pump Off

1. Make sure that valves 2 and 3 are closed.
2. Turn diffusion pump OFF and wait until oil reservoir is cool to the touch.
3. Turn fore pump OFF.

Use of Glass Bell Jar

Handle the bell jar with dry hands, always keeping at least two fingers under the rim so it won't slip. Set the bell jar on a towel to prevent damage to rim and gasket. Always use wire bell jar guard. Coat the inside of the bell jar with a thin layer of stopcock grease for the purpose of reducing the amount of metal sticking to the glass. This permits observation throughout the evaporation process, and the metal which did stick to the bell jar is easier to remove.

## APPENDIX II

### Maintenance of the $4\pi$ Counting Chamber

See section on  $4\pi$  Proportional Counters, page 35, for a description of the chambers, and figures 15 and 16 for pictures of them.

#### Center Wire Replacement: Cylindrical Chamber

1. Grasp a one foot length of 0.002 inch stainless steel wire about 1/4 inch from its end using lucite forceps.
2. Clean this end in stainless steel soldering flux (Joseph Ryerson and Son, Inc., Detroit, Michigan).
3. Drop a small globule of molten solder onto an asbestos board and immediately plunge the end of the wire into it and let it solidify.
4. Thread the wire through the lucite insulator so that the sphere of solder catches in the recess.
5. Clean the wire as described below.
6. Replace the lucite insulator bearing the cleaned center wire in the chamber by screwing it in loosely (leave it out about one turn).
7. Remove the old solder from the hollow tube of the kovar seal with a needle point file, and clean the entire seal with water and dry.
8. Thread the center wire through the hollow tube in the kovar seal and affix the seal to the chamber.
9. Thin the external connecting wire and insert it in the hollow tube alongside the 0.002 inch wire.

10. Stretch the center wire taut and solder the two wires in place.
11. Pull on the 0.002 inch wire to see if the connection is good.
12. Cut off the excess wire as close as possible to the solder joint.
13. Apply a globule of solder to the joint to cover the end of the 0.002 inch wire.
14. Turn the lucite insulator inside the chamber until the wire is taut.

Center Wire Replacement: Spherical Chamber (53)

1. Push the slug about 1/2 inch out of its teflon insulator.
2. Remove the old solder from the end of the slug with a needle point file.
3. Clean out the radial hole (in the side of the slug near the end).
4. Loop the 0.001 inch platinum wire through the radial hole, out the end, and back in again.
5. Place the end of the slug on a hot soldering iron, radial hole down.
6. Make a fillet of rosin core solder to secure the loop.
7. Pull on the ends of the 0.001 inch wire to see if the connection is good.
8. Cut off the excess wire and file smooth.
9. Clean the loops as described below.

Cleaning and Adjustment of  $4\pi$  Counter Chambers

The following remarks are partially the results of experience and partially a verification of some suggestions made by Mr. W. H. Bradley, President of Nuclear Measurements Corporation ( 53 ) and suggestions contained in the NMC Instruction Manual.

If the counter is contaminated or if a voltage plateau can not be obtained (with the methane flowing at 2-3 bubbles/sec) it may suffice to brush out the chamber with a camels hair brush to remove dust particles, etc., taking care not to touch the center wires. If, however, the chamber does not present a clean shiny surface after the brushing, it should be disassembled and washed thoroughly with distilled water, and dried in an oven (preferably at about  $75^{\circ}\text{C}$  since a hotter oven will melt the Apiezon W Wax which seals the gas inlet tubes to the chamber). The O-rings are treated in a like manner.

A more drastic cleaning is necessary only if the chamber is coated with a brown layer of oxidation products and/or if trouble is still experienced obtaining a plateau. They should then be placed on a lathe and the outer surface removed using in succession coarse carborundum paper (SiC-No. 180) followed by the finer SiC-No. 400 and lastly SiC-No. 600, so that the surface is made smooth and shiny. The chamber is then washed thoroughly with Tide solution, rinsed with distilled water and dried in an oven as described above.

It is very important that the chambers never be cleaned or wiped with any aromatic organic agent or carbon tetrachloride, since the counting rate would be seriously affected for a long period of time due to the continual emission of vapors of the agent which are capable of being absorbed onto the metal and O-ring surface.

In cleaning the center wires it is best to remove them from the chamber. First a solution of lacquer thinner is used, followed by a Tide solution and finally distilled water. To do this, a drop of liquid is forced partially out of the end of a medicine dropper, and the drop is traced over the wire taking care not to contaminate the insulator with any of the liquid. The drop is allowed to fall on a piece of absorbent paper and the process repeated several times with a new drop of the same solution. The electrodes are finally dried thoroughly.

Several other adjustments and corrections were made to the spherical counters. Platinum wire electrodes 0.001 inch in diameter (Sigmund Cohn, New York, No. 479) were substituted for the stainless steel electrodes originally used. The original insulators for the electrodes were replaced with teflon insulators. Dow Corning 702 high vacuum oil was used as the bubbling fluid. Finally the chamber was sealed tightly so that it did not leak. The combination of the above alterations was found to result in plateaus ~300 volts in length obtained with a gas flow rate of ~3 bubbles/sec.

## BIBLIOGRAPHY

1. J. D. Luntz, *Nucleonics* 13, No. 2, 7 (1955).
2. J. D. Luntz, *Nucleonics* 13, No. 6, 80 (1955).
3. F. E. Frost and J. M. Putnam, University of California, Radiation Laboratory Unclassified Report UCRL-2672 (November 1954).
4. E. T. Clarke and J. W. Irvine, Jr., *Phys. Rev.* 66, 231 (1944).
5. D. J. Hughes *et al.*, U.S. Atomic Energy Commission, Unclassified Document AECU-2040 (May 1952).
6. R. F. Taschek, private communication to W. W. Meinke (January 1955).
7. G. A. Jarvis *et al.*, *Phys. Rev.* 79, 929 (1950).
8. E. M. McMillan and R. D. Miller, *Phys. Rev.* 73, 80 (1948).
9. R. A. Glass, University of California Radiation Laboratory Unclassified Report UCRL-2560 (April 1954).
10. W. K. H. Panofsky and R. Phillips, *Phys. Rev.* 74, 1732 (1948).
11. C. P. Baker *et al.*, U.S. Atomic Energy Commission Declassified Document AECD-2189 (LADC-541) (June 1943).
12. J. P. Blaser *et al.*, *Helv. Phys. Acta* 24, 3 (1951).
13. R. L. Aamodt, V. Peterson, and R. Phillips, *Phys. Rev.* 88, 739 (1952).
14. W. H. Burgus *et al.*, University of California Radiation Laboratory Unclassified Report UCRL-4292 (February 1954).
15. P. Kafalas, Ph.D. Thesis, Massachusetts Institute of Technology (August 1954).
16. C. Mileikowsky and R. T. Pauli, *Arkiv f. Fysik* 4, 299 (1952).
17. B. Cork, L. Johnston, and C. Richman, *Phys. Rev.* 79, 71 (1950).

18. E. L. Kelly and E. Segre, Phys. Rev. 75, 999 (1949).
19. P. W. Davison, Phys. Rev. 75, 757 (1949).
20. B. Cork, Phys. Rev. 80, 321 (1950).
21. H. T. Gittings, Jr., Rev. Sci. Instr. 20, 325 (1949).
22. I. A. D. Lewis and A. C. Clark, J. Sci. Instr. 26, 80 (1949).
23. C. J. Brown, Los Alamos Scientific Laboratory Declassified Report LA-1059 (July 1949).
24. M. J. Poole, J. Sci. Instr. 26, 113 (1949).
25. M. M. Haring, Mound Laboratory Unclassified Report MLM-630 (December 1951).
26. A. K. Stebbins, III, M. S. Thesis, Purdue University (August 1951).
27. E. R. Shenk and A. E. Canfora, U.S. Pat. 2,549,022 (April 1951).
28. W. A. Higinbotham and S. Rankowitz, Rev. Sci. Instr. 22, 688 (1951).
29. G. M. B. Bouricius and F. C. Shoemaker, Rev. Sci. Instr. 22, 183 (1951).
30. R. J. Watts, Rev. Sci. Instr. 22, 356 (1951).
31. W. W. Buechner, R. D. Evans, and M. S. Livingston, U.S. Atomic Energy Commission Unclassified Document AECU-2616 (May 1952-May 1953).
32. W. Birnbaum et al., University of California Radiation Laboratory Unclassified Report UCRL-2756 (November 1954).
33. R. O. Lane and D. J. Zaffarano, Phys. Rev. 94, 960 (1954).
34. I. A. D. Lewis and B. Collinge, Rev. Sci. Instr. 24, 1113 (1953).
35. J. S. King, Ph.D. Thesis, University of Michigan (1953).
36. J. E. Rose, Rev. Sci. Instr. 8, 130 (1937).

37. F. N. D. Kurie, Rev. Sci. Instr. 19, 485 (1948).
38. J. W. M. DuMond, Rev. Sci. Instr. 6, 285 (1935).
39. R. Ruka, private communication (1954).
40. L. O. Olsen, C. S. Smith, and E. C. Crittenden, Jr., J. Appl. Phys. 16, 425 (1945).
41. W. C. Caldwell, J. Appl. Phys. 12, 779 (1941).
42. O. Haxel and F. G. Houtermans, Z. Physik 124, 705 (1948).
43. F. G. Houtermans, L. Meyer-Schützmeister, and D. H. Vincent, Z. Physik 134, 1 (1952).
44. L. Meyer-Schützmeister and D. H. Vincent, Z. Physik 134, 9 (1952).
45. R. Cohen, Ann. Physik (12th series) 7, 185 (1952).
46. D. B. Smith, British Atomic Energy Research Establishment Unclassified Report AERE-I/R-1210 (June 1953).
47. H. H. Seliger and L. Cavallo, J. Research National Bureau of Standards 47, 41 (1951).
48. C. J. Borkowski and T. H. Handley, Oak Ridge National Laboratory Unclassified Report CRNL-1056 (April 1951).
49. H. H. Seliger and A. Schwebel, Nucleonics 12, No. 7, 54 (1954).
50. L. Cavallo, private communication to W. W. Meinke (August 1952).
51. B. D. Pate and L. Yaffe, Can. J. Chem. 33, 610 (1955).
52. R. C. Hawkings, M. F. Merritt, and J. H. Craven, Proceedings of a Symposium "Recent Developments and Techniques in the Maintenance of Standards" held at the National Physical Laboratory (May 1951).
53. W. H. Bradley, private communication (June 1954).
54. E. Reible, private communication to W. A. Cassatt (August 1953).
55. V. G. Rexroth, Los Alamos Scientific Laboratory Unclassified Report LA-1239 (May 1951).



56. E. L. Kemp, Los Alamos Scientific Laboratory  
Unclassified Report LA-1207 (July 1950).
57. W. A. Cassatt, Jr., private communication (June 1953).
58. W. A. Cassatt, Jr., private communication to W. W.  
Meinke (March 1955).
59. M. Trott, private communication (August 1953).
60. D. R. Bach, Ph.D. Thesis, University of Michigan  
(September 1955).
61. B. Rossi and K. Greisen, *Revs. Modern Phys.* 13,  
240 (1941).
62. H. A. Bethe and J. Ashkin, in Experimental Nuclear  
Physics, E. Segre, editor (John Wiley and Sons,  
Inc., New York, 1953), p. 251.
63. A. W. Smith, Electrical Measurements in Theory and  
Application (McGraw-Hill Book Company, Inc., New  
York, 1948), Chap. III.
64. E. F. Westrum, private communication (1955).
65. F. Hudswell and C. J. Mandleberg, British Atomic  
Energy Research Establishment Unclassified Report  
AERE-C/R-861 (March 1951).
66. H. C. Thomas, private communication to W. W. Meinke  
(October 1953).
67. E. Nielsen and A. Weinstein, Brookhaven National  
Laboratory Unclassified Report BNL-259 (S-19)  
(September 1953).
68. I. B. Ackerman, private communication (February 1955).
69. L. E. Glendenin et al., Radiochemical Studies: The  
Fission Products (McGraw-Hill Book Co., Inc.,  
New York, 1951), National Nuclear Energy Series,  
Plutonium Project Record, Vol. 9, p. 1629.
70. W. E. Cohn and H. W. Kohn, *J. Am. Chem. Soc.* 70,  
1986 (1948).
71. R. Bouchez and G. Kayas, *Compt. rend.* 228, 1222 (1949).
72. W. L. Arons and A. K. Solomon, U. S. Atomic Energy  
Commission Unclassified Document AECU-2661 (1952).
73. J. Beukenkamp and W. Rieman, III, *Anal. Chem.* 22,  
582 (1950).

74. M. G. Kayas, *Compt. rend.* 228, 1002 (1949).
75. V. J. Linnenbom, *J. Chem. Phys.* 20, 1657 (1952).
76. W. W. Meinke, U. S. Atomic Energy Commission Declassified Document AECD-2738 (UCRL-432) (August 1949).
77. L. D. McIssac and A. Voigt, Iowa State College Unclassified Report ISC-271 (June 1952).
78. W. W. Scott, Standard Methods of Chemical Analysis (D. Van Nostrand Co., Inc., New York, 1939), p. 931.
79. W. F. Hillebrand and G. E. F. Lundell, *J. Am. Chem. Soc.* 42, 2609 (1920).
80. J. R. Haskins et al., *Phys. Rev.* 88, 876 (1952).
81. J. E. Duval and M. H. Kurbatov, *J. Am. Chem. Soc.* 75, 2246 (1953).
82. J. D. Gile, W. M. Garrison, and J. G. Hamilton, *J. Chem. Phys.* 18, 1685 (1950).
83. N. V. Sidgwick, The Chemical Elements and Their Compounds (Oxford University Press, London, 1950), p. 636.
84. W. W. Meinke, W. A. Cassatt, Jr. and K. L. Hall, U. S. Atomic Energy Commission Unclassified Report AECU-2944 (June 1954).
85. W. A. Cassatt, Jr., Ph.D. Thesis, University of Michigan (September 1954). see also U. S. Atomic Energy Commission Unclassified Report AECU-2958.
86. H. G. Hicks et al., California Research and Development Company Report LRL-65 (December 1953).
87. H. G. Hicks, private communication to W. W. Meinke (June 1955).
88. H. R. Haymond et al., *J. Chem. Phys.* 18, 391 (1950).
89. D. N. Sunderman and W. W. Meinke, *Science* 121, 777 (1955).
90. A. Langer, *J. Chem. Phys.* 10, 321 (1942).
91. G. Rouser and P. F. Hahn, *J. Am. Chem. Soc.* 74, 2398 (1952).

92. A. S. Newton, reported in "Chemical Procedures Used In Bombardment Work at Berkeley," by W. W. Meinke, U. S. Atomic Energy Commission Declassified Document AECD-2738 (UCRL-432) (August 1949).
93. G. G. Manov, Preliminary Report No. 13, Nuclear Science Series, National Research Council (July 1953).
94. C. E. Myers, *Nucleonics* 5, No. 5, 37 (1949).
95. J. G. Bayly, *Can. J. Research* 28A, 520 (1950).
96. L. R. Zumwalt et al., *Science* 107, 47 (1948).
97. C. V. Cannon, reported in Conference on Absolute  $\beta$  Counting, Preliminary Report No. 8, Nuclear Science Series, National Research Council (October 1950).
98. R. Loevinger, *Rev. Sci. Instr.* 24, 907 (1953).
99. L. H. Gray, *Brit. J. Radiology* 22, 677 (1949).
100. J. V. Dunworth, *Rev. Sci. Instr.* 11, 167 (1940).
101. J. Barnothy and M. Forro, *Rev. Sci. Instr.* 22, 415 (1951).
102. M. Deutsch, reported in Conference on Absolute  $\beta$  Counting, Preliminary Report No. 8, Nuclear Science Series, National Research Council (October 1950).
103. E. Bleuler and G. J. Goldsmith, Experimental Nucleonics (Rinehart and Co., Inc., New York, 1952), p. 56.
104. W. B. Mann, National Research Council of Canada Report CRM-408 (ca. 1950).
105. L. R. Zumwalt, U. S. Atomic Energy Commission Declassified Document UDDC-1346 (December 1947).
106. L. R. Zumwalt, U. S. Atomic Energy Commission Unclassified Document AECU-567 (September 1949).
107. Y. Saji, M. Sakisaka, and K. Miyake, *J. Phys. Soc. Japan* 8, 580 (1953).
108. G. K. Schweitzer and E. R. Stein, *Nucleonics* 7, No. 3, 65 (1950).
109. G. M. Walton, J. S. Thompson, and I. F. Croall, British Atomic Energy Research Establishment Unclassified Report AERE-C/R-1136 (March 1953).

110. U. L. Upson, *Nucleonics* 11, No. 12, 49 (1953).
111. A. C. Pappas, U. S. Atomic Energy Commission  
Unclassified Document AECU-2806 (September 1953).
112. G. A. Schweitzer and J. W. Nehls, *J. Phys. Chem.*  
56, 541-4 (1952).
113. G. W. Reed, Jr., private communication (January 1954).
114. W. S. Lyon and S. A. Reynolds, Oak Ridge National  
Laboratory Unclassified Report ORNL-955  
(January 1951).
115. P. Lerch, *Helv. Phys. Acta* 26, 663 (1953).
116. G. I. Gleason, J. D. Taylor, and D. L. Tabern, *Nucleonics*  
5, No. 5, 12 (May 1951).
117. S. G. Rudstam, *Nucleonics* 13, No. 2, 64 (1955).
118. F. D. Rosen and W. Davis, Jr., U. S. Atomic Energy  
Commission Declassified Document AECD-3184  
(November 1950).
119. R. G. Baker and L. Katz, *Nucleonics* 11, No. 2, 14  
(1953).
120. B. F. Burtt, *Nucleonics* 5, No. 2, 28 (1949).
121. W. E. Nervik and I. C. Stevenson, *Nucleonics* 10, No. 3,  
18 (1952).
122. E. D. Klema and A. C. Hanson, *Phys. Rev.* 73, 106 (1948).
123. R. E. Batzel, W. J. T. Crane and G. D. O'Kelley,  
*Phys. Rev.* 91, 939 (1953).
124. W. E. Nervik, University of California Radiation  
Laboratory Unclassified Report UCRL-2542 (April 1954).
125. C. F. G. Delaney, *Phys. Rev.* 81, 158 (1951).
126. W. F. Libby, "Sensitive Radiation Detection Techniques  
for Tritium Natural Radioactives, and Gamma Radiation"  
ATI-133901 (December 1951).
127. E. L. Eidinoff, reported in Conference on Absolute  
 $\beta$  Counting, Preliminary Report No. 8, Nuclear  
Science Series, National Research Council  
(October 1950).
128. J. Bernstein and R. Ballentine, *Rev. Sci. Instr.* 21,  
158 (1950).

129. H. R. Crane, *Nucleonics* 9, No. 6, 16 (1951).
130. R. K. Clark, *Rev. Sci. Instr.* 21, 753 (1950).
131. G. Failla and H. H. Rossi, U. S. Pat. 2,659,826 (November 1953).
132. W. Gross, S. Deutsch, and G. Failla, in *Annual Report on Research Project, NYO-4582* (April 1954).
133. A. D. Suttle, Jr., U. S. Atomic Energy Commission Unclassified Report AECU-2524 (August 1952).
134. W. L. Graf, C. L. Comar, and I. B. Whitney, *Nucleonics* 9, No. 4, 22 (October 1951).
135. F. L. Curtis, D. L. Clark, and J. J. Dauby, Mound Laboratory Unclassified Report MLM-801 (December 1952).
136. M. L. Curtis, Mound Laboratory Unclassified Report MLM-603 (September 1951).
137. D. C. Conway and J. C. Rasmussen, University of California Radiation Laboratory Unclassified Report UCRL-2075 (January 1953).
138. J. S. Hader, G. R. Hagee, and L. A. Setter, *Nucleonics* 12, No. 6, 29 (1954).
139. H. H. Seliger, *Phys. Rev.* 88, 408 (1952).
140. H. C. Martin, B. C. Diven, and R. F. Taschek, *Phys. Rev.* 93, 199 (1954).
141. E. H. Belcher, *J. Sci. Instr.* 30, 286 (1953).
142. D. C. Conway and J. C. Rasmussen, University of California Radiation Laboratory Report UCRL-2076 (January 1953).
143. N. Lindner and R. R. Osborne, California Research and Development Company Report RTA-22 (January 1953).
144. M. H. MacGregor, Ph.D. Thesis, University of Michigan (1953).
145. G. A. Sawyer, Ph.D. Thesis, University of Michigan (1950).
146. Massachusetts Institute of Technology Progress Report No. 29 (May 1953).
147. B. D. Pate and L. Yaffe, *Can. J. Chem.* 33, 15 (1955).

148. B. D. Fate and I. Yaffe, *Can. J. Chem.* 33, 929 (1955).
149. L. M. Fry and R. T. Overman, U. S. Atomic Energy Commission Declassified Document AECD-1800 (January 1948).
150. J. Brown et al., *Rev. Sci. Instr.* 19, 818 (1948).
151. J. Backus, *Phys. Rev.* 68, 59 (1945).
152. I. M. Langer and C. B. Cook, *Rev. Sci. Instr.* 19, 257 (1948).
153. H. Slatis, Beta and Gamma-Ray Spectroscopy, K. Siegbahn, editor (North-Holland Publ. Co., Amsterdam, 1955), p. 260.
154. F. W. Brown, III and A. B. Willoughby, *Rev. Sci. Instr.* 19, 820 (1948).
155. A. Rothen, *Rev. Sci. Instr.* 16, 26 (1945).
156. L. Harris and J. E. Beasley, *J. Opt. Soc. Am.* 42, 634 (1952).
157. W. B. Hillig, Ph.D. Thesis, University of Michigan (1953).
158. D. E. Hull, U. S. Atomic Energy Commission Declassified Document AECD-1816 (March 1948).
159. W. B. Mann and H. H. Deliger, *J. Research National Bur. Standards* 50, 197 (1953).
160. E. L. Duggan and K. C. Smith, *Science* 116, 305 (1952).
161. P. T. Gilbert, Jr., *Science* 114, 637 (1951).
162. D. Halliday, Introductory Nuclear Physics (John Wiley and Sons, Inc., New York, 1950).
163. T. F. Kohman, *Phys. Rev.* 65, 63 (1944).
164. T. F. Kohman, The Transuranium Elements: Research Papers (McGraw-Hill Book Co., Inc., New York, 1949), National Nuclear Energy Series, Plutonium Project Record, Vol. 14B, p. 1655.
165. F. Calvin et al., Isotopic Carbon (John Wiley and Sons, Inc., New York, 1949), Appendix III.
166. W. H. Baker, Mound Laboratory Unclassified Report ML-658 (March 1952).
167. E. Bleuler and G. J. Goldsmith, op. cit., p. 320.

168. L. J. Rainwater and C. S. Wu, *Nucleonics* 1, No. 2, 60 (1947).
169. L. J. Rainwater and C. S. Wu, *Nucleonics* 2, No. 1, 42 (1948).
170. A. C. G. Mitchell and L. H. Langer, *Phys. Rev.* 53, 505 (1938).
171. L. Szilard and T. A. Chalmers, *Nature* 135, 98 (1935).
172. E. Amaldi et al., *Proc. Roy. Soc. (London)* 149A, 522 (1935).
173. L. I. Silver, *Phys. Rev.* 76, 589 (1949).
174. B. Russell and A. Mattenberg, U. S. Atomic Energy Commission Declassified Document AEC-D-2926 (October 1945).
175. E. L. Jensen et al., *Phys. Rev.* 85, 112 (1952).
176. E. K. Sheline, R. B. Holtzman, and C. Y. Fan, *Phys. Rev.* 83, 919 (1951).
177. T. Westermark, *Phys. Rev.* 88, 573 (1952).
178. B. N. Cacciapuoti, *Nuovo Cimento* 15, 213 (1938).
179. B. Elbek, K. C. Nielsen, and C. B. Nielsen, *Phys. Rev.* 95, 96 (1954).
180. J. H. Hollander, I. Perlman, and G. T. Seaborg, *Revs. Modern Phys.* 25, 469 (1953).
181. W. F. Hornyak and T. Coor, *Phys. Rev.* 92, 675 (1953).
182. R. Sherr and R. H. Miller, *Phys. Rev.* 93, 1076 (1954).
183. G. Charpak, *J. phys. et radium* 16, 62-5 (1955).
184. F. J. Lemphill, private communication (January 1955).
185. L. J. Laslett, *Phys. Rev.* 76, 858 (1949).
186. J. H. Sreb, *Phys. Rev.* 81, 469 (1951).
187. E. E. Lockett and R. H. Thomas, *Nucleonics* 11, No. 3, 14 (1953).
188. A. H. Solomon, *Phys. Rev.* 79, 403 (1950).

189. J. W. Cobble and R. W. Atteberry, Phys. Rev. 80, 917 (1950).
190. R. Wilson and G. R. Bishop, Proc. Phys. Soc. (London) 62, 457 (1949).
191. W. K. Sinclair and A. F. Holloway, Nature 167, 365 (1951).
192. S. N. Van Voorhis, Phys. Rev. 49, 889 (1936).
193. J. Tobailem, J. phys. et radium 16, 48 (1955).
194. J. W. Irving, Jr. and E. T. Clarke, J. Chem. Phys. 16, 686-90 (1948).
195. F. O. Bartell and S. Softky, Phys. Rev. 84, 463 (1951).
196. A. G. Worthing and J. Geffner, Treatment of Experimental Data (John Wiley and Sons, Inc., New York, 1943) Chap. II.
197. W. F. Biller, Ph.D. Thesis, University of California Radiation Laboratory Unclassified Report UCRL-2067 (December 1952).
198. S. C. Fung, Ph.D. Thesis, University of California Radiation Laboratory Unclassified Report UCRL-1465 (September 1951).
199. W. A. Aron, B. G. Hoffman, and F. C. Williams, Atomic Energy Commission Unclassified Document AECU-663 (UCRL-121) (May 1951).
200. G. L. Schott and W. W. Meinke, Phys. Rev. 89, 1156 (1953).
201. T. Enns, Phys. Rev. 56, 872 (1939).
202. M. Lindner and I. Perlman, Phys. Rev. 78, 499 (1950).
203. F. A. Johnson, Proc. Roy. Soc. (Canada) 46, 135A (1952).
204. W. L. Bendel et al., Phys. Rev. 90, 888 (1953).
205. B. C. Halder and E. O. Wiig, Phys. Rev. 94, 1713 (1954).
206. E. P. Steinberg and L. E. Glendenin, Radiochemical Studies: The Fission Products (McGraw-Hill Book Co., Inc., New York, 1951); National Nuclear Energy Series, Plutonium Project Record, Vol. 9, p. 877.
207. K. Shure, Ph.D. Thesis, Massachusetts Institute of Technology (May 1951).



